This is to certify that the
dissertation entitled

MODELING AND ANALYSIS OF SOLAR DISTRIBUTED GENERATION

presented by

Eduardo Iván Ortiz Rivera

has been accepted towards fulfillment
of the requirements for the

Ph. D. degree in Electrical Engineering

Major Professor's Signature

May 11, 2006

Date

MSU is an Affirmative Action/Equal Opportunity Institution

MODELING AND ANALYSIS OF SOLAR DISTRIBUTED GENERATION

By

Eduardo Iván Ortiz Rivera

A DISSERTATION

Submitted to
Michigan State University
in partial fulfillment of the requirements
for the degree of

DOCTOR OF PHILOSOPHY

Department of Electrical and Computer Engineering

2006

ABSTRACT

MODELING AND ANALYSIS OF SOLAR DISTRIBUTED GENERATION

By

Eduardo Iván Ortiz Rivera

Recent changes in the global economy are creating a big impact in our daily life. The price of oil is increasing and the number of reserves are less every day. Also, dramatic demographic changes are impacting the viability of the electric infrastructure and ultimately the economic future of the industry. These are some of the reasons that many countries are looking for alternative energy to produce electric energy. The most common form of green energy in our daily life is solar energy. To convert solar energy into electrical energy is required solar panels, dc-dc converters, power control, sensors, and inverters.

In this work, a photovoltaic module, PVM, model using the electrical characteristics provided by the manufacturer data sheet is presented for power system applications. Experimental results from testing are showed, verifying the proposed PVM model. Also in this work, three maximum power point tracker, MPPT, algorithms would be presented to obtain the maximum power from a PVM. The first MPPT algorithm is a method based on the Rolle's and Lagrange's Theorems and can provide at least an approximate answer to a family of transcendental functions that cannot be solved using differential calculus. The second MPPT algorithm is based on the approximation of the proposed PVM model using fractional polynomials where the

shape, boundary conditions and performance of the proposed PVM model are satisfied. The third MPPT algorithm is based in the determination of the optimal duty cycle for a dc-dc converter and the previous knowledge of the load or load matching conditions.

Also, four algorithms to calculate the effective irradiance level and temperature over a photovoltaic module are presented in this work. The main reasons to develop these algorithms are for monitoring climate conditions, the elimination of temperature and solar irradiance sensors, reductions in cost for a photovoltaic inverter system, and development of new algorithms to be integrated with maximum power point tracking algorithms. Finally, several PV power applications will be presented like circuit analysis for a load connected to two different PV arrays, speed control for a dc motor connected to a PVM, and a novel single phase photovoltaic inverter system using the Z-source converter.

To my parents, Eduardo and Haydee,

to my sister, Enid, and to my wife, Yulia r

s

S

C

th

En

Ro

exn

ACKNOWLEDGMENTS

First, all the glory to God! This dissertation would not be possible without several contributions. It is a pleasure to thank my advisor, Professor Fang Z. Peng, for his guidance, assistance, support, and for providing me with a pleasant working environment. I would also like to thank Professors Steven Shaw, Hassan K. Khalil, Elias Strangas, and Robert Schlueter for their time and effort in being part of my committee.

I would like to extend special thanks to Professors Percy Pierre, Barbara O'Kelly, the National Consortium for Graduate Degrees for Minorities in Engineering and Science and the Alfred P. Sloan Foundation for providing the funding which made this work possible and for all their support during my stay at Michigan State University. I am very grateful to Professor Wesley G. Zanardelli, my friend and colleague, for his interest in my research, encouragement, friendly discussions, and excellent suggestions.

Special words of thanks go to my lab colleagues Alan Joseph, Jin Wang, Miaosen Shen, Fan Zhang, Yi Huang, Joel Anderson, Richard Badin, Honnyong Cha, Lihua Chen, Irving Balaguer, Zhiguo Pan, Varun Chengalvala and Kent Holland for all of their support. I would also like to thank the members of the Department of Electrical Engineering and College of Engineering whose help was much appreciated, including Roxanne Peacock, Sheryl Hulet and Professor Drew Kim. I am appreciative for the extended use of computer resources at Michigan State University.

A special note of thanks is extended to my parents Eduardo and Haydee for

th
no
to
ex
liv
Al
be
for

Pu
wo
tha
this
Lin
200
seve
to F
exa
and

their constant support, encouragement and unconditional love, without which I would never have accomplished this goal; to my sister Enid for always believing in me; to my lovely wife Yulia Trukhina for her support, love and care, for being a fine example of an excellent scientist herself, making me proud of her and wanting to live up to her standards; to my good friends Miguel Figueroa, Nelson Sepúlveda, Jeff Ahrens, Uchechukwu Wejinya, Ana Becerril, Sandra Soto, and Pedro Meléndez for being supportive and always ready to help. I would like to thank all my other friends for making my life in East Lansing, Michigan enjoyable and meaningful.

Finally, I would like to thank Professor Gerson Beauchamp from University of Puerto Rico, Mayagüez for all his support before, during and after this journey. I would like to thank Professor Sonia Díaz for driving my curiosity. I would like to thank Professor R. L. Tummala who prepared me during my previous degree for this challenge. I would like to thank Professor Claudio Rivetta from the Stanford Linear Accelerator Center for his hospitality during the summers of the 2001 and 2002 at Fermi National Accelerator Laboratory where I got a better understanding of several aspects of my research. I would also like to express my gratitude and thanks to Professor Raúl Marrero for his guidance, and his professional as well as personal example as a mentor during all his life at Barranquitas, Puerto Rico where I was born and grew up.

LIS

LIS

1

2

3

TABLE OF CONTENTS

LIST OF TABLES

LIST OF FIGURES

Int

The w
megaw
States
Depart
over 15
the ele
that a
constr
and po
the ot
renewa
green
in ma
enviro
green

Sin
distrib
in urb

CHAPTER 1

Introduction

The worldwide electric utility generation is estimated at over 3,000,000 installed megawatts (MW) and is growing by more than 80,000MW per year. In the United States alone, the electric utility generation is estimated at 722,200MW and the U.S. Department of Energy (DoE) forecasts that, for the coming decade, an average of over 15,000MW per year of new generation facilities will be added in order to supply the electricity growth and to replace the estimated 6,000MW per year of old plants that are expected to be retired. To solve this problem, the typical solution is the construction of a large central power station, more transmission lines, transformers, and poles to deliver the power to the end-user, often hundreds of miles away [3]. On the other hand, another alternative solution for providing power has been the use of renewable energies in distributed generation applications. The use of renewable and green energies (i.e. solar energy, wind energy, geothermic energy, etc.) is growing in many countries and the contribution to reduce global warming and protect the environment is increasingly important [4, 5, 6, 7, 8, 9]. The most common of these green energies in our daily life is solar energy.

Since the last three decades the interest to use solar energy in applications of distributed generation are growing very fast. Applications for the solar energy are in urban areas, motor drives, race vehicles, satellites, etc [5, 10, 11, 12, 13, 14, 15, 16.

like

is n

loca

the

alte

the

ene

use

for

ele

adv

sur

the

a F

[4.

un

Bu

tha

cha

16, 17, 18]. For some applications where small amounts of electricity are required, like emergency call boxes, PV systems are often justified even when grid electricity is not very far away. When applications require larger amounts of electricity and are located away from existing power lines, photovoltaic systems can in many cases offer the least expensive, most viable option [15]. Today, solar energy is considered as a real alternative resource of energy to be used for production of electrical energy around the world [19, 20, 21]. The key component to convert solar energy into electrical energy is the photovoltaic module, PVM, also known as a solar panel. Sometimes the use of photovoltaic modules (PVM's) can be more practical than the typical solutions for power generation.

An example of the last statement is that solar panels can supply power for the electronic equipment aboard a satellite over a long period of time, which is a distinct advantage over batteries [18, 22]. Also, it is possible to obtain useful power from the sun in terrestrial applications using solar panels, even though the atmosphere reduces the solar intensity [20, 23, 24, 25]. Inclusive for many remote locations, the cost of a PV generation system is less than the cost of extending the grid to that location [4, 26].

Unfortunately in PV circuit analysis, often it is assumed that the PVM is working under the following three assumptions [27]:

1. The environment conditions are constants.
2. The PVM is working under maximum power.
3. The PVM voltage output is constant, hence the PVM can be assumed as a constant voltage source.

But for practical purposes, these assumptions are not always valid due to the fact that in a regular day, the temperature, T, and the solar irradiance, E_i, levels are changing.

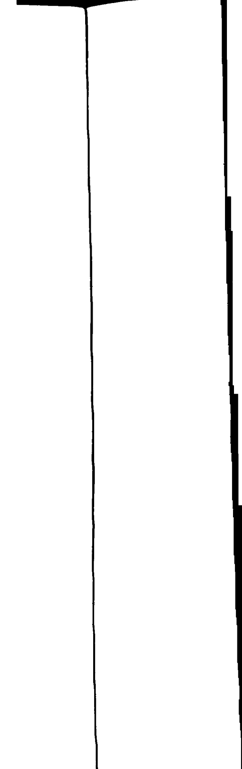

Figur

As
irradia
can be
the dif
Finally
data f
lowest
point
4 hou
the P
shadin
Al
physi

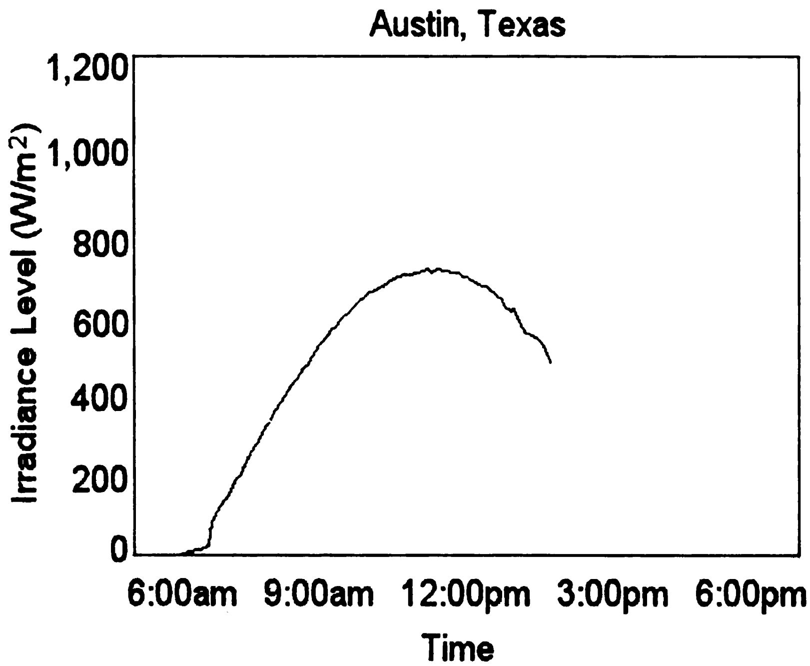

Figure 1.1. Irradiance level (W/m^2) at Austin, Texas during March 16, 2006 [1].

As examples of the last statement, figure 1.1 shows how in a normal day the irradiance level can change from $0W/m^2$ up to $700W/m^2$ [1]. Also, the irradiance level can be different in a region during the same period of time [2, 28]. Figure 1.2 shows the different irradiance levels around the state of Georgia during an instance of time. Finally, the temperature can change during the day; figure 1.3 shows the temperature data from a normal day at Barranquitas, Puerto Rico, where at 5:00am (5:00), the lowest temperature point is $16°C$ and at 3:00pm (15:00) the highest temperature point is $28°C$. In a typical day, the temperature can change up to $10°C$ in less than 4 hours. Hence, it is clear that these parameters will affect the maximum power and the PVM output voltage. Rapid changes in the temperature and the influence of shading will affect the maximum power supplied by the PVM [29, 30].

Also, the actual models to describe solar panel performance are more related to physics, electronics, and semiconductors than to power systems and these models do

Figu
durin

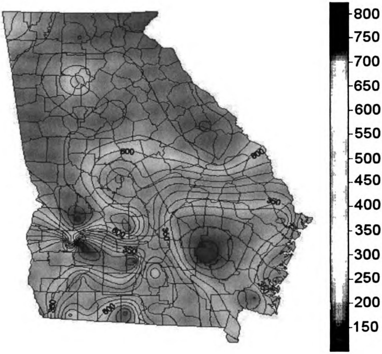

Figure 1.2. Irradiance level (W/m^2) in different regions around the state of Georgia during April 18, 2006 [2].

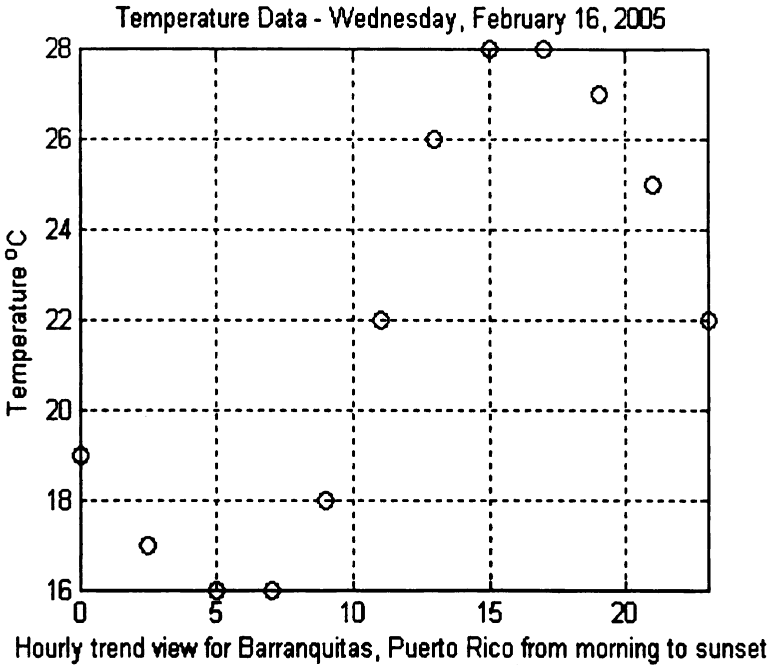

Figure 1.3. Daily temperature data (°C) from morning to sunset at Barranquitas, PR during February 16, 2005.

not necessarily consider the effects of the temperature and effective irradiance level [22, 23, 30, 31, 32, 33, 34, 35, 36, 37, 38, 39, 40, 41, 42, 43, 44]. Some of the models require several parameters such as the temperature coefficients, photon current, open circuit voltage, series/shunt resistance of the device, etc. Also some of the required parameters in those models are not available by the manufacturer data sheets so it is necessary to find the information in other sources. At the same time, these models can be impractical and too complex for common tasks in power systems such as power flow, harmonic analysis, sensitivity analysis, load matching for maximum power transferred from the source to the load. To solve these problems and to maximize the use of information provided by the manufacturer data sheets, Chapter 2 proposes a photovoltaic model based on the electrical characteristics, Standard Test Conditions (STC), and I-V Curves. This model will be more beneficial and practical for power system analysis [45].

In
PV p
Track
the m
track
provi

In
[46, 9
in en
MPF
rithm
know
last
to se
offer
tabl

I
seve
are
anal
and
used
too
an a
by t
thes
this

In addition to the PVM, to convert solar energy into electrical energy, a basic PV power generation system includes inverters, control (i.e. Maximum Point Power Tracking) and sensors. As a fact, a PVM will operate at the highest efficiency when the maximum power is supplied from the PVM [46, 47]. The maximum power point tracker, MPPT, is the typical algorithm to calculate the maximum power, P_{max}, provided by a PVM [46, 47, 48, 49].

In the past, many authors described different variations of the MPPT algorithm [46, 47, 48, 49, 50, 51, 52, 53, 54, 55] and their applications to control dc-dc converters in energy conversion [51, 52, 53, 54, 55, 56, 57]. Unfortunately, most of the existing MPPT methods to estimate the maximum power are based on trial and error algorithms where the voltage is increased until the maximum power is achieved, better known as the hill-climbing method [46, 48, 49]. Other MPPT algorithms compare the last sampled voltage and the current to the presently sampled voltage and the current to see which state will produce the maximum power [52]. Additionally, the literature offers other types of MPPT algorithms such that rippled based method [50], look-up table methods, [53] and fuzzy logic [54].

Disadvantages with these MPPT algorithms are that discrete algorithms require several iterations to calculate the optimal steady-state duty ratio [56]. Some of them are not designed for quick changes in the weather conditions [49, 58]. Also, for non-analytical methods, the time for the iterations will depend on the initial conditions and can create bifurcation problems [57, 59, 60]. Additionally, the dynamic models used to describe the interaction of solar panels, MPPT control, and converter are too complicated, with a lot of required parameters and the models cannot produce an analytical solution to obtain the optimal voltage and maximum power produced by the PV inverter creating the necessity to use long and tedious iterations. Also, these results are not very practical for straightforward power flow analysis. To solve this problem, Chapter 3 proposes an analytical method using the proposed PVM in

Cha

the

Met

for p

sam

and

that

valu

over

appli

solvi

A

nomi

PVM

tive c

P_{max}

like m

factor

filter

desig

Th

polyno

descri

the fa

our da

approx

Chapte

Chapter 2 to obtain a close approximation of the optimal voltage that will produce the maximum power. The name of the method is the Linear Reoriented Coordinates Method, LRCM, [61]. The LRCM is very useful as an alternative MPPT algorithm for power and utility applications [62]. The LRCM is a simple method which uses the same variables as the proposed dynamic model and is a time saver for calculating V_{op} and P_{max} reducing the long and tedious iterations. The simulated results will show that the proposed technique is very effective, giving a small error between the real values and estimated values, even if the effective intensity of light is changing rapidly over the PVM. In addition, other applications for LRCM will be shown including applications for fuel cells, economics, space optimization for floorplan design, and solving transcendental functions [63].

An additional MPPT algorithm is presented in Chapter 4. It is Fractional Polynomial Method, FPM. The main idea of the FPM is to approximate, the proposed PVM model given in Chapter 2, using fractional polynomials then using the derivative of the approximation of P(V) is possible to approximate analytically V_{op} and P_{max}. The literature provides several examples using fractional polynomials in areas like medicine (e.g. mathematical modeling of breast cancer [64, 65], modeling of risk factors in epidemiology [66]), signal processing and pattern recognition (e.g. digital filter design [67, 68, 69] and face recognition [70]), control systems (e.g. observer design [71]), biological and agricultural models [72, 73], etc.

The main advantage of a fractional polynomial is the reduction of high order polynomial models for curve fitting [73] and increased accuracy of the approximation describing more adequately a physical model. Also, fractional polynomials belong to the family of fractals. It is important to understand that the fractals can be found in our daily life, in the nature and physical world [74, 75] doing fractional polynomial approximation a useful tool to describe the PVM physical behavior [76]. Additionally, Chapter 4 provides an approximation method for converting fractional polynomials to the

model i

4

Cha

and ten

algoritl

the ope

these a

Pyrono

in the i

PVM s

measur

algoritl

Additio

program

Cha

tions of

and a p

[79]. It

for a PV

consider

Chapter

to the closest integer polynomials, keeping similar properties as the proposed PVM model in Chapter 2. These two non-traditional methods are fully explained in Chapter 4

Chapter 5 presents several algorithms to estimate the effective irradiance level, E_i, and temperature, T, over a PVM using the PVM model proposed in Chapter 2. These algorithms are based on the Fixed Point Theorem [77] and the online measurements of the open circuit voltage and short circuit current. The main purpose for developing these algorithms is to eliminate the use of pyronometers and thermocouples [78]. Pyronometers usually are very expensive and need calibration after sudden changes in the irradiation. The thermocouples usually are cheap but direct contact to the PVM surface is required and several thermocouples are required to obtain an accurate measure and often calibration is required. From the economic point of view, these algorithms can reduce the cost for a PV power system eliminating extra components. Additionally, these algorithms are very accurate, easy to understand, and can be programmed in a microprocessor or DSP board.

Chapter 6 presents the following sections: circuit analysis using PVM's, calculations of the optimal duty ratio to obtain P_{max} for different types of dc-dc converters and a proposed PVM transformerless inverter using a resonant Z-source converter [79]. It is important to understand that for each analysis the dynamic equations for a PVM were used under variable environmental conditions. This chapter can be considered as a tool for power systems analysis using photovoltaic modules. Finally, Chapter 7 presents a summary of the results and plans for future work.

CHAPTER 2

Photovoltaic Module Model

This chapter proposes an analytical model for the performance of photovoltaic modules to be used in distributed power generation. The proposed photovoltaic module (PVM) model uses the electrical characteristics provided by the manufacturer data sheet. The required characteristics are short-circuit current (I_{sc}), open-circuit voltage (V_{oc}) and the temperature coefficients of I_{sc} and V_{oc}. The proposed model takes into consideration the nominal values provided by the manufacturer data sheet under Standard Test Conditions (STC). Also, the proposed PVM model considers the changes and effects of the temperature and the effective irradiance levels over the PVM. Finally, simulations about V-I and P-V curves under different irradiance levels and temperatures are provided for different solar panel modules, data sheets.

2.1 Methods Proposed in the Past

Different conversion methods have been proposed in the past, some of them work point by point and others model the solar cell performance with analytical equations. Some of the models and the conversion equations are made up of the following:

1) Method of Anderson [34]:

$$I_2 = \frac{E_2 \cdot I_1}{E_1 + E_1 \cdot TCi \cdot (T_1 - T_2)} \tag{2.1}$$

$$V_2 = \frac{q \cdot V_1}{[1 + TCV \cdot (T_1 - T_2)] \cdot \left[q + k \cdot T \cdot \ln\left(\frac{E_1}{E_2}\right)\right]} \tag{2.2}$$

2) Method of Bleasser [35]:

$$I_2 = \frac{E_2}{E_1} \cdot I_1 \cdot (1 + TCi \cdot (T_1 - T_2)) \tag{2.3}$$

$$V_2 = V_1 - R_s \cdot (I_2 - I_1) + \frac{k \cdot T}{q} \cdot \ln\left(\frac{E_2}{E_1}\right) + TCV \cdot (T_2 - T_1) \tag{2.4}$$

3) IEC-891 procedure [41]:

$$I_2 = I_1 + I_{SC1} \cdot \left(\frac{I_{SR}}{I_{MR}} - 1\right) + TCi \cdot (T_2 - T_1) \tag{2.5}$$

$$V_2 = V_1 - R_s \cdot (I_2 - I_1) - K \cdot I_2 \cdot (T_2 - T1) + TCV \cdot (T_2 - T_1) \tag{2.6}$$

4) Photovoltaic Utility Scale Application (PVUSA) model [43]:

$$P = E_i \cdot (a + b \cdot E_i + c \cdot T + d \cdot WS) \tag{2.7}$$

5) Solar Cell, Semiconductor (one diode) Model [22]:

$$I(V) = I_{Ph} + I_{SR} - I_{SR} \cdot \exp\left(\frac{q \cdot V}{k \cdot T}\right) \tag{2.8}$$

6) Two-Exponential Model [37]:

$$I(V) \;=\; I_{Ph} + I_{S1} - I_{S1} \cdot \exp\left(\frac{V + I \cdot R_s}{\eta_1 \cdot V_{Th}}\right)$$

v
a
a
v
1
te
id
10
by
re
the

ma
und
qui
such
ity
the
K.
prog
ance.
d to
resist
age of

$$+I_{S2} - I_{S2} \cdot \exp\left(\frac{V + I \cdot R_s}{\eta_2 \cdot V_{Th}}\right) - \frac{V + I \cdot R_s}{R_p} \tag{2.9}$$

The variables P, I and V are the photovoltaic module output power, current and voltage. Index 1 indicates measured data, index 2 labels the new temperature T and irradiation E_i and the conversion results for I and V [38]. I_{ph}, I_{SC1} and I_{SR} are photocurrent, saturation and reverse saturation current. V_{Th} is the thermical voltage. R_s, R_p are the series/shunt resistance. k is Boltzmann constant, $1.38 \times 10^{-23} J/Kelvin$. TCi is the temperature coefficient of I_{sc}, $(A/°C)$. TCV is the temperature coefficient of V_{oc}, $(V/°C)$. K is the curve correction factor. η is the ideality factor. a, b, c and d are regression coefficients. q is the charge of electron, $1.6 \times 10^{-19} As$. WS is the wind speed, (m/s). The first three methods are working point by point [34, 35, 41], the PVUSA method is based on continuous data collection and regression model [43] and the last two methods are analytical equations to describe the performance of a solar cell, [22, 37].

All the given methods require several parameters that can be obtained from the manufacturer data sheet, such as the temperature coefficients, short circuit current under STC, and open circuit voltage under STC, etc. Unfortunately, some of the required parameters for these models cannot be found in the manufacturer data sheet, such that the photon current, the series/shunt resistance, thermal voltage, the ideality factor, the diode reverse saturation current, Boltzmann's constant, band gap for the material, etc. Also, the IEC-891 uses a fourth parameter curve correction factor K. The Two-Exponential model requires a curve-fitting and simulation computer program. Limitations with the PVUSA are: poor model performance at low irradiance, and requires sufficient data to calculate the regression coefficients a, b, c and d to perform the curve fitting. Also, three the methods consider the PVM internal resistance as a constant value where in reality it is not true due the changes in voltage of operation. Additionally, the literature offers other complex methods of PVM modeling using fuzzy logic, look-up tables or learning algorithms more suitable for physics but not necessary for power applications [36, 39]. In general, these models of the PV panels required additional parameter data not given by the manufacturer data sheets; it is difficult to obtain the needed data, and most of them are static models not designed for distributed power applications analysis [45].

2.2 Typical Requirements for a PVM Data Sheet

The Underwriters Laboratories has developed a sample of information requirements for photovoltaic modules [80]. A photovoltaic module datasheet should include the ratings of the short circuit current (I_{sc}), open circuit voltage (V_{oc}), optimal voltage (V_{op}) and optimal current (I_{op}) of an individual module when operating at maximum power (P_{max}). These ratings are to be based upon Standard Test Conditions (STC). The STC (also known as SRC or Standard Reporting Conditions) is defined with nominal cell temperature $25°C$, nominal irradiance level $1000W/m^2$ at spectral distribution of Air Mass 1.5 solar spectral content. Additionally, the ratings are tested at Nominal Operating Cell Temperature (NOCT). NOCT is defined as $20°C$ ambient air temperature, $800W/m^2$ irradiance with a $1m/s$ wind across the module from side to side. Finally, it is the purpose of the next section to propose to the reader a photovoltaic module model more suitable and useful for power system applications using the valuable information required from the manufactures.

2.3 Proposed Photovoltaic Module Model

The proposed model for the photovoltaic module (PVM) takes into consideration the relationship of the current with respect to the voltage, effective irradiance level, E_i and temperature, T of operation for the PVM, the characteristic constant for the I-V curves, the short-circuit current and the open-circuit voltage [45]. The proposed

PVM model is described by (2.10), (2.11), (2.12) and (2.13). The main advantage of the proposed PVM model is that for any photovoltaic module, it can be described in terms of the values provided by the manufacturer data sheet and the standard test conditions [45]. Also, the proposed PVM model is continuous and differentiable with respect to the voltage giving a unique relationship between voltage, current and power.

$$I(V) = \frac{Ix}{1 - exp\left(\frac{-1}{b}\right)} \cdot \left[1 - exp\left(\frac{V}{b \cdot Vx} - \frac{1}{b}\right)\right] \tag{2.10}$$

$$\begin{aligned} Vx &= s \cdot \frac{E_i}{E_{iN}} \cdot TCV \cdot (T - T_N) + s \cdot V_{max} \\ &\quad - s \cdot (V_{max} - V_{min}) \cdot exp\left(\frac{E_i}{E_{iN}} \cdot ln\left(\frac{V_{max} - V_{oc}}{V_{max} - V_{min}}\right)\right) \end{aligned} \tag{2.11}$$

$$Ix = p \cdot \frac{E_i}{E_{iN}} \cdot [I_{sc} + TCi \cdot (T - T_N)] \tag{2.12}$$

The power produced by a PVM is described in (2.13) and is calculated multiplying (2.10) by the voltage, V.

$$P(V) = \frac{V \cdot Ix}{1 - exp\left(\frac{-1}{b}\right)} \cdot \left[1 - exp\left(\frac{V}{b \cdot Vx} - \frac{1}{b}\right)\right] \tag{2.13}$$

The variables P, I and V are the photovoltaic module output power, current and voltage. I_{sc} is the short-circuit current at $25°C$ and $1000W/m^2$. V_{oc} is the open-circuit voltage at $25°C$ and $1000W/m^2$. V_{max} is the open-circuit voltage at $25°C$ and more than $1,200W/m^2$, (usually, V_{max} is close to $1.03 \cdot V_{oc}$). V_{min} is the open-circuit voltage at $25°C$ and less than $200W/m^2$, (usually, V_{min} is close to $0.85 \cdot V_{oc}$). T is the solar panel temperature in $°C$. E_i is the effective solar irradiation in W/m^2. A PVM is tested under Standard Test Conditions (STC) when the nominal temperature, T_N, is $25°C$ and the nominal effective solar irradiation, E_{iN}, is $1,000W/m^2$. TCi is the temperature coefficient of I_{sc} in $A/°C$. TCV is the temperature coefficient of V_{oc} in

$V/°C$. Sometimes the manufacturer provides TCV in terms of $(mV/°C)$ just divide TCV by 1000 to convert in terms of $(V/°C)$. b is the characteristic constant for the PVM based on the I-V Curve. The variable s is the number of PVM's with the same electrical characteristics connected in series and p is the number of PVM's with the same electrical characteristics connected in parallel as a note for a single PVM, s and p are 1. Ix is the short circuit current at any given E_i and T, and it can be calculated from (2.12) when the voltage, V is zero. Vx is the open circuit voltage at any given E_i and T, also Vx is the voltage of operation for the PVM when the current, I is zero (2.11). The range of existence of V will be from 0 to Vx and the range of existence of $I(V)$ will be from 0 to Ix.

The maximum power, P_{max}, produced by a PVM when the PVM is operating at the optimal voltage, V_{op}, is given by (2.14). Chapter 3 and Chapter 4 will be shown the uniqueness and existence of the V_{op} and how to approximate V_{op} and P_{max} using several nontraditional methods.

$$P_{max} = P(V_{op}) = V_{op} \cdot I(V_{op}) = \frac{V_{op} \cdot Ix}{1 - exp\left(\frac{-1}{b}\right)} \cdot \left[1 - exp\left(\frac{V_{op}}{b \cdot Vx} - \frac{1}{b}\right)\right] \qquad (2.14)$$

Finally, the PVM internal resistance, Ri, or conductance, Gi, can be calculated from the proposed PVM model as given in (2.15). The optimal internal resistance, Rop, is given by (2.16). Typically, the batteries have an internal resistance between 0.2Ω to 0.7Ω [81] and a short circuit could be very dangerous for the battery. Instead, the PVM internal resistance is much larger and the value depends on the voltage and power drawn from the PVM. Additionally, a PVM is a current limited system hence can be short-circuited without damage at difference of the batteries. Also, if a PVM connected to a resistive load, R, is operating at V_{op} then Ri is equal to the optimal resistance Rop, hence if Rop is equal to R then P_{max} is transferred to the load, but if Rop and R are different then the transferred power will be less than P_{max}. The value

Figure 2
under S

of *Rop* v

The

2.1 show

represent

the prod

panel is

power is

and the r

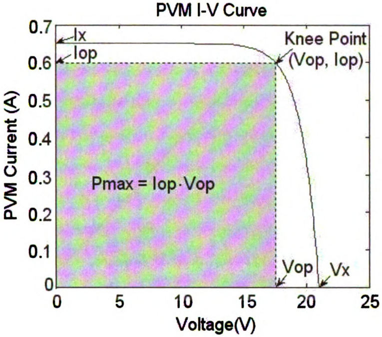

Figure 2.1. I-V Curve for a single Photovoltaic Module (note: Ix is I_{sc} and Vx is V_{oc} under STC).

of *Rop* will be very useful for PVM systems using load matching applications.

$$Ri = \frac{1}{Gi} = \frac{V}{I(V)} = \frac{V - V \cdot exp\left(\frac{-1}{b}\right)}{Ix - Ix \cdot exp\left(\frac{V}{b \cdot Vx} - \frac{1}{b}\right)} \tag{2.15}$$

$$Rop = \frac{1}{Gop} = \frac{V_{op}}{I(V_{op})} = \frac{V_{op}^2}{P_{max}} = \frac{V_{op} - V_{op} \cdot exp\left(\frac{-1}{b}\right)}{Ix - Ix \cdot exp\left(\frac{V_{op}}{b \cdot Vx} - \frac{1}{b}\right)} \tag{2.16}$$

The proposed PVM model can show the effects of T and E_i over a PVM. Figure 2.1 shows the I-V characteristics of an illuminated solar panel. The shaded rectangle represents the maximum power obtained by the solar panel. The knee point is when the product of the current and the voltage is the maximum power [45]. The solar panel is working in the optimal current (I_{op}) and voltage (V_{op}), hence the maximum power is delivered to the load by the solar panel. Figure 2.2 shows the P-V Curve and the relationship between P_{max} and the knee point.

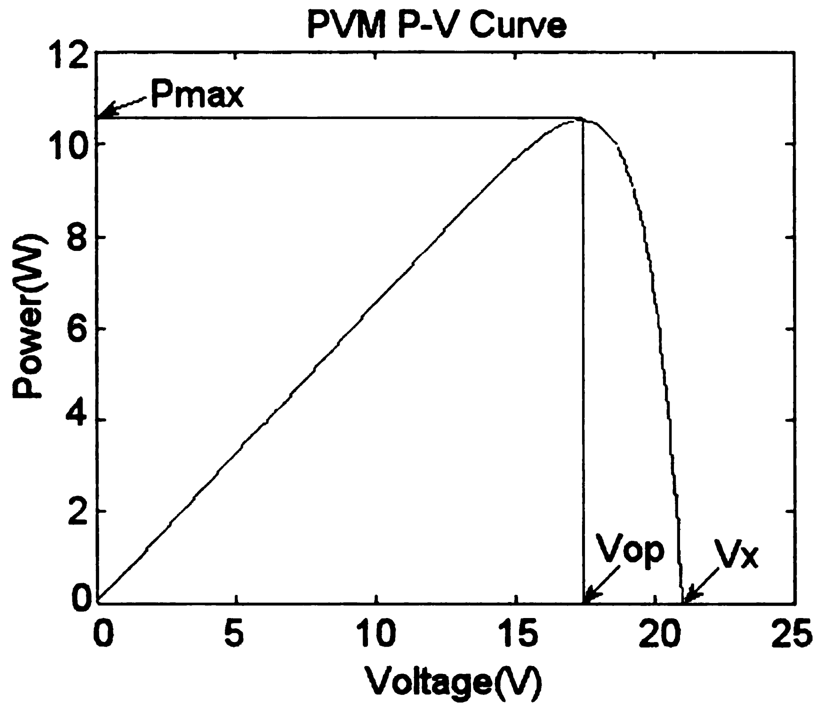

Figure 2.2. P-V Curve for a single Photovoltaic Module (note: Ix is I_{sc} and Vx is V_{oc} under STC).

Figure 2.3 shows the relationship between the internal impedance and voltage of operation for the PVM. The optimal internal impedance, R_{op}, has a direct relationship with the maximum power and is unique. If a resistive load with the same value as the optimal internal impedance is connected to a photovoltaic module then the maximum power is transferred. It is important to note that figure 2.3 can be used to maximize the efficiency of a solar power system when load matching is required. Figure 2.3 shows that the resistance is quasi-linear up to the point that the optimal resistance to produce the maximum power is obtained.

Figu
V_{oc} u

2.4

The P

capaci

model

capacit

Ano

where τ

propose

known r

PVM an

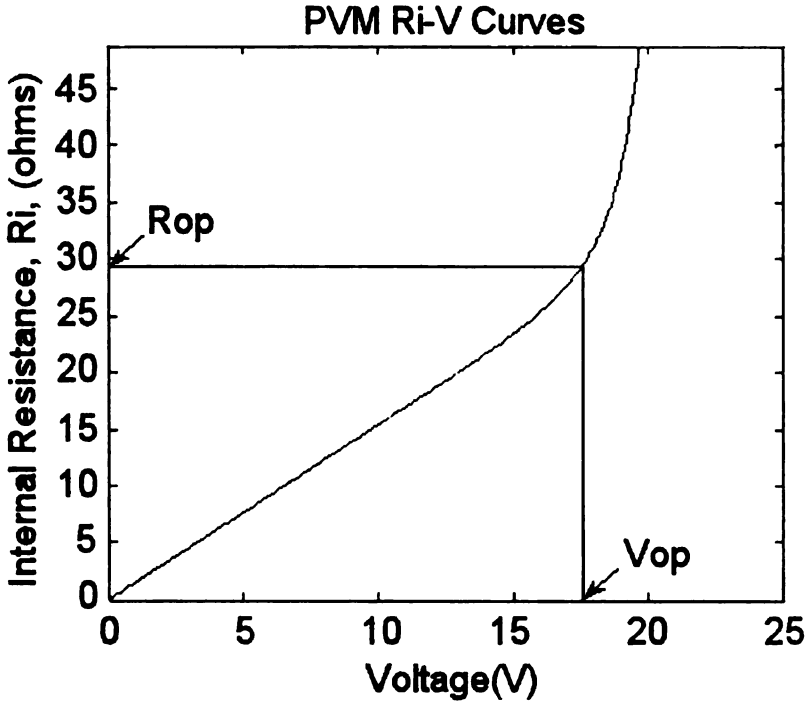

Figure 2.3. R-V Curve for a single Photovoltaic Module (note: Ix is I_{sc} and Vx is V_{oc} under STC).

2.4 Dynamic PVM model and the internal PVM capacitance

The PVM dynamic model is based on the PVM static model and considers the internal capacitance for the PVM, Cx. Figure 2.4 shows the schematic for the dynamic PVM model and it is modeled by the differential equation given in (2.17). The internal capacitance is measured using a capacitance meter.

Another way to measure the internal capacitance is using the time constant τ where τ is the product of Cx and a known resistive load, R. Figure 2.5 shows the proposed method to approximate the internal capacitance connecting the PVM to a known resistive load, R. Figure 2.6 shows the measurements of the voltage in the PVM and the resistive load using an oscilloscope then the required time to obtain

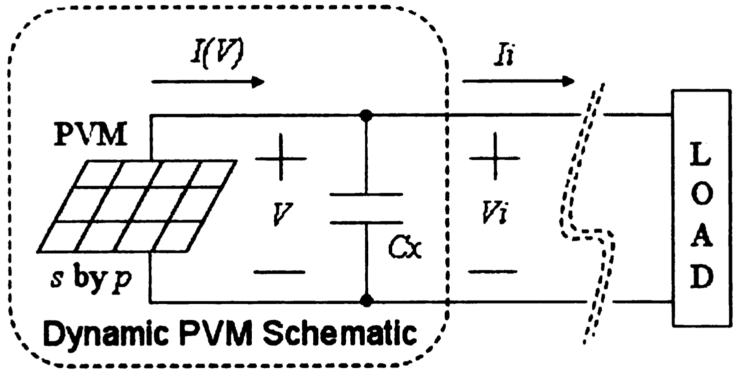

Figure 2.4. Schematic for a dynamic PVM model including the internal capacitance, Cx.

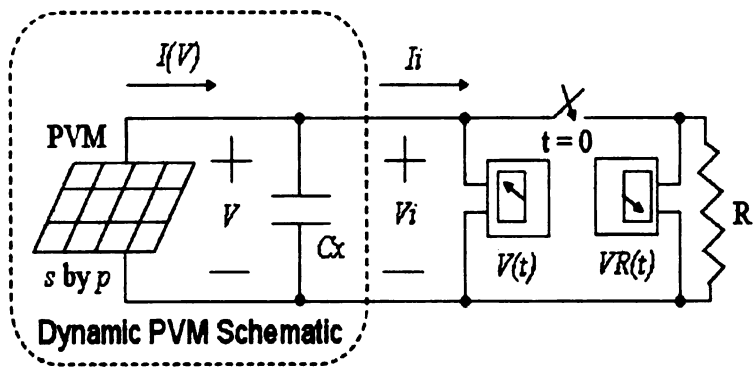

Figure 2.5. Proposed method to approximate the internal resistance Cx.

around 0.6321 of the final voltage, Vo is calculated. The calculated time will be known as the time constant, τ. Finally to approximate the Cx, just divide τ by R. The typical value for Cx is on the range of $1nF$ to $10nF$ but this value can vary depending the type of PVM.

$$\frac{\partial V}{\partial t} = \frac{I(V) - Ii}{Cx} = \frac{Ix - Ix \cdot exp\left(\frac{V}{b \cdot Vx} - \frac{1}{b}\right)}{Cx - Cx \cdot exp\left(\frac{-1}{b}\right)} - \frac{Ii}{Cx} \tag{2.17}$$

Figu

2.5

Now ar

perform

ship wi

the fill f

for any

algorith

single P

given in

Another

shows th

0.6234 b

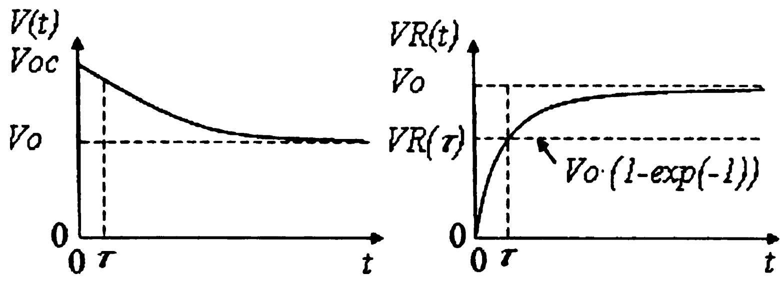

Figure 2.6. Outputs for $V(t)$ and $VR(t)$ after the switch is close at time $t = 0$.

2.5 How to Calculate the Characteristic Constant?

Now arise the questions, how the characteristic constant, b, is related to the PVM performance and how to calculate it? The PVM performance has an inverse relationship with the characteristic constant, b, where the smaller the b the greater will be the fill factor and the produced power for the PVM [45]. The characteristic constant for any PVM is positive definite with a typical range for b from 0.01 to 0.18. An algorithm based on the Fixed Point Theorem, and the electrical characteristics for a single PVM (i.e. p and s are 1) under STC, is used to calculate b. The algorithm is given in (2.18). The variable ε is the maximum allowed error to stop the iteration. Another way to approximate b without using iterations is given in (2.19). Figure 2.7 shows that V_b is the voltage of operation that will produce the current I_b which it is 0.6234 by I_{sc}.

$$\begin{aligned} while|b_{n+1} - b_n| &> \varepsilon \\ b_{n+1} &= \frac{V_{op} - V_{oc}}{V_{oc} \cdot ln\left[1 - \frac{I_{op}}{I_{sc}} \cdot \left(1 - exp\left(\frac{-1}{b_n}\right)\right)\right]} \end{aligned} \tag{2.18}$$

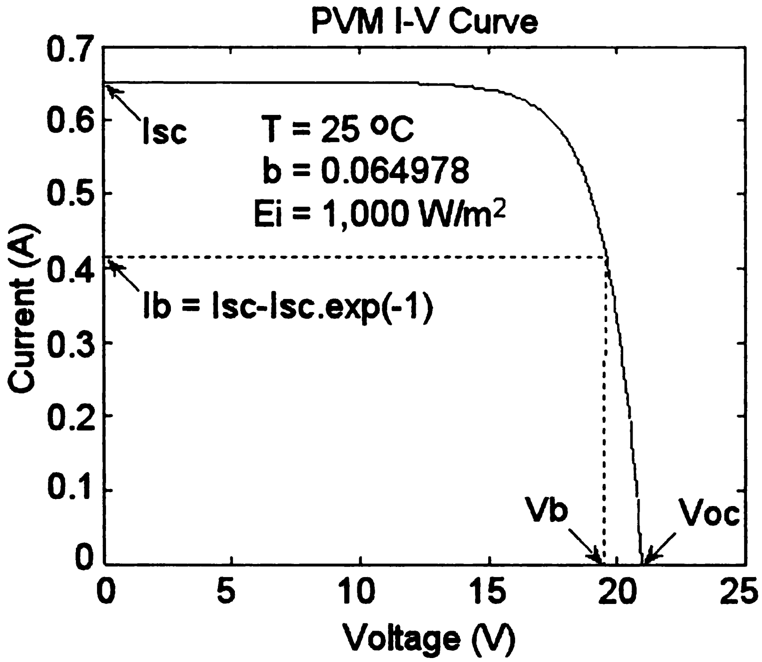

Figure 2.7. Non-Iterative method using the PVM I-V Curve to calculate b.

$$\begin{aligned} I_{sc} \cdot (1 - exp\,(-1)) &= \frac{I_{sc}}{1 - exp\left(\frac{-1}{b}\right)} \cdot \left[1 - exp\left(\frac{V_b}{b \cdot Vx} - \frac{1}{b}\right)\right] \\ &\approx I_{sc} \cdot \left[1 - exp\left(\frac{V_b}{b \cdot Vx} - \frac{1}{b}\right)\right] \rightarrow b \approx 1 - \frac{V_b}{V_{oc}} \qquad (2.19) \end{aligned}$$

2.6 Relationship Between the PVM Performance and the Fill Factor

The fill factor, (2.20) is a figure of merit for solar panel design [22]. It is defined as the rectangular area covered by P_{max} (i.e. I_{op} multiplied by V_{op}) divided by the total rectangular area produced by I_{sc} and V_{oc}. Using figure 2.2, the inequality (2.21) can be found for a single PVM where the maximum power will be less than the area of the V-I Curve and more than a quarter of the product of I_{sc} and V_{oc} [62].

$$fillfactor = \frac{P_{max}}{I_{sc} \cdot V_{oc}} = \frac{I_{op} \cdot V_{op}}{I_{sc} \cdot V_{oc}} \tag{2.20}$$

$$I_{sc} \cdot V_{oc} > \int_{0}^{V_{oc}} I(V)dV > P_{max} > \frac{1}{4} \cdot I_{sc} \cdot V_{oc} \tag{2.21}$$

Before to prove the inequality (2.21), consider the limits for $I(V)$ when b tends to 0 and ∞ as presented on (2.22) and (2.23). Now, it is trivial to prove the upper part of the inequality (2.21) and it can be done by inspection.

$$\lim_{b \longrightarrow 0} \left[I_{sc} - I_{sc} \cdot \frac{1 - \exp\left(\frac{V}{b \cdot V_{oc}}\right)}{1 - \exp\left(\frac{1}{b}\right)} \right] = I_{sc} \tag{2.22}$$

$$\lim_{b \longrightarrow \infty} \left[I_{sc} - I_{sc} \cdot \frac{1 - \exp\left(\frac{V}{b \cdot V_{oc}}\right)}{1 - \exp\left(\frac{1}{b}\right)} \right] = I_{sc} - I_{sc} \cdot \frac{V}{V_{oc}} \tag{2.23}$$

The first part of the upper inequality is the maximum power for an ideal PVM when b is equal to 0. This is the ideal maximum power for a PVM with fill factor equal to one and it can be seen as the maximum rectangular area that can be obtained between I_{sc} and V_{oc}. The second part in the upper inequality is the integral of (2.10) evaluated from 0 to V_{oc} under STC hence the total area under the curve of $I(V)$ will be always more than any rectangular area inside of the curve $I(V)$.

$$\int_{0}^{V_{oc}} I(V)dV = \int_{0}^{V_{oc}} I_{sc} \cdot \frac{1 - exp\left(\frac{V}{b \cdot V_{oc}} - \frac{1}{b}\right)}{1 - exp\left(\frac{-1}{b}\right)} dV = I_{sc} \cdot V_{oc} \cdot \frac{1 - b + b \cdot \exp\left(\frac{-1}{b}\right)}{1 - \exp\left(\frac{-1}{b}\right)} \tag{2.24}$$

To prove the lower part of (2.21) consider $I_L(V)$. $I_L(V)$ is the limit of (2.10) when b tends to ∞ under STC as prove on (2.23). $I_L(V)$ is a straight line equation where any value in $I_L(V)$, without include the boundaries i.e. $V \in (0 \quad V_{oc})$ under STC, will be always less than any value produced by $I(V)$. The inequality for the last statement is given in (2.25).

$$I(V) = I_{sc} - I_{sc} \cdot \frac{1 - \exp\left(\frac{V}{b \cdot V_{oc}}\right)}{1 - \exp\left(\frac{1}{b}\right)} > I_{sc} - I_{sc} \cdot \frac{V}{V_{oc}} = I_L(V) \tag{2.25}$$

The maximum power produced for an ideal PVM modeled by $I_L(V)$, i.e. b equal to ∞, is calculated using differential calculus and is shown in (2.26). Now, it is clear that the maximum power produced by $I_L(V)$ will be always less than any maximum power produced by $I(V)$ more than that the inequality (2.21) is satisfied.

$$\begin{aligned} P(V) &= V \cdot I_L(V) = I_{sc} \cdot V - I_{sc} \cdot \frac{V^2}{V_{oc}} \\ &\Rightarrow \frac{\partial P}{\partial V} = I_{sc} - 2 \cdot I_{sc} \cdot \frac{V}{V_{oc}} = 0 \\ &\Rightarrow V_{op} = \frac{V_{oc}}{2} \Rightarrow P(V_{op}) = \frac{I_{sc} \cdot V_{oc}}{4} \end{aligned} \tag{2.26}$$

Additionally after prove (2.21), the inequality for the fill factor is given in (2.27). Finally, it is proved that the fill factor is more than one quarter and less than the total area inside of the I-V Curve divided by the short circuit current, I_{sc}, and open circuit voltage, V_{oc}.

$$1 > \int_0^{V_{oc}} \frac{I(V)dV}{I_{sc} \cdot V_{oc}} > fillfactor > \frac{1}{4} \tag{2.27}$$

2.7 PVM Model Verification

The proposed model was tested using different manufacturer data sheets. Tables 2.1 and 2.2 shows the electrical characteristics for the SX-10, SX-5 and other PVM products. Figures 2.8-2.13 show different simulations for the SX-10 module using the information provided by the manufacturer SOLAREX. Figures 2.8-2.10 show simulation results for the photovoltaic module under different temperatures of operation (i.e. $0°C$, $25°C$, $50°C$ and $75°C$) with the irradiation level at $1000W/m^2$. Figures

2.11-2.13 show the simulation results for photovoltaic module SX-10 with the temperature at $25°C$ and the effective irradiance level changing (i.e. $200W/m^2$, $400W/m^2$, $600W/m^2$, $800W/m^2$, and $1000W/m^2$). The effects of change in the irradiance level are more drastically visible than the effects of temperature over the solar panel. The changes in temperature can be used to determine now the photovoltaic modules will operate in tropical areas versus non-tropical areas.

Typically, a PVM datasheet includes the I-V curves under changes in the temperature. Figure 2.8 shows the simulation for the I-V Curves under different temperatures. The simulated I-V curves are similar to the I-V curves provided by the manufacturer SOLAREX SX-10 and SX-5. At the same time other plots, not provided by the manufacturer, can be calculated using the proposed model such as P-V curves, R-V curves and I-P curves. Unfortunately, the manufacturer data sheet does not provide these figures despite the fact that this information is very important for solar power systems where the irradiance level changes quickly. An example is when the clouds are hiding the sun for a period of time, and then the irradiance level increases and the temperature remains constant. Figure 2.9 shows how the temperature can affect the maximum power supplied by the photovoltaic module under a constant irradiance level. Figures 2.10 and 2.13 show how the internal resistance of the photovoltaic module SX-10 changes when the output voltage changes.

As a final test for verification of the proposed PVM model, the experimental measures for the voltage and current for the solar panels BP SOLAREX SA-05 [82] were done at Lansing, Michigan (May 10, 2005) with T = 25C and the sun irradiating at the maximum intensity light (1:30pm). The test shows how accurate is the proposed PVM model comparing between the measured and estimated data. Figures 2.14, 2.15 and 2.16 show the direct relationship between the experimental measures and estimation for any of the cases related to the I-V, P-V and R-V curves of the PVM SA-05. Finally, all of these curves, equations, and relationships give valuable

Table 2.1. Photovoltaic Module Specifications

Datasheet	I_{sc}	V_{oc}	I_{op}	V_{op}	b
Siemens SP75	$4.80A$	$21.7V$	$4.40A$	$17.0V$	0.08717
Shell SQ80	$4.85A$	$21.8V$	$4.58A$	$17.5V$	0.06829
SLK60M6	$7.52A$	$37.2V$	$6.86A$	$30.6V$	0.07292
Solarex SA-5	$0.38A$	$25.0V$	$0.34A$	$15.0V$	0.13900
Solarex SX-5	$0.30A$	$20.5V$	$0.27A$	$16.5V$	0.08474
Solarex SX-10	$0.65A$	$21.0V$	$0.59A$	$16.8V$	0.08394

Table 2.2. Photovoltaic Module Specifications (cont.)

Datasheet	TCi	TCV	V_{min}	V_{max}
Siemens SP75	$2.06mA/°C$	$-77mV/°C$	$18.45V$	$22.243V$
Shell SQ80	$1.4mA/°C$	$-81mV/°C$	$20.25V$	$21.810V$
SLK60M6	$2.2mA/°C$	$-127mV/°C$	$32.55V$	$37.312V$
Solarex SA-5	$0.3mA/°C$	$-60mV/°C$	$21.00V$	$25.500V$
Solarex SX-5	$0.2mA/°C$	$-80mV/°C$	$17.43V$	$21.115V$
Solarex SX-10	$0.2mA/°C$	$-80mV/°C$	$17.85V$	$21.630V$

information to be considered for photovoltaic power systems and distributed power generation design.

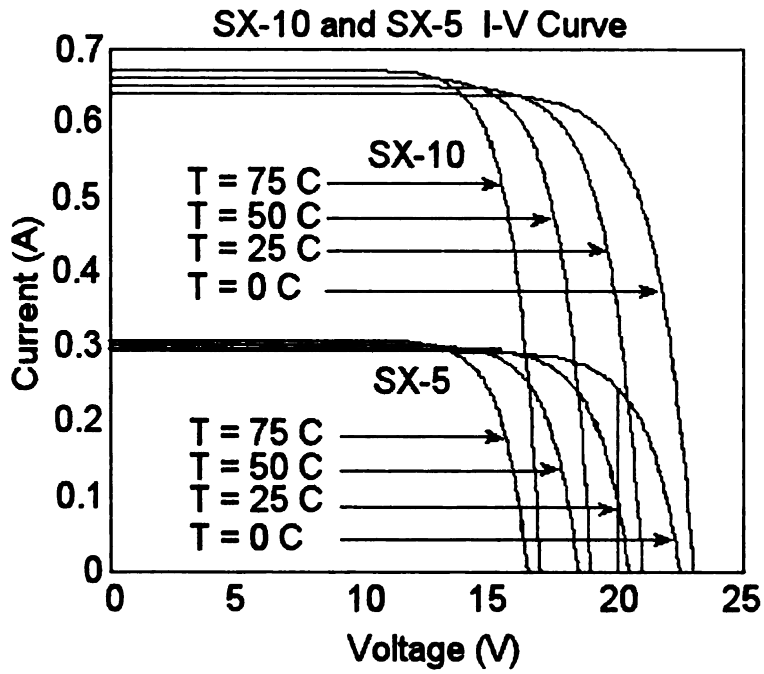

Figure 2.8. I-V Curves for the SX-10 and SX-5 under different temperatures.

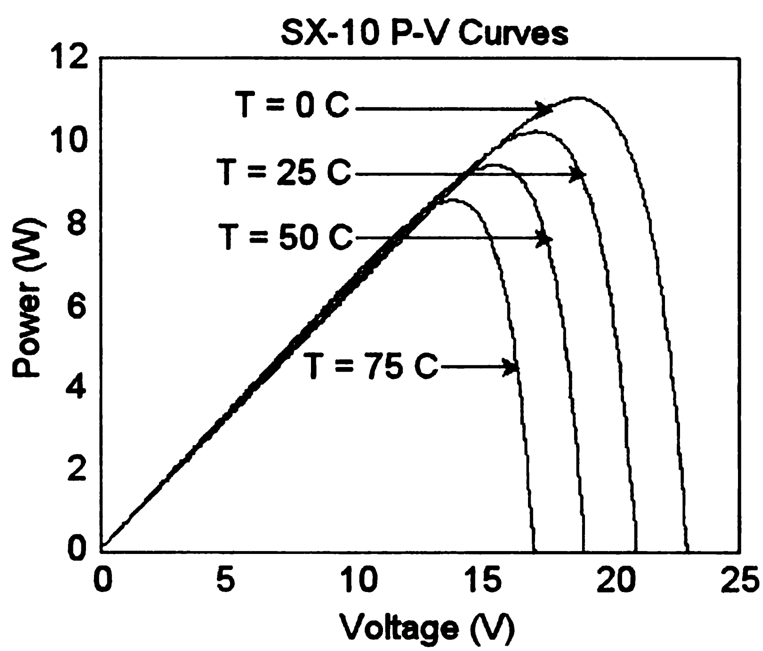

Figure 2.9. P-V Curves for the SX-10 module under different temperatures.

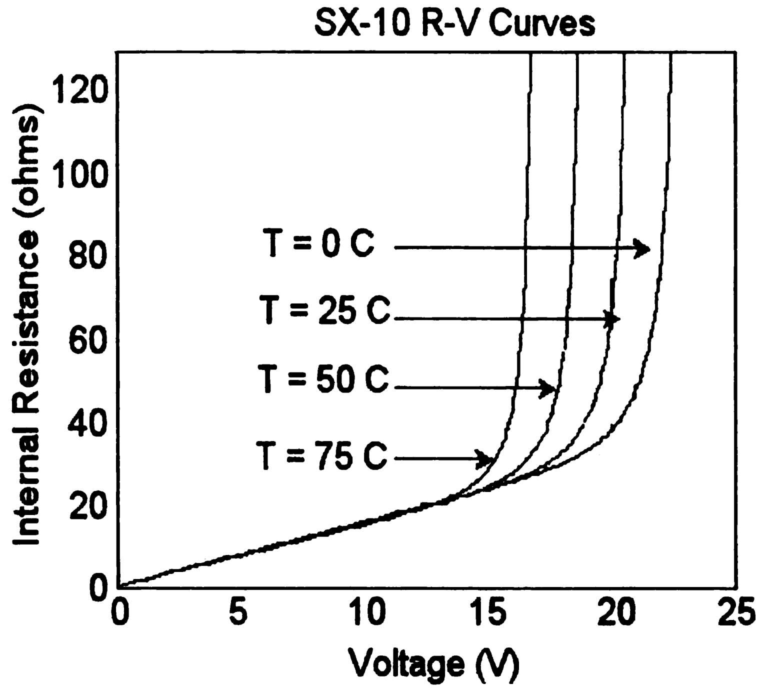

Figure 2.10. R-V Curves for the SX-10 module under different temperatures.

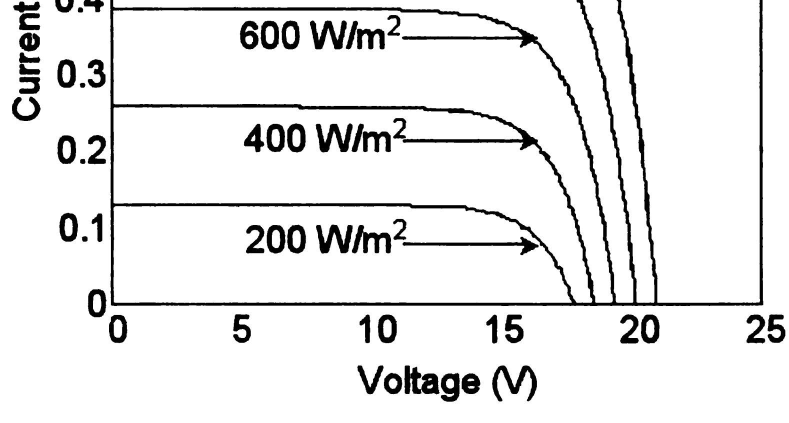

Figure 2.11. I-V Curves for the SX-10 and SX-5 modules under different effective irradiance levels.

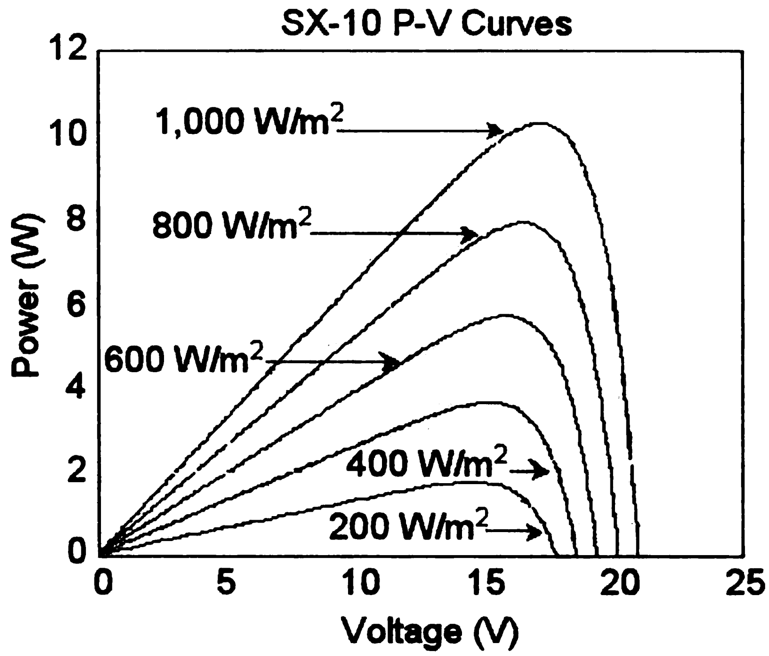

Figure 2.12. P-V Curves for the SX-10 module under different effective irradiance levels.

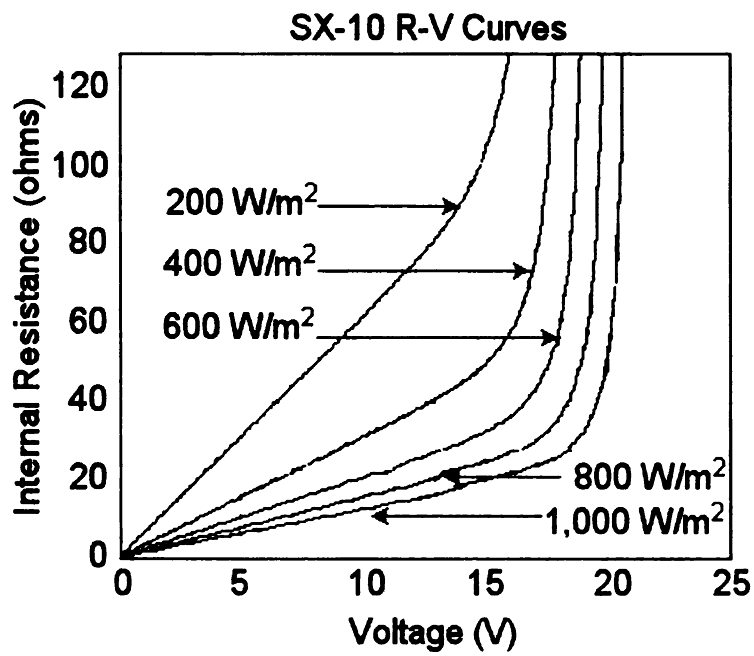

Figure 2.13. R-V Curves for the SX-10 module under different effective irradiance levels.

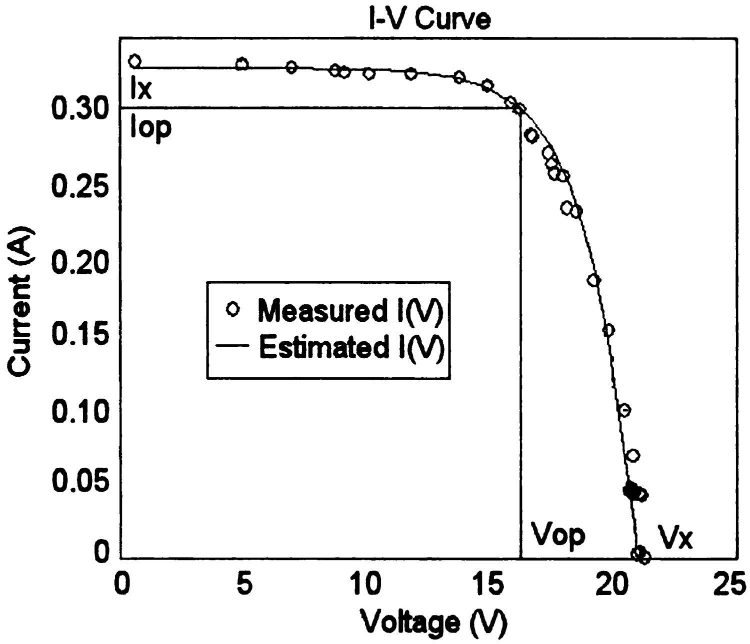

Figure 2.14. Experimental measures and estimation for the SA-05 I-V Curve.

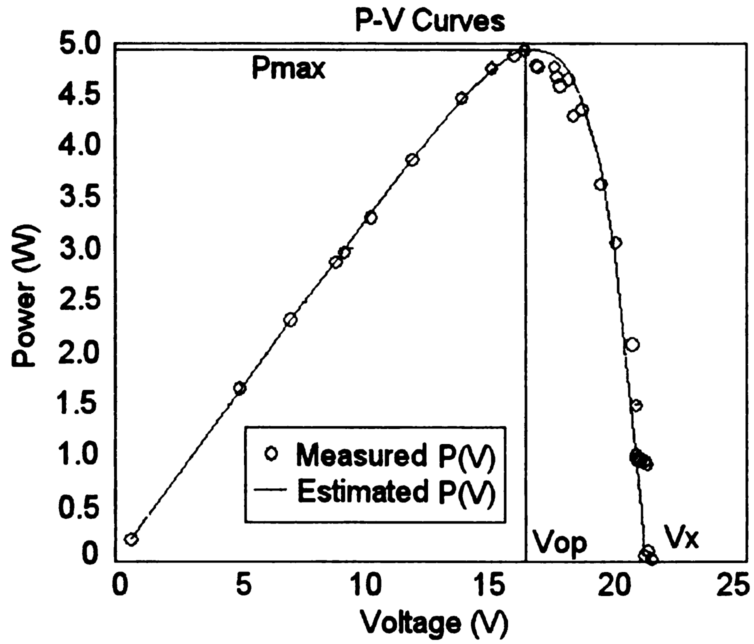

Figure 2.15. Experimental measures and estimation for the SA-05 P-V Curve.

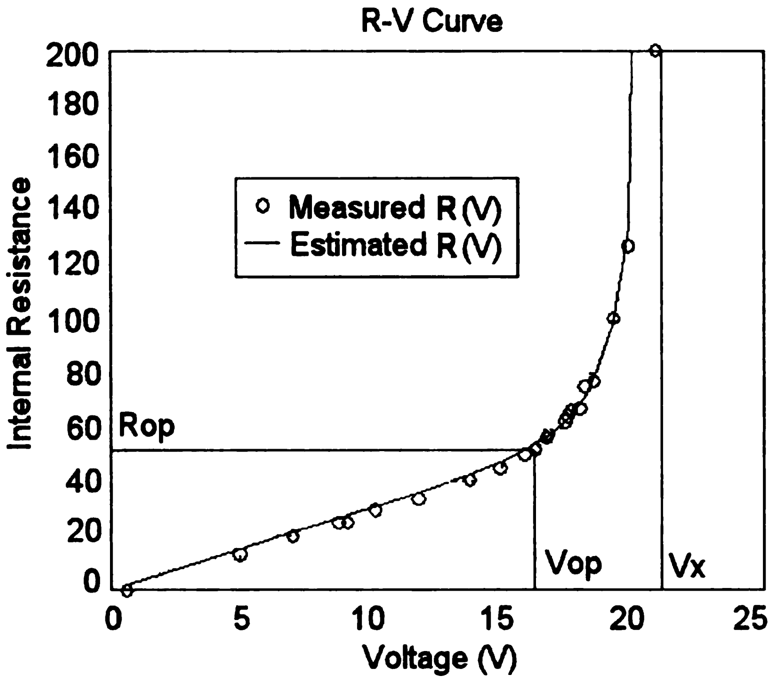

Figure 2.16. Experimental measures and estimation for the SA-05 R-V Curve.

v
T
T
tr
ot
sc
ca
in
(P
sin
fue
A/I
con
func

CHAPTER 3

Linear Reoriented Coordinates Method

This chapter presents a non-traditional method and algorithm to calculate the inverse solution for a one-dimensional function without the diffeomorphism property. The proposed method is called the Linear Reoriented Coordinates Method (LRCM). The LRCM is a very powerful and useful too to calculate the symbolic solutions for transcendental functions where the inverse function is not possible to calculate using other traditional methods and only analytic solutions can be calculated but symbolic solutions are not possible to obtain. The description and conditions for the application of the method are presented in the chapter. The main application presented in the chapter will be to determine the maximum power for a photovoltaic module (PVM) using the proposed PVM given in the Chapter 2. Additional examples and simulations for the LRCM related to maximum profit and revenue for a company, fuel cells and to optimize the maximum rectangular area for a floorplan for an 8-bit A/D converter given space constraints, are presented. Finally, the LRCM should be consider as a method that can provide at least an approximate answer to a family of functions that cannot be solved using differential calculus.

3.1 Introduction

For the last several centuries, the solution for transcendental functions has been a challenge for physics, engineers and mathematicians. A transcendental function is defined as function which does not satisfy a polynomial equation, whose coefficients are polynomials themselves, (i.e. $F(x) = \alpha_n x^n + ... + \alpha_1 x + \alpha_0, \forall \alpha_i \in \Re$). Some examples for transcendental functions are exponential functions, logarithmic functions, and trigonometric functions [83]. The most useful transcendental functions for science are exponential functions. They have an incredible number of applications, but it is not always possible to solve them symbolically. Examples for modeling with transcendental functions are in RLC circuits [84], fuel cells [85], photovoltaic modules [45], maximum area for space optimization given shape constraints [86], [87], [88], neural networks [89], robotics [90], etc.

Unfortunately, the only way to solve them it is numerically, sometimes with long and tedious iterations and the use of computers with complex algorithms [90], [91], [92], [93]. Now, for any kind of function, the traditional and effective way to calculate the maximum or minimum values is using differential calculus. But in many cases in physical sciences, engineering or math when it is required modeling using transcendental functions are very complex to work with them.

If a function $y = f(x)$ has the diffeomorphism property then it is possible to obtain the maximum value y_{max}. It is determined when the first derivative of $f(x)$ is calculated with respect to x, then the function $f'(x) = 0$ is solved with respect to x to find the optimal x and y_{max}. Diffeomorphism is defined as a map between manifolds which is differentiable and has differentiable inverse. In other words, for a one-dimensional system, it is a change of coordinates that does not change information given by the original system [94]. A function $f(x)$ has the diffeomorphism property if it is smooth, it has an inverse and the inverse is smooth. If a function has the diffeomorphism property, then it is possible to find the inverse for the given function.

The inverse function is defined as follows.

If $f : X \to Y$ is $1-1$ and onto then the correspondence that goes backwards from Y to X is also a function and is called f inverse, denoted f^{-1}. This map is easily described by $f^{-1} : Y \to X$ and $f^{-1}(y) = x$ if and only if $y = f(x)$. This relationship is easy to remember for a real function since switching coordinates of a point in the plane puts us at the reflection of the original point about the line $y = x$. Thus the graph of f^{-1} must be the reflection of the graph of f about the line $y = x$. This is a great help if the graph of f is already known. It's the $1-1$ condition that is really critical for constructing an inverse function. If f is $1-1$ but not onto we can simply replace the codomain with the range $f(X)$ so that $f : X \to f(X)$ in then $1-1$ and onto so we can talk about an inverse $f^{-1} : f(X) \to X$. The domain of the function is equal to the range of the inverse and the range of the function is equal to the domain of the inverse. Finally, a unique inverse only will exist in $1-1$ functions or the unique inverse will exists only over the restricted domain [83].

Unfortunately, it is not always possible to find the symbolic inverse for a given function, $x = f^{-1}(y)$, [95]. But then the question arises, is it at least possible to approximate the inverse of one-dimensional function and how good it is this approximation? To answer these questions, this paper proposes a non-traditional method to approximate the symbolic inverse for one-dimension transcendental functions. Also, the paper provides the different conditions where the method can be applied and which type of functions can be satisfied.

3.2 Rolle's and Lagrange's Theorems

The main idea for the LRCM is based in the Rolle's and Lagrange's Theorems (Mean Value Theorem or Fundamental Theorem Calculus) as shown in figure 3.1; and it is valid in any domain $[a \quad b]$ but first we need to understand if it is possible to approximate the inverse of a one-dimensional function. The Lagrange Inversion Theorem (LIT) [83] determines the Taylor series expansion of the inverse function of analytic function. Consider the function, $y = f(x)$, where if f is analytic at a point x_0 and $f'(x_0) \neq 0$. Then it is possible to invert or solve the equation for y, $x = f^{-1}(y) = h(y)$ where h is analytic at the point $y_0 = f(x_0)$. The reversion of series is given by the series expansion of $h(y)$ in (3.1).

$$h(y) = x_0 + \sum_{k=1}^{\infty} \frac{(y - y_0)^k}{k!} \cdot \frac{\partial^{k-1}}{\partial x^{k-1}} \left(\frac{(x - x_0)^k}{(f(x) - y_0)^k} \right) \Bigg|_{x=x_0} \tag{3.1}$$

This equation will give the inverse function $h(y)$, but unfortunately it is required to do long calculations. Depending the type of functions (or the use of computers), the result most of the time will be an infinite series polynomial (Taylor series). In the case of transcendental functions, it will be required to take into consideration the restrictions on the domain making it difficult to calculate the inverse. But how can these problems be solved and how can an approximate inverse function be found without the use of Taylor series, long iterations and be a good approximation? The Linear Reoriented Coordinates Method (LRCM) can be a solution for these problems for at least a family of functions!

Theorem 3.1 (Rolle's Theorem, Fig. 3.2). If $f(x)$ is differentiable on $(a,\ \ b)$, continuous on $[a,\ \ b]$ and $f(a) = f(b)$, then $\exists$ c-value in $(a,\ \ b)$ such that $f'(c) = 0$.

Corollary 3.1 (Modified Rolle's Th.). If for $f(x)$ $\exists!$ maximum value f_{max} then $\exists!$ $x(f'(x_{op}) = 0)$ in $\Re \times [0\ \ x_{max}]$.

Theorem 3.2 (Lagrange's Theorem, Fig. 3.3). If g is continuous and differentiable on $[a,\ \ b]$, then $\exists$ c-value in $[a,\ \ b]$ such that, $g'(c) = (g(b) - g(a))/(b - a)$.

Corollary 3.2. If $f(x) = x \cdot g(x)$ and $f(x_{op}) = x_{op} \cdot g(x_{op}) = f_{max}$ then $g'(x_{op}) = -g(x_{op})/x_{op}$.

Theorem 3.3 (Cauchy Mean Value Theorem). If g and f are continuous and

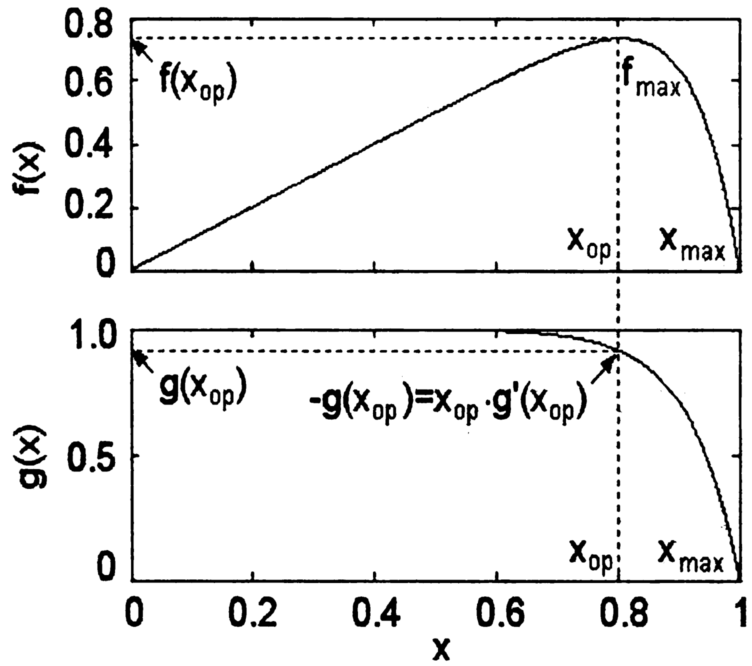

Figure 3.1. Linear Reoriented Coordinates Method (LRCM).

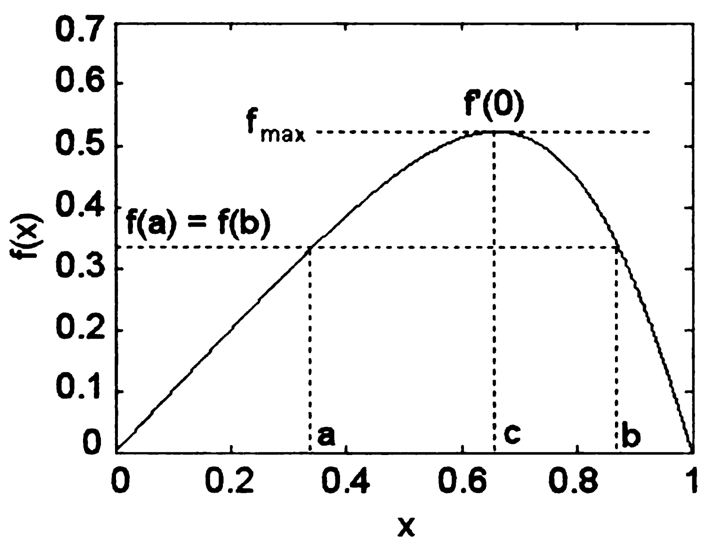

Figure 3.2. Rolle's Theorem.

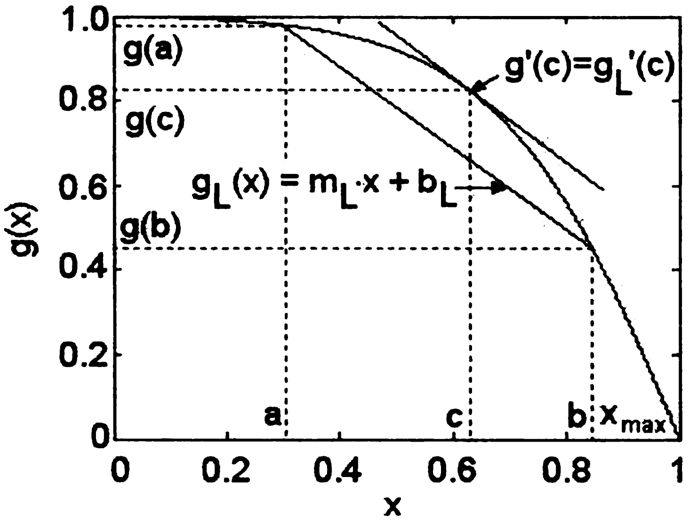

Figure 3.3. Lagrange's Theorem.

differentiable on $[a,\ b]$, then c-value in $[a,\ b]$ such that, $f'(c)/g'(c) = (f(b) - f(a))/(g(b) - g(a)))$. The proofs for each theorem and corollary are well known and are skipped in the paper.

3.3 Linear Reoriented Coordinates Method

3.3.1 Description for the LRCM

The LRCM is a method to find the approximate maximum value for a function $f(x)$, where $f'(x) = r(x) = 0$, which cannot be solved using traditional methods of differential calculus, [62]. The LRCM can also be seen as a method to find the approximate symbolic solution x for the equation $r(x) = 0$ without symbolic solutions. The function $f(x)$ is defined as $f(x) = x \cdot g(x)$ and the maximum value of $f(x)$ is defined as f_{max} where $f_{max} = x_{op} \cdot g(x_{op})$ and x_{op} is the optimal value for f_{max}. The main idea for the LRCM is to find the optimal points to calculate f_{max}. These points are $(x_{op},\ g(x_{op}))$ and are calculated using $g'(x)$ and the linear slope ml of $g(x)$

evaluated at the point x_{op}.

3.3.2 Conditions for the LRCM

The necessary conditions for the application of the LRCM to calculate the maximum value f_{max} and the approximate optimal x, x_{ap} for a function $f(x)$, are:

1. $f(x) = x \cdot g(x)$ in $\Re \times [0 \ \ x_{max}]$
2. $f \in C^1(\Re \times [0 \ \ x_{max}])$
3. $g \in C^1(\Re \times [0 \ \ x_{max}])$
4. $g'(x) < 0$ in $\Re \times [0 \ \ x_{max}]$
5. $g''(x) \leq 0$ in $\Re \times [0 \ \ x_{max}]$
6. *Corollary 1* is satisfied in $\{x \in \Re \times [0 \ \ x_{max}]\}$
7. $g'(x_{op}) = -g(x_{op})/x_{op}$
8. $f_{max} = x_{op} \cdot g(x_{op})$

3.3.3 Approximation for x_{op} and f_{max}

Now, consider a function, $f(x)$, that satisfies the conditions for the LRCM hence it is desire to approximate x_{op}. The first step is to use the straight line given by (3.2) where $gl(x)$ is always positive in $\{x \in \Re \mid [0 \ \ x_{max}]\}$. The derivative of $gl(x)$ with respect to x is always negative and unique in $\{x \in \Re \mid [0 \ \ x_{max}]\}$. The derivatives of $gl(x)$ and $g(x)$ can be intersected in the point x_{ap} where it is the optimal point x_{op} plus an error, ϵ, as given in (3.3). For an small ϵ, the optimal value for x_{op} is approximated by (3.4), if ϵ is 0 then (3.4) is the solution for x_{op}.

$$gl(x) = bl + ml \cdot x = g(0) - \frac{g(0)}{x_{max}} \cdot x \tag{3.2}$$

$$gl'(x) = ml = -\frac{g(0)}{x_{max}} = gl'(x_{ap}) = gl'(x_{op} + \epsilon) \tag{3.3}$$

$$x_{op} \approx x_{op} + \epsilon = g'^{-1}\left(\frac{-g(0)}{x_{max}}\right) \tag{3.4}$$

The approximation of x_{op} is substituted in $f(x)$ to approximate f_{max} as given in (3.5). Finally, the error for the approximation of f_{max} is given by (3.6).

$$f(x_{ap}) = x_{ap} \cdot g(x_{ap}) = f_{ap} \approx f_{max} \tag{3.5}$$

$$Error = 100 \cdot \frac{f(x_{op}) - f(x_{ap})}{f(x_{op})} \tag{3.6}$$

3.3.4 Validation for the LRCM

Consider $f(x) = x \cdot g(x)$, and the derivative of $f(x)$ with respect to x, $f'(x) = g(x) + x \cdot g'(x)$ where $g(x)$ has the diffeomorphism property. Now using the Lagrange's Theorem and the Cauchy's Mean Value Theorem to find the optimal value x_{op} that it will produce the maximum value of $f(x) \implies f_{max} = x_{op} \cdot g(x_{op}) = f(x_{op})$ in the domain $[0 \;\; x_{max}]$ (Rolle's Thm.). Let's apply the Cauchy's Mean Value Theorem to $f(x)$ and $g(x)$ where both functions have the diffeomorphism property to solve for x_{op}.

$$f'(x_{op}) = \frac{f(r) - f(x_{max})}{r - x_{max}} = \frac{f(r)}{r - x_{max}} \tag{3.7}$$

$$g'(x_{op}) = \frac{g(r) - g(x_{max})}{r - x_{max}} = \frac{g(r)}{r - x_{max}} \tag{3.8}$$

$$r = \frac{f(r)}{g(r)} = \frac{f'(x_{op})}{g'(x_{op})} = \frac{g(x_{op})}{g'(x_{op})} + x_{op} \tag{3.9}$$

Using the *Corollary 3.2*, if $r = 0$ then the approximation for x_{op} is given by (3.10) and the approximation error is 0.

$$x_{op} = g'^{-1}\left(\frac{-g(0)}{x_{max}}\right) \tag{3.10}$$

Now, if $f(x)$ does not have the diffeomorphism property then x_{op} can not be solved (i.e. $x_{op} = f'^{-1}(0)$ is not possible to solve). Now, consider the function $g(x)$ to determine x_{op}, instead to use $f(x)$ because $f'(x) = g(x) + x \cdot g'(x)$. There is a linear slope (mL) with the same value as $g'(x_{op})$ to find f_{max}, $mL = g'(x_{op})$ (Lagrange's Thm.). Using Lagrange's Theorem, there is a function $gl(x) = ml \cdot x + bl$, where $gl(0) = g(0)$, $gl(x_{max}) = g(x_{max}) = 0$ and $gl'(x_{ap}) = g'(x_{ap})$, as given in (3.11) and (3.12).

$$mL = g'(x) \approx gl'(x) = \frac{-g(0)}{x_{max}} \tag{3.11}$$

$$x_{ap} \approx x_{op} \Longrightarrow x_{ap} = g'^{-1}\left(\frac{-g(0)}{x_{max}}\right) \tag{3.12}$$

Now, the approximate x_{op} can be calculated using (3.12)! Finally, an approximate f_{max} is calculated using x_{ap}, $f_{max} \approx f(x_{ap}) = x_{ap} \cdot g(x_{ap})$. The error of angle ε for x_{ap} and f_{max} will be calculated using (3.13),

$$\varepsilon = \tan^{-1}\left(g(x_{ap}) + x_{ap} \cdot g'(x_{ap})\right) \tag{3.13}$$

If $\varepsilon = 0$, then f_{max} is found, $g'(x_{op}) = gl(x_{op})$, $x_{ap} = x_{op}$ and the inverse map of the derivative of $f(x)$ is found.

3.4 LRCM as a MPPT Algorithm

Figure 3.4 shows that at any particular intensity of light, there is a unique point for the maximum power; this value is named the maximum power point (MPP). The MPP is calculated exactly by solving for the voltage when (3.14) is equal to zero then this voltage (V_{op}) is substituted in (2.13) to obtain the MPP. Unfortunately, it is not possible to find a symbolic solution hence the only way to solve (3.14) is numerically and this solution requires long and tedious iterations, making the solution not practical.

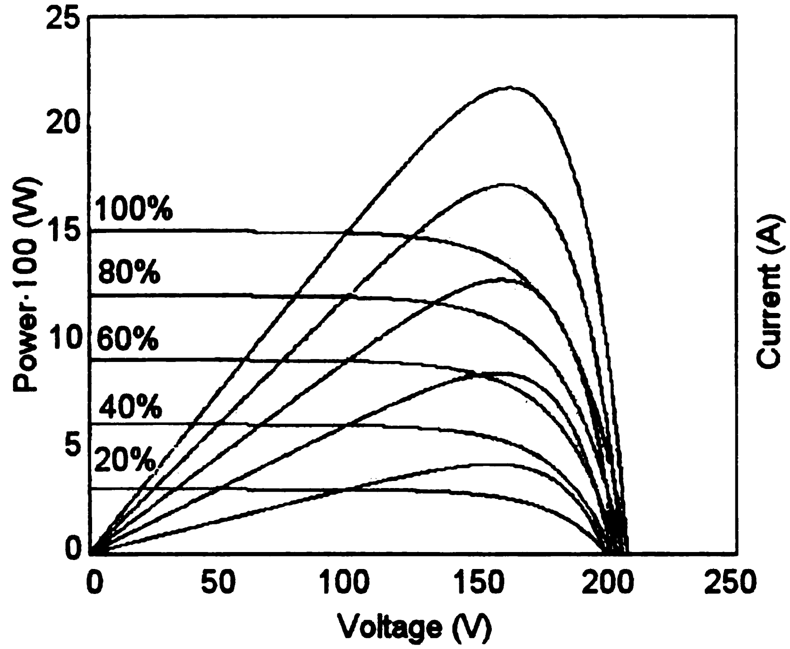

Figure 3.4. P-V and I-V Characteristics for different intensities of light.

$$\frac{\partial P(V)}{\partial V} = \frac{Ix - Ix \cdot exp\left(\frac{V}{b \cdot Vx} - \frac{1}{b}\right)}{1 - exp\left(\frac{-1}{b}\right)} - V \cdot \frac{-Ix \cdot exp\left(\frac{V}{b \cdot Vx} - \frac{1}{b}\right)}{b \cdot Vx - b \cdot Vx \cdot exp\left(\frac{-1}{b}\right)} \tag{3.14}$$

Chapter 1 shows the traditional MPPT algorithms given by the literature. These MPPT algorithms are versions of the numerical algorithm that relates the derivative of the current with respect to the voltage equaled to the negative of the current divided by the voltage, as given in (3.15). Unfortunately, a general (symbolic) solution cannot be found using these algorithms, most of them depends on the record of previous conditions and it is not guarantee that these algorithms can work properly under nonconstant weather conditions.

$$\frac{\partial P}{\partial V} = I + V \cdot \frac{\partial I}{\partial V} = 0 \Rightarrow \frac{\partial I}{\partial V} = -\frac{I}{V} \tag{3.15}$$

In the other hand, the Linear Reoriented Coordinates Method (LRCM) can be an

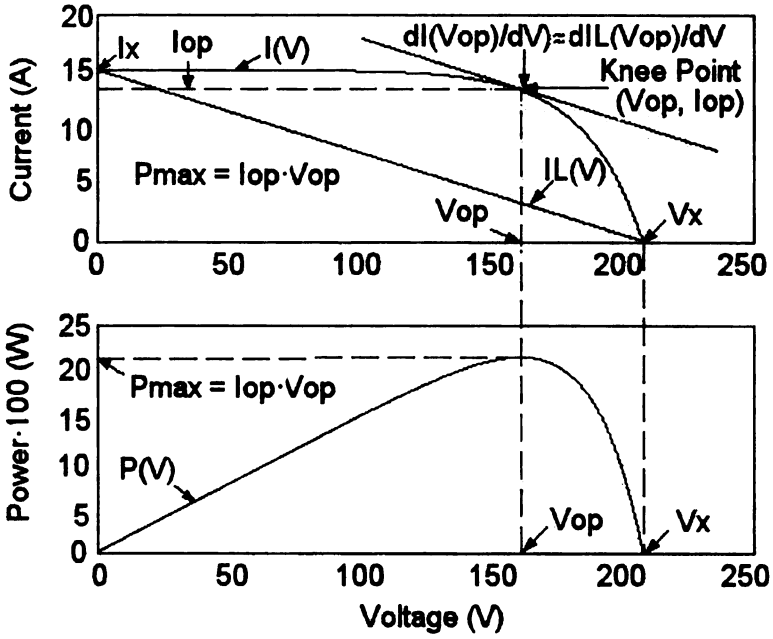

Figure 3.5. Relationship between the P-V curve, I-V curve and the LRCM.

useful tool to approximate the solution of (3.14) with respect to V and be used as an MPPT algorithm. For PV applications, the main idea for the LRCM will be to find the I-V curve knee point as seen in Figure 3.5. The I-V curve knee point is the optimal current (I_{op}) and the optimal voltage (V_{op}) that produces P_{max}. Using the boundaries of the I-V Curve i.e. initial and final values, a linear current equation, $I_L(V)$ can be determined as given in (3.16). Also, $I_L(V)$ can be considered as the limit of (2.10) when b tends to infinite. The current equation, (2.10) and the linear current equation, (3.16) are differentiated and set equal to each other to solve for V, this solution will be known as V_{ap}. The derivatives of $I(V)$ and $I_L(V)$ with respect to V are given by (3.18) and (3.17). It is important to remember that the slope of the I-V Curve at the knee point is approximated by the slope of the linear current equation, (3.19) hence the solution V_{ap} is a close approximation of V_{op}.

$$I_L(V) = I(0) - I(0) \cdot \frac{V}{Vx} = \lim_{b \longrightarrow \infty} \left[I_{sc} - I_{sc} \cdot \frac{1 - \exp\left(\frac{V}{b \cdot V_{oc}}\right)}{1 - \exp\left(\frac{1}{b}\right)} \right] = I_{sc} - I_{sc} \cdot \frac{V}{V_{oc}} \quad (3.16)$$

$$\frac{\partial I_L(V)}{\partial V} = -\frac{Ix}{Vx} \quad (3.17)$$

$$\frac{\partial I}{\partial V} = \frac{-Ix \cdot exp\left(\frac{V}{b \cdot Vx} - \frac{1}{b}\right)}{b \cdot Vx - b \cdot Vx \cdot exp\left(\frac{-1}{b}\right)} \quad (3.18)$$

$$\frac{\partial I_L(V)}{\partial V} \approx \frac{\partial I(V)}{\partial V} \Rightarrow -\frac{Ix}{Vx} \approx \frac{-Ix \cdot exp\left(\frac{V}{b \cdot Vx} - \frac{1}{b}\right)}{b \cdot Vx - b \cdot Vx \cdot exp\left(\frac{-1}{b}\right)} \quad (3.19)$$

Now, the equation of the approximate optimal voltage, V_{ap} is given in (3.20). To prove that V_{op} will be always equal to or more than V_{ap} for any given b more than zero, V_{ap} is substituted into (3.14) resulting in (3.21), where (3.21) is more than zero for any given b more than zero.

$$V_{ap} = Vx + b \cdot Vx \cdot \ln\left(b - b \cdot \exp\left(-\frac{1}{b}\right)\right) \leq V_{op} \quad (3.20)$$

$$\frac{\partial P}{\partial V} = \frac{Ix \cdot \left[\ln\left(b - b \cdot \exp\left(\frac{-1}{b}\right)\right) \cdot \left(b \cdot \exp\left(\frac{-1}{b}\right) - b\right) + (b+1) \cdot \exp\left(\frac{-1}{b}\right) - b\right]}{1 - \exp\left(\frac{-1}{b}\right)} \geq 0 \quad (3.21)$$

Now, let's substitute V_{ap} into (2.10) to obtain I_{ap} then to approximate P_{max} multiply V_{ap} by I_{ap} as given in (3.23). If V_{ap} solves (3.14) equal to zero hence we found the exact solutions for P_{max}, I_{op} and V_{op}. Also, R_{op} can be approximated by (3.24). It is important to note that (3.25) always will be true under any value of b.

$$I_{ap} = Ix \cdot \frac{1 - b + b \cdot exp\left(\frac{-1}{b}\right)}{1 - exp\left(\frac{-1}{b}\right)} \quad (3.22)$$

$$P_{ap} = Ix \cdot Vx \cdot \frac{\left[1 - b + b \cdot exp\left(\frac{-1}{b}\right)\right] \cdot \left[1 + b \cdot \ln\left(b - b \cdot \exp\left(-\frac{1}{b}\right)\right)\right]}{1 - exp\left(\frac{-1}{b}\right)} \quad (3.23)$$

$$R_{ap} = \frac{Vx}{Ix} \cdot \frac{\left[1 + b \cdot \ln\left(b - b \cdot \exp\left(-\frac{1}{b}\right)\right)\right] \cdot \left[1 - exp\left(\frac{-1}{b}\right)\right]}{1 - b + b \cdot exp\left(\frac{-1}{b}\right)} \tag{3.24}$$

$$P_{max} = V_{op} \cdot I_{op} \geq V_{ap} \cdot I_{ap} = P_{ap} \tag{3.25}$$

Additionally after proving (2.21) and (2.27) in the Chapter 2, the whole inequality for the maximum power and fill factor using the LRCM are given by (3.26) and (3.27).

$$I_{sc} \cdot V_{oc} > \int_0^{V_{oc}} I(V)dV > P_{max} \geq P_{ap} > \frac{1}{4} \cdot I_{sc} \cdot V_{oc} \tag{3.26}$$

$$1 > \int_0^{V_{oc}} \frac{I(V)dV}{I_{sc} \cdot V_{oc}} > fillfactor \geq \frac{I_{ap} \cdot V_{ap}}{I_{sc} \cdot V_{oc}} > \frac{1}{4} \tag{3.27}$$

Finally for PVM applications, the LRCM is a simple method where, instead of calculating the optimal voltage (rated voltage) and maximum power solutions using the power equation, the solutions are obtained using the current equation and the linear current equation to obtain the approximations of I_{op}, V_{op} and P_{max}. Also, the LRCM has the advantage of giving an approximated symbolic solution for V_{op}, I_{op}, and P_{max} under any T or E_i. The LRCM can produce the same results as other methods that use Taylor series, continuous fraction expansion, iterations or other approximations, and it is more practical for simulations and power flow analysis providing symbolic solutions. The following results will show that the proposed technique is very effective, giving a small error between the actual values and estimated values, even when the effective intensity of light is changing over the photovoltaic modules or solar panels.

3.5 LRCM Results for a PVIS with MPPT

Figures 3.6 and 3.7 show the simulation results for a PVM with the estimated curve for P_{max} and the knee points. The parameters for the simulation results are, T is T_N,

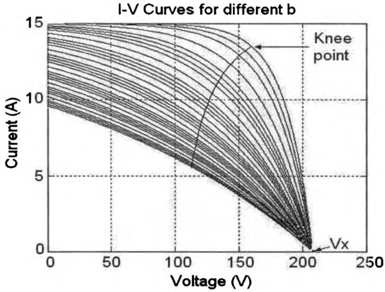

Figure 3.6. I-V Curves with estimated knee points.

Vx is $208V$, I_{sc} is $15A$, b is between 0.08 to 0.4 and E_i is given by (3.28).

$$E_i = (1 - b) \cdot E_{iN} \tag{3.28}$$

Figure 3.6 shows the I-V curves for different characteristic constants and the estimated curve for P_{max}. The characteristic constant will determine Ix and the location of the knee point. The P_{max} will be more for small characteristic constant; hence an I-V curve with b equal to 0.1 produces a bigger P_{max} than an I-V curve with b equal to 0.3. Figure 3.7 shows the P-V Curve for different characteristic constants and the estimated curve for P_{max}. The approximation of P_{max} is very close to P_{max}. Figure 3.8 illustrates the estimated error using the LRCM to approximate P_{max} versus the normalized voltage, i.e. V_{op} divided by Vx with the maximum error is approximately 0.3%. Figure 3.9 shows the P-V curve when T is T_N , Vx is $208V$, I_{sc} is $15A$, b is 0.08 and E_i is $900W/m^2$. It is shown that the approximation of V_{op}, V_{ap}, gives Pap where it has a similar value for P_{max} produced by V_{op}.

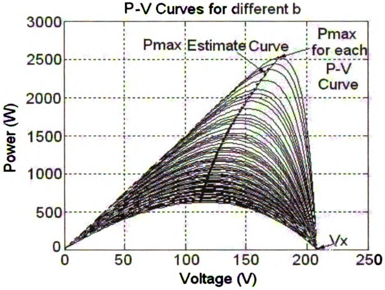

Figure 3.7. P-V Curves with estimated maximum points for the P_{max} curve.

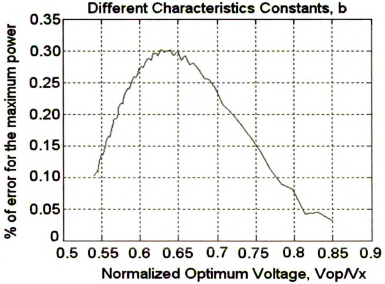

Figure 3.8. Error Curve for P_{max} and P_{max} estimated under different normalized optimum voltage.

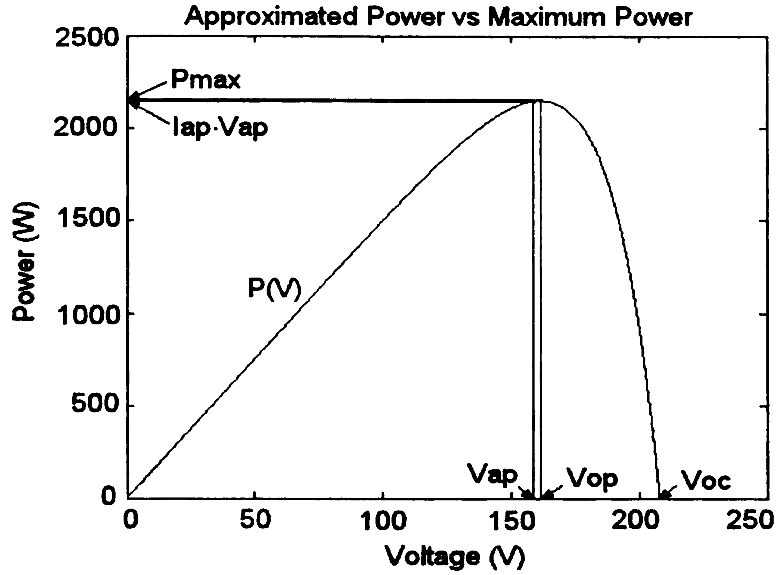

Figure 3.9. P-V curve showing the closeness between P_{max} and P_{max} approximated by P_{ap}.

Finally, to prove how good is the range of our approximation for P_{max} using the LRCM as a general case for any type of PVM consider the functions (3.29) and (3.30). X, Y and Z are the normalize current, normalize voltage and normalize power for any PVM. These variables describe a normalize PVM where X is V/Vx and Y is I/Ix. The range of existence for X and Y is from 0 to 1. Using the LRCM, it possible to approximate the optimal normalize current X_{ap} as given in (3.31). X_{ap} is substituted in (3.30) then the approximate maximum normalize power, Z_{ap}, produced by any PVM is given by (3.32). To calculate the approximate maximum power, P_{ap}, just multiply Z_{ap} by Ix and Vx.

$$Y = \frac{I}{Ix} = \frac{1 - exp\left(\frac{X}{b} - \frac{1}{b}\right)}{1 - exp\left(\frac{-1}{b}\right)} \tag{3.29}$$

$$Z = \frac{V \cdot I}{Vx \cdot Ix} = X \cdot Y = \frac{X - X \cdot exp\left(\frac{X}{b} - \frac{1}{b}\right)}{1 - exp\left(\frac{-1}{b}\right)} \tag{3.30}$$

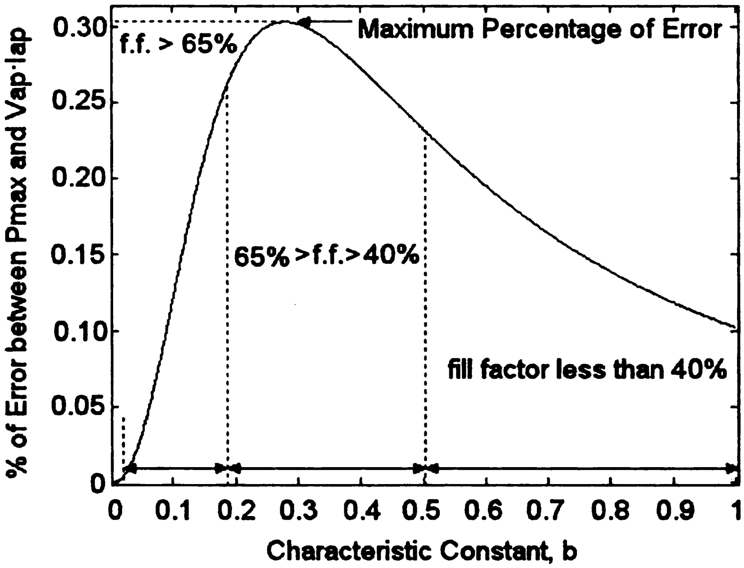

Figure 3.10. Maximum percentage of error curve for P_{max} versus the characteristic constant, b.

$$X_{ap} = 1 + b \cdot \ln\left(b - b \cdot \exp\left(\frac{-1}{b}\right)\right) \tag{3.31}$$

$$Z_{ap} = \frac{\left[1 + b \cdot \ln\left(b - b \cdot \exp\left(\frac{-1}{b}\right)\right)\right] \cdot \left[1 - b + b \cdot \exp\left(\frac{-1}{b}\right)\right]}{1 - \exp\left(\frac{-1}{b}\right)} \tag{3.32}$$

Figure 3.10 shows the maximum percentage of error between P_{max} and Pap for any PVM where b changes from 0.001 to 1. P_{max} was calculated using Matlab for any given b. The typical values of b for any PVM are from 0.01 to 0.18 hence the error for the approximation using the LRCM will be from 0.01% to 0.25% for any given PVM. An excellent result for the LRCM considering that there is no analytical solution for (3.14). Finally, the LRCM has the advantage to guarantee an approximate symbolic solution for the PVM exponential functions (2.10), (2.13) and (3.14) without symbolic solutions. It has been proved that the LRCM has a maximum error for the estimation of P_{max} near to 0.3% where b is changing to obtain different V-I characteristic curves.

3.6 Additional Examples using the LRCM

Example 3.1: Consider the function $f(x)$ in $\{x \in \Re \mid [0 \ \ r]\}$ given by (3.33) with the diffeomorphism property to find the maximum value f_{max} using differential calculus. The derivative of $f(x)$ is given by (3.34) hence the operation points x_{op} and f_{max} are given by (3.35).

$$f(x) = A \cdot x \cdot \left(r^2 - x^2\right)^{0.5} \tag{3.33}$$

$$f'(x) = A \cdot \left(r^2 - x^2\right)^{0.5} - A \cdot x^2 \cdot \left(r^2 - x^2\right)^{0.5} = 0 \tag{3.34}$$

$$\left(x_{op} = \frac{r}{\sqrt{2}},\ \ f(x_{op}) = \frac{A \cdot r^2}{2} = f_{max}\right) \tag{3.35}$$

Now let's find the maximum value for the same function $f(x)$ using LRCM.

1) Calculate $g'(x)$ using $g(x)$ where $g(r)$ is $A \cdot r$ and $g(0)$ is 0.

$$g(x) = A \cdot \left(r^2 - x^2\right)^{0.5} \tag{3.36}$$

$$g'(x) = -A \cdot x \cdot \left(r^2 - x^2\right)^{0.5} \tag{3.37}$$

2) Calculate $gl(x)$ using (3.2) then calculate $gl'(x)$

$$gl(x) = A \cdot r - A \cdot x \Longrightarrow gl'(x) = -A \tag{3.38}$$

3) Calculate x_{op} using the LRCM hence $g'(x) \approx gl'(x)$

$$x_{ap} = x_{op} = \frac{r}{\sqrt{2}} \tag{3.39}$$

4) To approximate f_{max}, x_{ap} is substituted in $f(x)$.

$$f(x_{ap}) = \frac{A \cdot r^2}{2} = f_{max} \tag{3.40}$$

5) Finally, ε is the final angle error for the approximation with $\varepsilon = 0°$ i.e. 0% of error for the approximation of x_{op}. Both results x_{op} and f_{max} can be solved and a symbolic solution is obtained with angle error of 0° i.e. $f'(x_{ap}) = 0$.

Example 3.2: A basic principle in microeconomics is to obtain the maximum profit and maximum revenues with the minimum costs [96]. Consider the function (3.41) that describes the profit for the company **X** given the number of employees, n. Figure 3.11 shows the profit versus the number of employees contracted by the company **X**. The variable m is the maximum number of employees to be contracted that will not create a deficit to the company **X**, and k is a factor that relates the rate of profit per employee. It is desired to maximize the profits for a company only contracting the number of employees necessary to maximize the profit. Unfortunately, (3.41) does not have the diffeomorphism property. Now, if (3.41) is divided by n, (3.42) is obtained and has the diffeomorphism property that satisfies the conditions to apply the LRCM. The derivative of (3.42) given by (3.43) and the boundaries of (3.42) can be used to calculate the optimal number of employees, n_x to provide the maximum profit for the company **X**. Using the LRCM, n_x is calculated using (3.44) where m is 52 and k is 10.06784 hence n_x is 36 with a profit of 284,600\$.

$$Profit(n) = n \cdot k - n \cdot (k-1) \cdot \left(\frac{k}{k-1}\right)^{\frac{n}{m}} \tag{3.41}$$

$$rate = k - (k-1) \cdot \left(\frac{k}{k-1}\right)^{\frac{n}{m}} \tag{3.42}$$

$$\frac{\partial rate}{\partial n} = \frac{1-k}{m} \cdot \ln\left(\frac{k}{k-1}\right) \cdot \left(\frac{k}{k-1}\right)^{\frac{n}{m}} \tag{3.43}$$

$$n_x = \frac{\ln(k-1) + \ln[\ln(k-1) - \ln(k)]}{\ln(k-1) - \ln(k)} \tag{3.44}$$

Example 3.3: The next example is to determine the inverse of a function $f(x)$ without diffeomorphism. The main goal is to determine the maximum rectangular

Figure 3.11. Profit vs # of employees contracted by the company **X**.

area inside of the function $g(x)$. $g(x)$ describes the shape constraint relation for a floorplan for an 8-bit A/D converter and it is required to maximize the rectangular area inside of $g(x)$. Floorplan design is the first task in VLSI layout and perhaps the most important one [88]. In practical designs, the dimensions of some modules are restricted by physical designs and therefore can not be varied continuously [87]. $f(x)$ in $\{x \in \Re \mid [0 \;\; 25]\}$ represents the rectangular area occupied by a floorplan for an 8-bit A/D converter.

$$f(x) = \frac{x \cdot 25 \cdot \tan^{-1}(25 - x)}{\tan^{-1}(25)} \tag{3.45}$$

Using differential calculus, it can be calculated $f'(x)$ and simplified to be solved by x but it cannot be solve for x, as given in (3.46).

$$\tan^{-1}(25 - x) - \frac{x}{1 + (25 - x)^2} = 0 \tag{3.46}$$

Consider the LRCM using the following steps:

1) Calculate $g'(x)$ using $g(x)$, $g(25)$ is 0 and $g(0)$ is 25

$$g(x) = \frac{25 \cdot \tan^{-1}(25 - x)}{\tan^{-1}(25)} \tag{3.47}$$

$$g'(x) = \frac{-25}{\tan^{-1}(25) + \tan^{-1}(25) \cdot (25 - x)^2} \tag{3.48}$$

2) Calculate $gl(x)$ using (3.2) then calculate $gl'(x)$

$$gl(x) = 25 - x \Longrightarrow gl'(x) = -1 \tag{3.49}$$

3) Calculate the approximate value of x_{op} using the LRCM hence $g'(x) \approx gl'(x)$

$$x_{op} \approx x_{ap} = 25 - \sqrt{\frac{25}{\tan^{-1}(25)} - 1} \tag{3.50}$$

4) To approximate f_{max}, x_{ap} is substituted in $f(x)$ hence $f_{max} \approx f(x_{ap})$.

$$f_{max} \approx \frac{25}{\tan^{-1}(25)} \cdot \tan^{-1}\left(\sqrt{\frac{25}{\tan^{-1}(25)} - 1}\right) \cdot \left(25 - \sqrt{\frac{25}{\tan^{-1}(25)} - 1}\right) \tag{3.51}$$

5) The percentage of error for the approximation of f_{max} is less than 2.3% and was calculated using (3.6). This final result proved how good is the approximation for f_{max} considering that there is not analytical solution for (3.46).

Finally, the dimensions for the maximum rectangular area for a floorplan for an 8-bit A/D converter are for x-axis is 21.0845 units and for $g(x)$-axis is 21.5693 units.

Example 3.4: Figure 3.12 shows the characteristic curve for a Fuel Cell [85] where voltage output (V) versus the current density (A/cm^2) relationship with an area for the reactor of $1cm^2$. The voltage, V, and the power, P, in terms of the current, I, are described by (3.52) and (3.53). To obtain the maximum power, P_{max}, is required

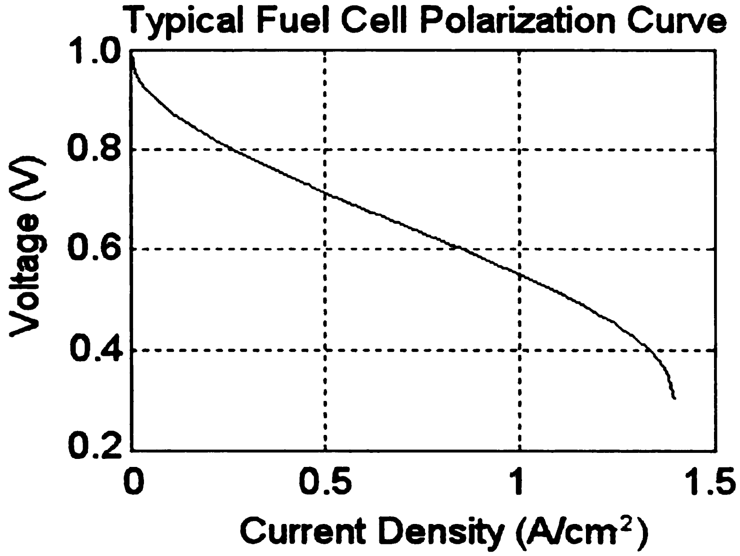

Figure 3.12. V-I Characteristic Curve for a Fuel Cell.

to solve the derivative of the power with respect to the current equal to zero.

$$V(I) = 0.3 + \frac{0.7}{\pi} \cdot \cos^{-1}\left(\frac{I}{0.7} - 1\right) \tag{3.52}$$

$$P(I) = I \cdot V(I) = 0.3 \cdot I + \frac{0.7}{\pi} \cdot I \cdot \cos^{-1}\left(\frac{I}{0.7} - 1\right) \tag{3.53}$$

$$\frac{\partial P(I)}{\partial I} = 0.3 + \frac{0.7}{\pi} \cdot \cos^{-1}\left(\frac{I}{0.7} - 1\right) - \frac{I}{\pi} \cdot \left[1 - \left(\frac{I}{0.7} - 1\right)^2\right]^{-0.5} \tag{3.54}$$

Unfortunately, it is not possible to solve (3.54) with respect to I due the absence of the diffeomorphism property. The LRCM can provide a good approximation for P_{max}.

$$\frac{\partial V(I)}{\partial I} = -\frac{1}{\pi} \cdot \left[1 - \left(\frac{I}{0.7} - 1\right)^2\right]^{-0.5} \tag{3.55}$$

$$Vl(I) = 1 - \frac{I}{2} \Longrightarrow \frac{\partial V(I)}{\partial I} = -\frac{1}{2} \tag{3.56}$$

Table 3.1. Comparison for LRCM Results and Optimal Values

	Voltage	Current	Power
Optimal	0.4902 V	1.1602 A	0.5687 W
Approx.	0.4538 V	1.2398 A	0.5626 W
Error	7.44 %	6.88 %	1.07 %

After use (3.55) and (3.56), it is possible to solve for the approximate optimal current (I_{ap}) given by (3.57).

$$I_{ap} = 0.7 + 0.7 \cdot \sqrt{1 - \frac{4}{\pi^2}} \tag{3.57}$$

Finally, I_{ap} can be substituted in the voltage and power equations, (3.53) and (3.52). Table 3.1 shows the results of the LRCM for the voltage, current and power. The row with the approximation error values for each variable was calculated using (3.6).

Example 3.5: Consider the function $g(x)$ described by (3.58). It is desire to calculate the maximum rectangular area inside of $g(x)$ $\forall$ x in $\{x \in \Re \mid [0 \;\; 4]\}$. The rectangular area inside of $g(x)$ can be calculated using $f(x) = x \cdot g(x)$, the derivative of $f(x)$ with respect to x is given by (3.59). Unfortunately is not possible to solve (3.59) equal to 0 but using the LRCM is possible to approximate the maximum rectangular area inside of $g(x)$.

$$g(x) = \exp(8) - \exp(4) + \exp(x) - \exp(2 \cdot x) \tag{3.58}$$

$$f'(x) = \exp(8) - \exp(4) + (1 + x) \cdot \exp(x) - (1 + 2 \cdot x) \cdot \exp(2 \cdot x) \tag{3.59}$$

1. Calculate the linear equation $gl(x)$ using the boundaries of $g(x)$ where $g(0)$ is $\exp(4) + \exp(8)$ and $g(4)$ is 0,

$$gl(x) = (\exp(4) + \exp(8)) \cdot \left(1 - \frac{x}{4}\right) \tag{3.60}$$

2. Determine $g'(x)$ and $gl'(x)$

$$g'(x) = exp(x) - 2 \cdot exp(2 \cdot x) \tag{3.61}$$

$$gl'(x) = -\frac{1}{4} \cdot (\exp(4) + \exp(8)) \tag{3.62}$$

3. Substitute $y = \exp(x)$ on $g'(x)$

$$g'(x) = exp(x) - 2 \cdot exp(2 \cdot x) = y - 2 \cdot y^2 \tag{3.63}$$

4. Using $g'(x)$ and $gl'(x)$ solve for y

$$g'(x_{ap}) \approx gl'(x_{ap}) \Longrightarrow y - 2 \cdot y^2 \approx -\frac{1}{4} \cdot (exp(8) + exp(4)) \tag{3.64}$$

$$y = \frac{1}{4} + \frac{1}{4} \cdot \sqrt{1 + 2 \cdot \exp(4) + 2 \cdot \exp(8)} = 19.7309 \tag{3.65}$$

5. Calculate x_{ap} then approximate the maximum area using x_{ap},

$$x_{ap} = \ln(y) = 2.96411 \Longrightarrow f(x_{ap}) = x_{ap} \cdot g(x_{ap}) = 7,618.51 \tag{3.66}$$

Finally, f_{max} is $7,631.62$ hence the percentage of error for the approximation $f(x_{ap})$ using (3.6) is 0.171524%. Again, $f'(x) = 0$ is not possible to solve with respect to x due the absence of the diffeomorphism property in $f(x)$ but using the LRCM at least, it is possible to estimate the optimal value for x with small percentage of error!

CHAPTER 4

Fractional Polynomial Method

This chapter presents a non-traditional method for the approximation of the photovoltaic module, PVM, exponential model using fractional polynomials where the shape, boundary conditions and performance of the original system are satisfied. The use of fractional polynomials will provide an analytical solution to determine the optimal voltage, V_{op}, optimal current, I_{op}, and maximum power, P_{max} for the PVM operation. An additional method to calculate a sufficiently close integer polynomial is given in the chapter using the information obtained from the Fractional Polynomial Method, FPM. Examples and simulations to validate the proposed methods are given in the chapter using data sheets for different types of PVM's. Finally, the proposed methods are excellent in approximating the PVM exponential model and provide a different way to approximate exponential functions that are not possible to solve using differential calculus.

4.1 Introduction

In engineering and sciences, an accurate mathematical modeling for a physical system, object, event or pattern can determine the behavior and characteristics of the proposed design–saving time, space, money and materials. Examples of mathematical modeling and simulations are in circuit analysis, design of mechanical systems, nuclear explosion simulation, power grid simulations, etc. An inaccurate mathematical model can result in serious problems not expected in the final design of the system. The performance and behavior of the system can be diminished because of inaccurate modeling. One of the most dramatic examples is the Tacoma Narrows Bridge, USA, in 1940, where the natural resonance of the bridge coincided with the frequency of the wind creating a collapse of the bridge, an effect not considered in the original design [97].

At the same time, a very complex mathematical model can be hard to analyze and impractical. So a compromise should be taken between the complexity and the number of parameters used to describe a physical system [98]. If the correct assumptions are made, an approximation of the mathematical model that keeps the main properties of the physical system can be obtained. An example is the mathematical model for a resistance in circuit analysis where the temperature effect is neglected on the nominal value for the resistance.

Chapter 2 proposes a PVM model based on the manufacturer data sheet. Unfortunately, the proposed PVM model cannot be programmed into a microchip because most of the Arithmetic Logic Units (ALU) will only perform arithmetic operations or it cannot be used as a PV source simulator in programs like Saber or P-Spice. This is because often these sources are simulated using polynomials instead of exponentials. To solve this problem, a method to approximate the photovoltaic module model using fractional exponents and polynomials is presented in this chapter.

The chapter describes how the proposed PVM model can be approximated by fractals and polynomials. The obtained polynomial keeps the properties of the given exponential function and can be used in programs like Saber and Pspice. Also, the chapter describes the relationship of exponential functions, with fractal functions and how it can be approximated by polynomials. Additionally, the fractional polynomial that describes the power for the PVM can be used to estimate the maximum power at any temperature or irradiance level. Finally, the proposed Fractional Polynomial Method, FPM can be applied to other types of transcendental functions.

4.2 Fractional Polynomial Method

In this section, a method for the approximation of exponential functions in the range of existence is described. The idea is to approximate the exponential functions as described in and using fractional polynomials. These fractional polynomials should keep the same boundaries, shape and performance of and . The question of how to approximate $I(V)$ as a fractional polynomial, keeping the boundary conditions and properties of $I(V)$ using the data provided by the PVM manufacturer data sheet, is addressed in this chapter. The Fractional Polynomial Method, FPM, is also useful in obtaining analytically the optimal current and voltage and at the same time able to provide P_{max}.

Now, consider the fractional polynomials (4.1) and (4.2) that satisfy the same boundary conditions of and , where n is a positive integer number and q is a non-integer number greater than or equal to 0 but less than 1 i.e. $0 \leq q < 1$.

$$I_f(V) = Ix - Ix \cdot \left(\frac{V}{Vx}\right)^{n+q} \tag{4.1}$$

$$P_f(V) = V \cdot I_f(V) = V \cdot Ix - V \cdot Ix \cdot \left(\frac{V}{Vx}\right)^{n+q} \tag{4.2}$$

The derivatives of (4.1) and (4.2) with respect to V are given in (4.3) and (4.4). To approximate the variables V_{op} and I_{op}, (4.4) is set equal to 0 then solve for V, the approximation of V_{op} will be given by V_{opf} then substitute V_{opf} in (4.1) to approximate I_{op} given by I_{opf}. Finally, P_{max} is approximated multiplying V_{opf} by I_{opf}, as described in (4.7). It is important to note that (3.14) cannot be solved with respect to V when it is equal to 0 but on the other hand (4.4) can be solved with respect to V giving a close approximation for V_{op}, I_{op} and P_{max}.

$$\frac{\partial I_f(V)}{\partial V} = -Ix \cdot (n+q) \cdot \left(\frac{V}{Vx}\right)^{n+q-1} \leq 0 \tag{4.3}$$

$$\frac{\partial P_f(V)}{\partial V} = Ix - Ix \cdot (n+q+1) \cdot \left(\frac{V}{Vx}\right)^{n+q} \tag{4.4}$$

$$V_{opf} = Vx \cdot \left(\frac{1}{n+q+1}\right)^{\frac{1}{n+q}} \tag{4.5}$$

$$I_{opf} = Ix \cdot \left(\frac{n+q}{n+q+1}\right) \tag{4.6}$$

$$P_{maf} = V_{opf} \cdot I_{opf} = Vx \cdot Ix \cdot \left(\frac{n+q}{n+q+1}\right) \cdot \left(\frac{1}{n+q+1}\right)^{\frac{1}{n+q}} \tag{4.7}$$

To find the relationship between (2.10) and (4.1), both functions are evaluated under Standard Test Conditions and set equal to each other as given in (4.8) then solve for $n+q$ as given in (4.9).

$$P_{max} = \frac{V_{op} \cdot I_{sc}}{1 - exp\left(\frac{-1}{b}\right)} \cdot \left[1 - exp\left(\frac{V_{op}}{b \cdot V_{oc}} - \frac{1}{b}\right)\right] = V_{op} \cdot I_{sc} \cdot \left[1 - \left(\frac{V_{op}}{V_{oc}}\right)^{n+q}\right] \tag{4.8}$$

$$n+q = \frac{1}{\ln\left(\frac{V_{op}}{V_{oc}}\right)} \cdot \ln\left[\frac{1 - \exp\left(\frac{V_{op}}{b \cdot V_{oc}}\right)}{1 - \exp\left(\frac{1}{b}\right)}\right] \tag{4.9}$$

The next three points summarize the proposed FPM for the approximation of a photovoltaic module model using fractional polynomials. It can be used as an analytical method to approximate P_{max} and satisfy the boundary conditions which are necessary to provide the best approximation of $I(V)$ and $P(V)$.

1- The boundary conditions are satisfied in $I_f(V)$ and $P_f(V)$. Additional conditions are given in Table 4.1.

2- For any value of V, more than 0 and less or equal than Vx, n-derivatives of

Table 4.1. Conditions satisfied by the proposed fractional approximation method

V	$P(V)$	$\frac{\partial P(V)}{\partial V}$	$I(V)$	$\frac{\partial I(V)}{\partial V}$
$V=0$	$P(0)=0$	$\frac{\partial P(0)}{\partial V}>0$	$I(0)=Ix$	$\frac{\partial I(0)}{\partial V}\leq 0$
$V=Vx$	$P(Vx)=0$	$\frac{\partial P(Vx)}{\partial V}<0$	$I(Vx)=0$	$\frac{\partial I(Vx)}{\partial V}<0$
$V=V_{oc}$	$P(V_{op})=P_{max}$	$\frac{\partial P(V_{op})}{\partial V}=P_{max}$	$I(V_{op})=I_{op}$	$\frac{\partial I(V_{op})}{\partial V}<0$

$I_f(V)$ with respect to V are less than 0 where $k = 1, 2, 3, ..., n$.

$$\frac{\partial^k I(V)}{\partial^k V} = \frac{-Ix}{b^k - b^k \cdot exp\left(\frac{-1}{b}\right)} \cdot exp\left(\frac{V}{b \cdot Vx} - \frac{1}{b}\right) = \frac{1}{b^{k-1}} \cdot \frac{\partial I(V)}{\partial V} < 0 \tag{4.10}$$

3- Analytical solution to solve for the maximum power, P_{max}.

$$\frac{\partial P_f(V_{opf})}{\partial V} = 0 \Longrightarrow V_{opf} = \frac{^{-1}\partial P_f(0)}{\partial V} \Longrightarrow P_{max} = P_{maf} = V_{opf} \cdot I(V_{opf}) \tag{4.11}$$

In the next section, approximation of the fractional polynomial to a close integer polynomial that keeps most of the properties of $I_f(V)$ is discussed.

4.3 Integer Polynomial Approximation Method

Some disadvantages of the fractional polynomial are that it cannot be programmed in an Arithmetic Logic Unit, it is not easy to handle for Lyapunov analysis and cannot be used as a custom voltage-current source for simulators like Pspice or Saber. So the purpose of this section is to provide an additional method to approximate a fractional polynomial using a close approximation for an integer polynomial where the boundary conditions are satisfied. The idea of the Integer Polynomial Approximation Method, IPAM, is to linearize only the non-integer part of (4.1) in the point of reference Vx where the non-integer part of (4.1) is given by (4.12) then (4.12) is evaluated on Vx as given in (4.13). The function $yl(V)$ is an straight line calculated by the linearization of (4.12) in the point of reference Vx. The straight line parameters m and b are calculated by (4.14) and (4.15) then are substituted in (4.16).

$$y(V) = \left(\frac{V}{Vx}\right)^q \tag{4.12}$$

$$y(Vx) = yl(Vx) = \left(\frac{Vx}{Vx}\right)^q = 1 \tag{4.13}$$

$$m = \frac{\partial}{\partial V}\left(\frac{V}{Vx}\right)^q \bigg|_{V=Vx} = q \tag{4.14}$$

$$b = y(Vx) - m \cdot \frac{V}{Vx}\bigg|_{V=Vx} = 1 - q \tag{4.15}$$

Finally, $yl(V)$ is the linearization of $y(V)$ and is given by (4.16). Using (4.16), the integer polynomial $I_p(V)$ that approximate the fractional polynomial $I_f(V)$ is obtained and given by (4.17). Now, it is possible to program $I_p(V)$ in an ALU or used as a custom source in programs like Saber or Pspice.

$$y(V) = b + m \cdot \frac{V}{Vx} = 1 - q + q \cdot \frac{V}{Vx} \tag{4.16}$$

$$I_p(V) = Ix - Ix \cdot \left(\frac{V}{Vx}\right)^n \cdot yl = Ix - Ix \cdot \left(\frac{V}{Vx}\right)^n \cdot \left(1 - q + q \cdot \frac{V}{Vx}\right) \tag{4.17}$$

To calculate the power just multiply $I_p(V)$ by V as given in (4.18). The maximum power is calculate by taking the derivative of $P_p(V)$ with respect to V as given on (4.19) then set (4.19) equal to zero and solve for V, is substituted in (4.18) to find the maximum power.

$$P_p(V) = V \cdot I_p(V) = V \cdot Ix - V \cdot Ix \cdot \left(\frac{V}{Vx}\right)^n \cdot \left(1 - q + q \cdot \frac{V}{Vx}\right) \tag{4.18}$$

$$\frac{\partial P_p(V)}{\partial V} = Ix \cdot \left[1 - (1-q)\cdot(n+1)\cdot\left(\frac{V}{Vx}\right)^n - q\cdot(n+2)\cdot\left(\frac{V}{Vx}\right)^{n+1}\right] \tag{4.19}$$

It is important to note that (4.17) and (4.18) satisfy the famous Weierstrass approximation theorem [99], therefore the maximum approximation errors for (4.17) and (4.18) are sufficiently close to the maximum errors for the approximations of (4.1) and (4.2) using fractional polynomials. Unfortunately if n is more than three, there is no general solution for (4.19) when it is equal to 0. A similar statement was proved first by Paolo Ruffini and Neils Henrik Abel. The theorem is known as the Abel-Ruffini theorem and it was published in the year 1813 [99]. For a polynomial like (4.17) with n more than three, at thought we can determine the limits for roots using Maclaurin's theorem [100] but this does not mean that the solutions (4.19) can be found; it means that only the range of existence for the solutions of V can be found. Also, if (4.19) can be solved, V will have n solutions making $n-1$ impractical and there is only one useful solution for V which is a unique positive real value in the range of existence from 0 to Vx.

On the other hand, $I_p(V)$ can be very useful for Lyapunov analysis. Consider a PVM connected in parallel to a capacitor, C, and a resistance, R, as shown in figure 4.1. It is desired to prove that the voltage, V, is asymptotically under any value of R. The dynamic function for the voltage is given by (4.20) where $V \in [0 \quad Vx]$.

$$\frac{\partial V}{\partial t} = \frac{I_p(V)}{C} - \frac{V}{C \cdot R} = \frac{Ix}{C} - \frac{(1-q) \cdot Ix \cdot V^n}{C \cdot Vx^n} - \frac{q \cdot Ix \cdot V^{n+1}}{C \cdot Vx^{n+1}} - \frac{V}{C \cdot R} \tag{4.20}$$

The equilibrium point of (4.20) is given by (4.21) where $\overline{V} \in (0 \quad Vx)$ hence the normalized equation that shift the equilibrium to zero is given by (4.22) where $\widetilde{V} = V - \overline{V}$.

$$\overline{V} = R \cdot I_p(\overline{V}) = R \cdot Ix - \frac{R \cdot (1-q) \cdot Ix \cdot \overline{V}^n}{Vx^n} - \frac{R \cdot q \cdot Ix \cdot V^{n+1}}{Vx^{n+1}} \tag{4.21}$$

$$\frac{\partial \widetilde{V}}{\partial t} = \frac{(1-q) \cdot Ix}{C \cdot Vx^n} \cdot \left(\overline{V}^n - \left(\widetilde{V} + \overline{V}\right)^n\right) + \frac{q \cdot Ix}{C \cdot Vx^{n+1}} \cdot \left(\overline{V}^{n+1} - \left(\widetilde{V} + \overline{V}\right)^{n+1}\right) \tag{4.22}$$

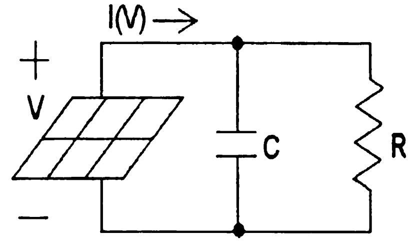

Figure 4.1. PVM connected to a RC Load.

Now, the Binomial Theorem [99] defined in (4.23) can be used to simplify (4.22) as demonstrated by (4.24). Due that the range of existence for V is from zero to Vx, the functions $g_n(V)$ and $g_{n+1}(V)$ are always positive functions.

$$\left(\widetilde{V}+\overline{V}\right)^{n+1} = \sum_{k=0}^{n+1}\binom{n+1}{k}\cdot\widetilde{V}^{k}\cdot\overline{V}^{n+1-k} = \overline{V}^{n} + \sum_{k=1}^{n+1}\binom{n+1}{k}\cdot\widetilde{V}^{k}\cdot\overline{V}^{n+1-k} \tag{4.23}$$

$$\begin{aligned}\frac{\partial\widetilde{V}}{\partial t} &= -\frac{(1-q)\cdot Ix}{C\cdot Vx^{n}}\cdot\sum_{k=1}^{n}\binom{n}{k}\cdot\widetilde{V}^{k}\cdot\overline{V}^{n-k} - \frac{q\cdot Ix}{C\cdot Vx^{n+1}}\cdot\sum_{k=1}^{n+1}\binom{n+1}{k}\cdot\widetilde{V}^{k}\cdot\overline{V}^{n+1-k}\\ &= -\frac{(1-q)\cdot Ix}{C\cdot Vx^{n}}\cdot g_n(\widetilde{V}) - \frac{q\cdot Ix}{C\cdot Vx^{n+1}}\cdot g_{n+1}(\widetilde{V})\end{aligned} \tag{4.24}$$

Let's apply the Lyapunov function, $\Omega = 0.5\cdot\widetilde{V}^2$, to check the stability of V using (4.24). The derivative of Ω clearly shows that V is asymptotically stable for any value of R as given in (4.25).

$$\frac{\partial\Omega}{\partial t} = \widetilde{V}\cdot\frac{\partial\widetilde{V}}{\partial t} = -\frac{(1-q)\cdot Ix}{C\cdot Vx^{n}}\cdot g_n(\widetilde{V})\cdot\widetilde{V} - \frac{q\cdot Ix}{C\cdot Vx^{n+1}}\cdot g_{n+1}(\widetilde{V})\cdot\widetilde{V} \le 0 \tag{4.25}$$

4.4 Examples using FPM and IPAM

In this section, Tables 2.1 and 2.2 will be used to compare the relationships between the proposed PVM model in Chapter 2 and the fractional approximation method. The first example will show how to apply the proposed method to approximate the performance for a PVM SX-5. The first step is to calculate variables n and q using (4.9), the calculations are given by (4.26) where n is 10 and q is 0.6078.

$$n + q = \frac{1}{\ln\left(\frac{16.5}{20.5}\right)} \cdot \ln\left[\frac{1-\exp\left(\frac{16.5}{0.08474 \cdot 20.5}\right)}{1-\exp\left(\frac{1}{0.08474}\right)}\right] = 10.6078 \tag{4.26}$$

Consider Ix equal to I_{sc} and Vx equal to V_{oc}, the approximations of the optimal current and optimal voltage are given by (4.27) and (4.28).

$$I_{opf} = Ix \cdot \left(\frac{n+q}{n+q+1}\right) = 0.3 \cdot \left(\frac{10+0.6078}{10+0.6078+1}\right) \tag{4.27}$$

$$V_{opf} = Vx \cdot \left(\frac{1}{n+q+1}\right)^{\frac{1}{n+q}} = 20.5 \cdot \left(\frac{1}{10+0.6078+1}\right)^{\frac{1}{10+0.6078}} \tag{4.28}$$

The approximation of the maximum power is the multiplication of (4.27) by (4.28) and it is given by (4.29). The fractional polynomial and integer polynomial, that describes the PVM SX-5 under STC, are given by (4.30) and (4.31). Table 4.2 shows the results for four PVM's given on Tables 2.1 and 2.2. Figure 4.2 shows the I-V Curves for a Solarex SX-5 with their fractional and integer polynomial approximations under STC. The fractional and integer approximations of $I(V)$ are very close to the I-V Curve. Figure 4.3 shows how good $I_f(V)$ and $I_p(V)$ are when the maximum error for the approximations of $I(V)$ for the SX-5 is $7.5mA$.

$$P_{maf} = I_{opf} \cdot V_{opf} = 0.27A \cdot 16.23V = 4.46W \tag{4.29}$$

Table 4.2. PVM parameter approximation using the FPM under STC

PVM Model	$I_{opf}(A)$	$V_{opf}(V)$	R_{opf} (Ω)	P_{maf} (W)	n	q
Solarex SX-5	0.27	16.23	60.11	4.46	10	0.6078
Solarex SX-10	0.60	16.77	27.95	10.00	11	0.0869
SLK60M6	6.96	30.19	4.34	210.10	12	0.4576
Siemens SP75	4.37	17.12	3.92	74.82	10	0.1799
Shell SQ80	4.51	17.82	3.95	80.32	13	0.1461

$$I_f(V) = Ix - Ix \cdot \left(\frac{V}{Vx}\right)^{n+q} = 0.3 - 0.3 \cdot \left(\frac{V}{20.5}\right)^{10.6078} \tag{4.30}$$

$$I_p(V) = 0.3 \cdot \left[1 - 0.3922 \cdot \left(\frac{V}{20.5}\right)^{10} - 0.6078 \cdot \left(\frac{V}{20.5}\right)^{11}\right] \tag{4.31}$$

The second example uses the I-V Characteristics given by the data sheet for a PVM SLK60M6 under different temperature and irradiance levels. It is desire to approximate the I-V Curves and P-V Curves using fractional polynomial and integer polynomial approximations. First the variables Ix, Vx, n and q are calculated using (2.11), (2.12), and (4.9) then these variables are substituted in (4.1), (4.2), (4.17), and (4.18) then $I_f(V)$, $P_f(V)$, $I_p(V)$ and $P_p(V)$ are simulated. Figures 4.4 and 4.5 show the I-V Curves, P-V Curves and their approximations for a PVM SLK60M6 under different cell temperatures and radiations. Clearly, it can be seen that the I-V Curves, P-V Curves and their approximations are very close to the results given by the SLK60M6 data sheet.

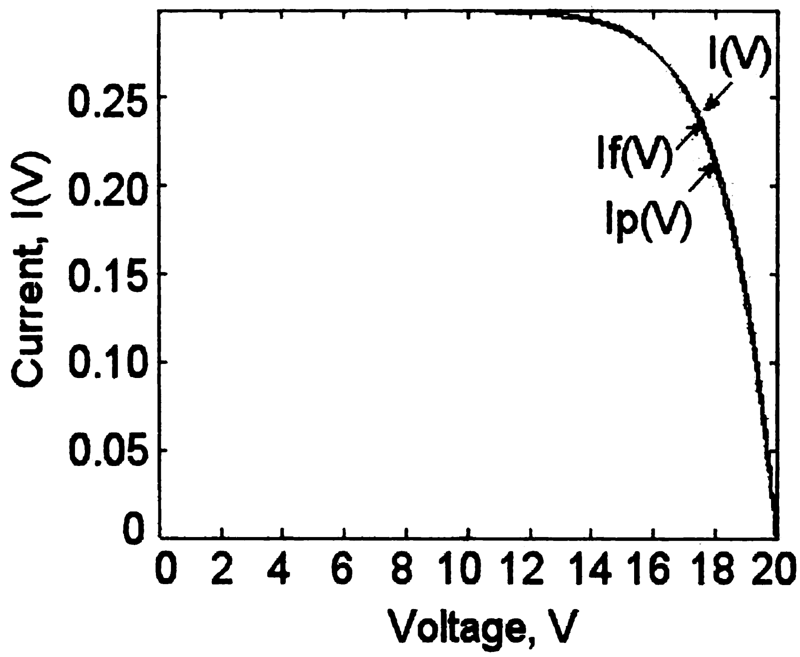

Figure 4.2. I-V curves and the approximations for a PVM SX-5 under STC.

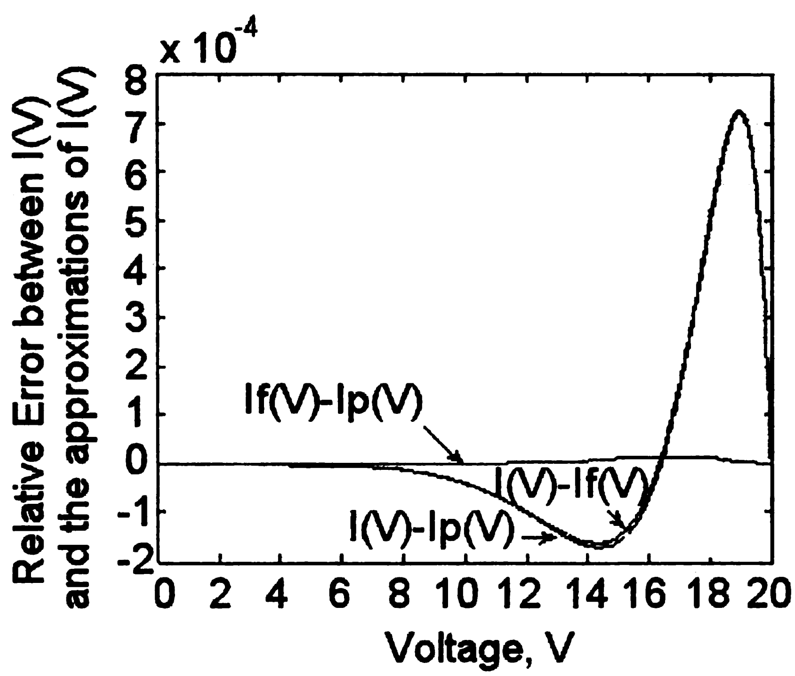

Figure 4.3. Error curves between *I(V)* and the approximations of *I(V)*.

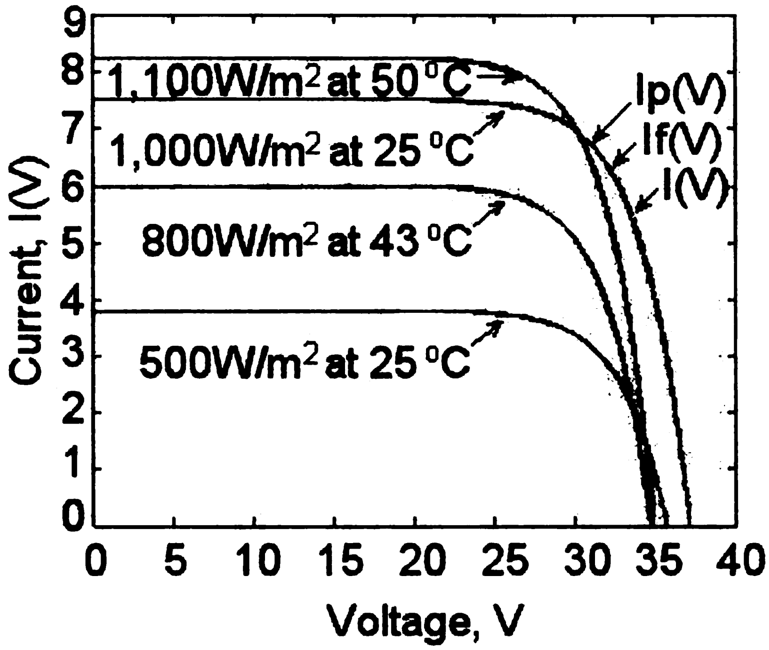

Figure 4.4. I-V Curves for a PVM SLK60M6 under different cell temperature and irradiance.

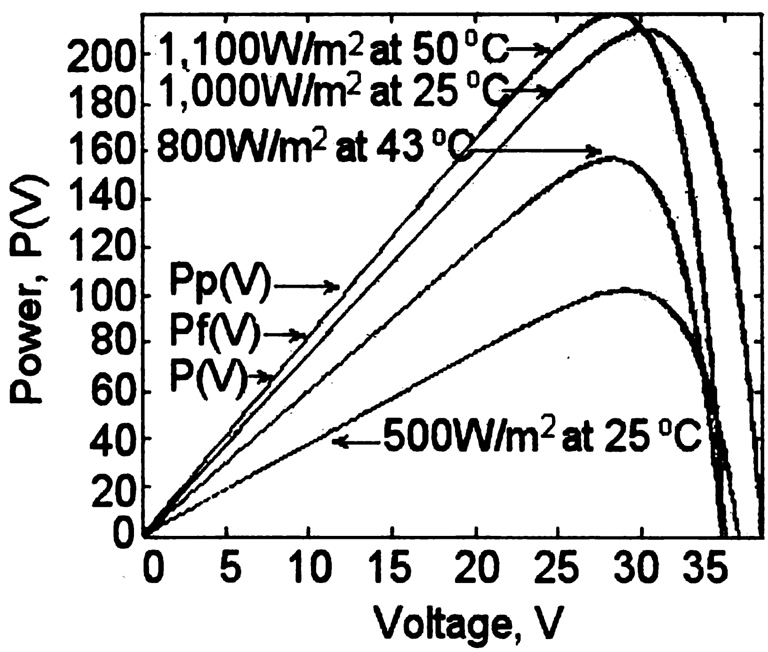

Figure 4.5. P-V Curves for a PVM SLK60M6 under different cell temperature and irradiance.

CHAPTER 5

Fixed Point Algorithms to Estimate T and E_{iN} over a PVM

The purpose of this chapter is to present four algorithms to calculate the effective irradiance level, E_i and temperature, T, of operation for a photovoltaic module, PVM. The main reasons to develop these algorithms are for monitoring climate conditions, the elimination of temperature and solar irradiance sensors, reductions in cost for a photovoltaic inverter system, and development of new algorithms to be integrated with maximum power point tracking algorithms. The first three algorithms use only the short circuit current, open circuit voltage, the operating current and voltage for the PVM, avoiding the use of pyranometers and thermocouples. The last algorithm can estimate the irradiance level using only the open circuit voltage and the PVM temperature of operation. Finally, simulations and experimental results are presented in the chapter.

5.1 Introduction

The environmental conditions are an important factor in the performance of any photovoltaic module, PVM. An accurate measurement of the temperature, T and effective irradiance level, E_i is needed to improve the design of PV power systems and maximum power point tracking, MPPT algorithms. Also, the measured data is useful for online PV system characterization [101, 102], reliability of the weather conditions and meteorological data collection on a long term basis [103]. Also, with the measured data, it will be possible to determine if a PV system is cost–effective [4] and to predict the annual energy production for a PVM in a specific geographic region [104].

The typical sensor used to measure the solar irradiance over a PVM is a pyranometer [105]. A pyranometer is defined as an instrument for measuring the solar radiation and diffuse sky radiation, i.e. effective irradiance on a plane surface [106]. Typically, pyronometers are used in terrestrial and space applications [4, 1, 2, 102, 103, 104, 105, 106, 107, 108, 109, 110]. Usually, for a low cost pyranometer a reasonable accuracy should be $\pm 5\%$ and for a high cost pyranometer a reasonable accuracy should be $\pm 2\%$ [107, 108]. Disadvantages with a pyranometer are that usually the price can be between 300 U.S. dollars and 1,800 U.S. dollars [108], the sensitivity may change with time and exposure to radiation [104], long periods of high temperature ($> 50°C$) can damage the accuracy of the instrument [106] and often the pyranometers need to be calibrated every day whenever there is significant change in weather conditions [106].

In addition to the solar irradiance, the temperature can affect the output of a PVM. The average temperature for a PVM should be measured using multiple thermocouples attached to the rear surface [111]. An advantage, thermocouples can measure a wide range of temperatures and are cheap and standard devices in the industry [112]. Thermocouples in photovoltaic applications are used mainly for safety reasons monitoring the average temperature variations in a PVM [106]. The main limitations using thermocouples are limitations in the range of accuracy, noise, connection problems, decalibration [112] and the positioning over the surface of the PVM, where it can affect the PVM performance, or under the PVM, where inaccurate measurements of the PVM temperature could be obtained [111].

To avoid the use of sensors and to solve the problems exposed before, this chapter proposes several Fixed-Point Iteration, FPI, algorithms using voltage and current measurements to calculate T and E_i over a PVM. These algorithms can be integrated with other algorithms related to MPPT (e.g. Linear Reoriented Coordinates Method, LRCM [62]) or to monitor the PVM performance [101]. The PVM mathematical model is described in the chapter, and it is based on the manufacturer data sheets [102]. Finally, this chapter describes the algorithms and compares the algorithm results to the measured results.

5.2 Algorithms to Estimate the Effective Irradiance Level and Temperature over a PVM

To understand the proposed algorithms and their validity, the following paragraphs will explain the definition and theorems related to Fixed-Point Iteration, FPI and their relationship with the PVM mathematical model. A fixed point is defined as a number x such that x is the solution of $x = g(x)$ [77]. *Theorem 5.1* and *Theorem 5.2* are the basis for the conditions of existence and uniqueness for the proposed algorithms.

Theorem 5.1 (*Fixed Point Existence*): Assume that $g(x)$ is continuous on $[a,\ b]$, and that $a \leq$ g(x) $\leq b\ \forall\ x \in [a,\ b]$ then $\exists$ a fixed-point c in $[a,\ b]$. The proof can be found in [77].

Theorem 5.2 (*Fixed Point Uniqueness*): Assume that $g(x)$ satisfies *Theorem 5.1*, $\partial g(x)/\partial x$ is continuous on $(a,\ b)$ and $\exists$ a positive constant $P < 1$ where $|g'(x)| \leq P$, then $g(x)$ has a unique fixed point c on $(a,\ b)$. The proof is in [77]. *Theorem 5.2* is also known as the *Contraction Mapping Theorem.*

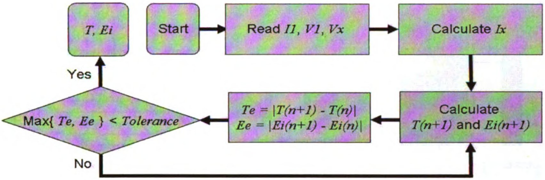

Figure 5.1. Flowchart for *Algorithm 5.1* to calculate T and E_i.

For additional FPI theorems, definitions and applications please refer to [77],[113] and [114]. Now the proposed algorithms will be presented with their descriptions and applications.

Algorithm 5.1: Fixed-Point Iteration to calculate T and E_i given Vx, V_1 and I_1. The algorithm considers the data provided by the PVM data sheet. Figure 5.1 shows the flowchart for *Algorithm 5.1*. The first step is to calculate Ix using (5.1). The second step is to iterate (5.2) and (5.3) to calculate T and E_i using T_N and E_{iN} as initial conditions.

$$Ix = \frac{I_1 - I_1 \cdot exp\left(\frac{-1}{b}\right)}{1 - exp\left(\frac{V_1}{b \cdot Vx} - \frac{1}{b}\right)} \tag{5.1}$$

$$\begin{aligned} T(n+1) &= T_N + \frac{E_i(n) \cdot (Vx - V_{max})}{TCV \cdot E_{iN}} + \frac{E_i(n)}{TCV \cdot E_{iN}} \\ &\cdot (V_{max} - V_{min}) \cdot exp\left(\frac{E_i}{E_{iN}} \cdot ln\left(\frac{V_{max} - V_{oc}}{V_{max} - V_{min}}\right)\right) \end{aligned} \tag{5.2}$$

$$E_i(n+1) = \frac{Ix \cdot E_{iN}}{I_{sc} + TCi \cdot (T(n) - T_N)} \tag{5.3}$$

Figure 5.2 presents an integrated PVM converter system using a DSP Board to control the maximum power to the load and to calculate T and E_{iN} without pyranometers or thermocouples. *Algorithm 5.1* is programmed to the DSP Board. Finally, the pro-

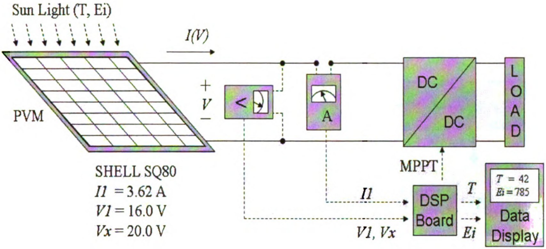

Figure 5.2. Integrated PVM converter system, using a DSP Board programmed with the *Algorithm 5.1.*

posed algorithm is able to find a unique solution for the effective irradiance level and temperature of operation over a PVM because (5.2) and (5.3) satisfy *Theorem 5.1* and *Theorem 5.2.*

Algorithm 5.2: This fixed iteration algorithm considers the use of Ix and Vx to calculate T and E_{iN}. First, *Algorithm 5.2* reads Ix and Vx then iterates (5.2) and (5.3) as presented on the *Algorithm 5.1* description.

Algorithm 5.3: Fixed-Point Iteration to Calculate T and E_i given V_1, V_2, I_1 and I_2. *Algorithm 5.3* is designed for a variable load with faster dynamics than T and E_i dynamics. The basic principle for *Algorithm 5.3* is the following: if the power in the load is changing but T and E_i are constants then the new operation point (V_2, I_2) will remain in the same I-V curve as the old operation point (V_1, I_1); hence, it is possible to calculate T and E_i. Figure 5.3 shows the flowchart for *Algorithm 5.3* where the first step is to read V_1, V_2, I_1 and I_2, as an initial value, $Vx(1)$ is equal to V_1 then iterate (5.4) and (5.5) to calculate Ix and Vx. Finally, Vx and Ix are sent

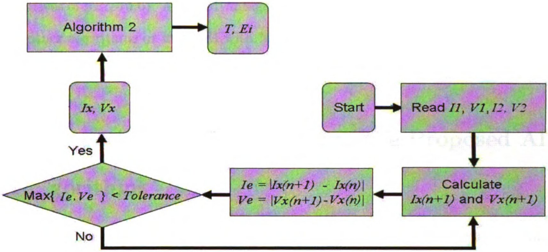

Figure 5.3. Flowchart for *Algorithm 5.3* to calculate Ix and Vx, integrated with *Algorithm 5.2.*

to *Algorithm 5.2* to calculate T and E_i.

$$Ix(n+1) = \frac{I_1 - I_1 \cdot exp\left(\frac{-1}{b}\right)}{1 - exp\left(\frac{V_1}{b \cdot Vx(n)} - \frac{1}{b}\right)} \tag{5.4}$$

$$Vx(n+1) = \frac{V_1}{1 + b \cdot ln\left[1 - \frac{I_1}{I_2} + \frac{I_1}{I_2} \cdot exp\left(\frac{V_2}{b \cdot Vx(n)} - \frac{1}{b}\right)\right]} \tag{5.5}$$

Algorithm 5.4: Fixed-Point Iteration to calculate E_i and Ix given Vx, and T. *Algorithm 5.4* is designed using the fact that the thermocouples are cheap. Hence using one sensor for the open circuit voltage, it is possible to calculate E_i. The algorithm reads T and Vx then iterates (5.6) to find E_i.

$$E_i(n+1) = \frac{(T - T_N) \cdot TCV \cdot E_{iN}}{Vx - V_{max} + (V_{max} - V_{min}) \cdot \left(\frac{V_{max} - V_{oc}}{V_{max} - V_{min}}\right)^{\frac{E_i(n)}{E_{iN}}}} \tag{5.6}$$

Finally, the proposed algorithms are valid to calculate T and E_i because *Theorem 5.1* and *Theorem 5.2* are satisfied due the continuity of the functions and partial derivatives of (5.2)-(5.6). As an advantage, the proposed algorithms can be integrated with other algorithms or methods with MPPT without affecting the performance of the PVM.

5.3 Experimental Results using the Proposed Algorithms

The electric specifications for four PVM (Table 2.1 and Table 2.2) were used to validate and test the proposed algorithms. Figure 5.2 shows an integrated PV converter system where *Algorithm 5.1* and *Algorithm 5.2* were simulated. Table 5.1 and Table 5.3 show the measured and expected parameters for the four PVM's using *Algorithm 5.1* and *Algorithm 5.2* respectively. The results for the *Algorithm 5.1* and *Algorithm 5.2* are given in the Table 5.2 and Table 5.4 respectively. The number of iterations required to calculate T and E_i were less than 5 for both algorithms. The maximum relative error to approximate E_i is less than 3% and the maximum absolute error between the measured T and the calculated T was only ±6°C showing a good performance. Also, the algorithms converge very fast with a good performance with the uniqueness property presented in *Theorem 5.2*. The LRCM [62] was integrated with *Algorithm 5.2* to approximate the maximum power produced by the PVM's on real time conditions, *Pap* as shown in Table 5.4. Finally, these algorithms can track the meteorological conditions for a long term because the collected data can be stored and recorded without interfering with the PVM performance.

Table 5.1. Measured Values for *Algorithm 5.1*

Datasheet	I_1	V_1	Vx	E_i	T
Siemens SP75	$3.00A$	$18.0V$	$19.8V$	$1,000W/m^2$	$45°C$
Shell SQ80	$3.62A$	$16.0V$	$20.0V$	$800W/m^2$	$46°C$
SLK60M6	$8.20A$	$10.0V$	$35.0V$	$1,100W/m^2$	$50°C$
Solarex SA-5	$0.28A$	$19.5V$	$25.3V$	$1,000W/m^2$	$20°C$

Table 5.2. Calculated Values using *Algorithm 5.1*

Datasheet	$Iterations(n)$	$E_i(Appr.)$	$T(Appr.)$
Siemens SP75	5	$955.7W/m^2$	$47.976°C$
Shell SQ80	4	$785.7W/m^2$	$42.271°C$
SLK60M6	4	$1,084W/m^2$	$44.045°C$
Solarex SA-5	4	$966.5W/m^2$	$19.552°C$

Table 5.3. Measured Values for *Algorithm 5.2*

Datasheet	I_1	V_1	Vx	E_i	T
Siemens SP75	$3.00A$	$18.0V$	$19.8V$	$1,000W/m^2$	$45°C$
Shell SQ80	$3.62A$	$16.0V$	$20.0V$	$800W/m^2$	$46°C$
SLK60M6	$8.20A$	$10.0V$	$35.0V$	$1,100W/m^2$	$50°C$
Solarex SA-5	$0.28A$	$19.5V$	$25.3V$	$1,000W/m^2$	$20°C$

Table 5.4. Calculated Values using *Algorithm 5.2*

Datasheet	$Iterations(n)$	$E_i(Appr.)$	$T(Appr.)$	Pap
Siemens SP75	5	$795.4W/m^2$	$44.980°C$	$64.7W$
Shell SQ80	4	$810.3W/m^2$	$42.845°C$	$60.9W$
SLK60M6	4	$794.7W/m^2$	$39.204°C$	$162W$
Solarex SA-5	4	$1,015W/m^2$	$72.656°C$	$5.12W$

CHAPTER 6

Proposed PV Power Applications

In this chapter, several PV applications will be shown like a PVM connected to different loads, an additional MPPT algorithm and other PV applications. The first sections show how to analyze a PV circuit using the PVM model given in Chapter 2. The MPPT algorithm proposed in this chapter is based in the control of the optimal duty cycle for a dc-dc converter and the previous knowledge of the load or load matching conditions. The procedure to calculate the optimal duty ratio for a buck, boost and buck-boost converters, to transfer the maximum power or required power, from a PVM to a load is presented in this chapter. Additionally, the existence and uniqueness of the optimal internal impedance, to transfer the maximum power from a PVM using load matching and how to obtain it using the optimal duty ratio, is shown. Finally, a Photovoltaic Inverter System, PVIS, is proposed for single-phase power applications. The proposed PVIS has three stages, a photovoltaic module connected to a buck-boost converter and a resonant Z-source converter. The PVIS takes into consideration changes in temperature and irradiance level, the dynamic model for a PVM, buck-boost converter model, Z-source converter operation principle in resonance to provide a frequency of 50Hz and voltage output (rms) of 120V.

6.1 Introduction

In the previous chapters, solutions were provided to many problems in the area of PV power systems, which includes better modeling to describe a PVM, improved algorithms to track the maximum power from a PVM, better design and control PV inverter systems, more accurate methods to estimate the temperature and effective irradiance level over the PVM, etc.

It is the purpose of this chapter to provide several PV applications related to the area of power systems. The first sections should be consider as a guidance for PV circuit analysis some of the examples are a PVM connected to a resistance, RLC load. Also, it is shown that the analysis for two PV arrays, with different electrical characteristics, connected in series to a power load. The following section will show how to calculate the optimal duty ratio for a dc-dc converter using the PVM electrical characteristics and the load matching conditions.

Finally, the last section of this chapter will be propose a transformer-less photovoltaic inverter system for single phase applications. Figure 6.1 shows the typical configuration for a photovoltaic inverter system. The main components are a PV array, a dc-dc converter to keep the PVM operating at the maximum power, an inverter to match the required frequency and to convert the dc voltage to ac voltage, a transformer to amplify and keep the desired output voltage and filters to clean the noise and reduction of harmonics.

Disadvantages with this configuration are the use of transformers, which are usually expensive, will decrease the efficiency, heavy and physically large [115]! To achieve good performance with this configuration, several sensors and a control design which takes into consideration the synchronization between the different current, voltages, maximum power and effects of the environment over the PVM are required. To avoid the use of transformers, minimize the number of required components, and to operate the PVM in the optimal performance under changes in T and E_i, it is proposed in

T

c

o

G

fi

di

th

pow

T

Tables

voltage

t

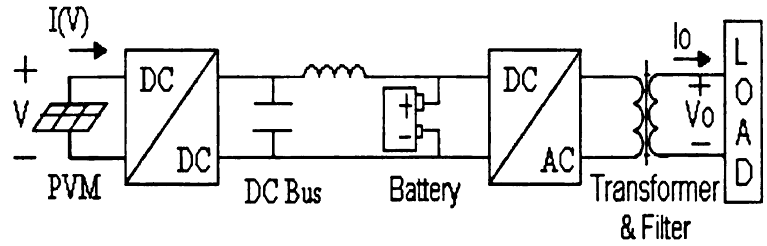

Figure 6.1. PV Inverter System for utility applications.

this chapter a dynamic photovoltaic inverter system using a resonant Z-source converter. The PV array will have the function to supply power to the load and to charge the batteries. The resonant Z-source converter will have two functions to reduce or eliminate the harmonics, and to amplify the ac voltage to the required rated voltage.

6.2 LRCM and FPM applied to commercial PV modules

This section details additional commercial PV modules not presented in the previous chapters. These commercial PV modules were added as a reference material. Some of the PVM manufacturers are UniSolar (US), SunWize (OEM, SW), BP Solar (BP), GE Photovoltaic (GEPV), Sanyo (ND, NE), Sharp (HIP, PC). The electrical specifications of each PVM under STC were evaluated using the Linear Reoriented Coordinates Method (LRCM) and Fractional Polynomial Method (FPM) to approximate the optimal current, the optimal voltage, the optimal resistance, and the maximum power.

Table 6.1 shows the electrical specifications for additional PV modules under STC. Tables 6.2 and 6.3 show the approximations of the optimal current, I_{op}, the optimal voltage, V_{op}, the optimal resistance, R_{op} and the maximum power, P_{max}.

Table 6.1. Electrical specifications for commercial PV modules under STC

PVM Model	$I_{sc}(A)$	$V_{oc}(V)$	$I_{op}(A)$	$V_{op}(V)$	R_{op} (Ω)	P_{max} (W)	b
US-3	0.40	12.0	0.33	8.1	24.55	2.67	0.1890
US-5	0.37	23.8	0.30	16.5	55.00	4.95	0.1864
OEM5	0.38	20.5	0.31	16.4	52.90	5.08	0.1183
SWPV-10	0.66	21.0	0.59	16.8	28.47	9.91	0.0891
OEM10	0.70	21.0	0.61	16.4	26.89	10.00	0.1068
US-11	0.78	23.8	0.62	16.5	26.61	10.23	0.1966
OEM20	1.38	21.0	1.22	16.5	13.52	20.13	0.0995
SWPV-20	1.21	21.0	1.19	16.8	14.12	19.99	0.0487
SX-20	1.29	21.0	1.19	16.8	14.12	19.99	0.0782
US-21	1.59	23.8	1.27	16.5	12.99	20.96	0.1941
SX-30	1.94	21.0	1.78	16.8	9.44	29.90	0.0802
US-32	2.40	23.8	1.27	16.5	8.51	32.01	0.1880
BP340	2.54	21.8	2.31	17.3	7.49	39.96	0.0859
OEM40	2.68	21.0	2.40	16.7	6.96	40.08	0.0907
US-42	3.17	23.8	2.54	16.5	6.50	41.91	0.1925
BP350	3.17	21.8	2.89	17.3	5.99	50.00	0.0851
SW50	3.40	21.0	3.05	16.4	5.38	50.02	0.0964
GEPV-050	3.30	22.0	2.90	17.3	5.97	50.17	0.1013
SW55	3.65	21.0	3.30	16.7	5.06	55.11	0.0873
SW60	3.95	21.0	3.60	16.7	4.64	60.12	0.0845
US-64	4.80	23.8	3.88	16.5	4.25	64.02	0.1880
BP365	3.99	22.1	3.69	17.6	4.77	64.94	0.0787
GEPV-072	4.80	21.0	4.40	17.0	3.86	74.80	0.0767
BP375	4.75	21.8	4.35	17.3	3.98	75.25	0.0834
NE-80U1	5.30	21.3	4.67	17.1	3.66	79.86	0.0926
BP375	4.80	22.1	4.55	17.6	3.87	80.08	0.0689
SW85	5.70	21.4	4.88	17.4	3.57	84.91	0.0964
SW90	5.90	21.4	5.17	17.4	3.37	89.96	0.0895
SW100	6.70	21.0	6.00	16.7	2.78	100.20	0.0907
SW115	7.70	21.0	6.89	16.7	2.42	115.06	0.0909
US-116	4.80	43.2	3.88	30.0	7.73	116.40	0.1872
SW120	8.00	21.0	7.18	16.7	2.33	119.91	0.0899
ND-L3EIU	8.10	21.3	7.16	17.2	2.40	123.15	0.0894
BP3160	4.80	44.2	4.55	35.1	7.71	159.71	0.0697
165-PC	5.40	44.5	4.72	35.0	7.42	165.20	0.1031
175-PC	5.43	44.6	4.95	35.4	7.15	175.23	0.0850
HIP-190BA3	3.75	67.5	3.47	54.8	15.79	190.16	0.0725

Table 6.2. PVM parameter approximation using the LRCM under STC

PVM Model	$I_{ap}(A)$	$V_{ap}(V)$	R_{ap} (Ω)	P_{ap} (W)
US-3	0.3264	8.2100	25.1514	2.6799
US-5	0.3028	16.3261	53.9246	4.9428
OEM5	0.3351	15.3231	45.7229	5.1352
SWPV-10	0.6012	16.4744	27.4037	9.9040
OEM10	0.6253	15.9827	25.5605	9.9938
US-11	0.6315	16.1608	25.5898	10.2060
OEM20	1.2428	16.1791	13.0183	20.1073
SWPV-20	1.1510	17.9072	15.5578	20.6115
SX-20	1.1891	16.8145	14.1404	19.9943
US-21	1.2907	16.2004	12.5519	20.9095
SX-30	1.7845	16.7519	9.3874	29.8939
US-32	1.9606	16.3000	8.3137	31.9582
BP340	2.3217	17.2020	7.4092	39.9383
OEM40	2.4371	16.4296	6.7415	40.0402
US-42	2.5776	16.2264	6.2953	41.8244
BP350	2.9004	17.2300	5.9406	49.9734
SW50	3.0725	16.2656	5.2939	49.9760
GEPV-050	2.9660	16.8983	5.6973	50.1209
SW55	3.3313	16.5285	4.9616	55.0605
SW60	3.6163	16.6155	4.5946	60.0863
US-64	3.9212	16.3000	4.1568	63.9164
BP365	3.6761	17.6790	4.8092	64.9890
GEPV-072	4.4321	16.8655	3.8053	74.7490
BP375	4.3538	17.2828	3.9696	75.2453
NE-80U1	4.8094	16.6070	3.4530	79.8691
BP375	4.4692	18.0263	4.0334	80.5639
SW85	5.1506	16.5738	3.2178	85.3657
SW90	5.3723	16.7788	3.1232	90.1411
SW100	6.0927	16.4296	2.6966	100.1006
SW115	6.9999	16.4215	2.3459	114.9495
US-116	3.9244	29.6099	7.5450	116.2013
SW120	7.2809	16.4520	2.2596	119.7864
ND-L3EIU	7.3761	16.7026	2.2644	123.2011
BP3160	4.4656	35.9961	8.0608	160.7430
165-PC	4.8439	34.0784	7.0354	165.0711
175-PC	4.9683	35.2525	7.0955	175.1454
HIP-190BA3	3.4781	54.6566	15.7146	190.1003

Table 6.3. PVM parameter approximation using the FPM under STC

PVM Model	$I_{opf}(A)$	$V_{opf}(V)$	R_{opf} (Ω)	P_{maf} (W)	n	q
US-3	0.3264	8.1922	25.0989	2.6739	4	0.4346
US-5	0.3033	16.3270	53.8355	4.9516	4	0.5452
OEM5	0.3357	15.4388	45.9875	5.1831	7	0.5811
SWPV-10	0.6003	16.5362	27.5466	9.9267	10	0.0552
OEM10	0.6247	16.0512	25.6940	10.0272	8	0.2966
US-11	0.6335	16.1670	25.5200	10.2418	4	0.3244
OEM20	1.2411	16.2410	13.0861	20.1566	8	0.9345
SWPV-20	1.1476	17.8728	15.5743	20.5105	18	0.3857
SX-20	1.1865	16.8510	14.2026	19.9931	11	0.4600
US-21	1.2943	16.2054	12.5210	20.9740	4	0.3764
SX-30	1.7808	16.7929	9.4302	29.9040	11	0.1824
US-32	1.9644	16.3018	8.2986	32.0232	4	0.5096
BP340	2.3170	17.2489	7.4446	39.9650	10	0.3884
OEM40	2.4332	16.4876	6.7761	40.1176	9	0.8588
US-42	2.5841	16.2306	6.2809	41.9419	4	0.4107
BP350	2.8943	17.2748	5.9687	49.9976	10	0.4959
SW50	3.0665	16.3139	5.3200	50.0272	9	0.1959
GEPV-050	2.9626	16.9680	5.7274	50.2691	8	0.7803
SW55	3.3251	16.5792	4.9861	55.1268	10	0.2331
SW60	3.6088	16.6597	4.6164	60.1221	10	0.5779
US-64	3.9288	16.3018	4.1493	64.0465	4	0.5096
BP365	3.6673	17.7131	4.8300	64.9600	11	0.3659
GEPV-072	4.4238	16.9115	3.8228	74.8133	11	0.7596
BP375	4.3441	17.3237	3.9879	75.2558	10	0.7024
NE-80U1	4.8045	16.6816	3.4721	80.1473	9	0.6970
BP375	4.4566	18.0357	4.0470	80.3783	12	0.9784
SW85	5.1504	16.6728	3.2372	85.8709	9	0.3703
SW90	5.3684	16.8620	3.1410	90.5222	10	0.0989
SW100	6.0830	16.4876	2.7104	100.2939	9	0.8588
SW115	6.9889	16.4801	2.3580	115.1785	9	0.8289
US-116	3.9321	29.6166	7.5320	116.4548	4	0.5305
SW120	7.2689	16.5084	2.2711	119.9976	9	0.9422
ND-L3EIU	7.3685	16.7770	2.2768	123.6220	10	0.0737
BP3160	4.4526	36.0123	8.0879	160.3497	12	0.8183
165-PC	4.8392	34.2271	7.0729	165.6308	8	0.6285
175-PC	4.9579	35.3444	7.1290	175.2325	10	0.5008
HIP-190BA3	3.4712	54.7818	15.7820	190.1561	12	0.4484

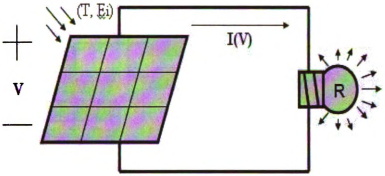

Figure 6.2. PVM connected to an incandescent light bulb.

6.3 PV modules connected to resistive loads

Figure 6.2 shows a PVM connected to a light bulb. It is desired to calculate the power, current, and voltage supplied by the PVM to a 350Ω light bulb under STC conditions. The PVM parameters are I_{sc} is 0.0182A, V_{oc} is 8.0V and b is 0.10. Using Kirchoff's Voltage Law, it is possible to set the relationship between the current supplied by the PVM and received by the light bulb as given in (6.1).

$$I(V) = 0.0185 - 0.0185 \cdot \exp(1.25 \cdot V - 10) = \frac{V}{R} \tag{6.1}$$

The supplied voltage is calculated using numerical analysis where $V = 5.9177V$, V is then substituted in (6.1) where $I(5.9177) = 0.0169A$. Finally, the power supplied to the load is $0.1W$.

Figure 6.3 shows a $150W$ load connected to two different PV arrays at $25°C$ and $900W/m^2$. Remembering the definition for a PV array, the interconnection of two or more PV modules with the same electrical characteristics in series (s) or parallel (p), the dimension for the PV array is given by ($s \times p$) and the total amount of PV modules that form the PV array can be calculated multiplying s by p. The array PV1 has 9 (i.e. 3×3) SX-10 PV modules connected in 3 series ($s = 3$) and 3 parallel ($p = 3$)

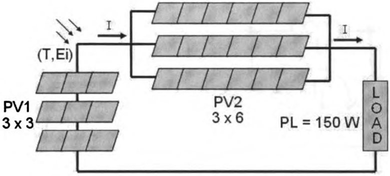

Figure 6.3. Two distinct PV Arrays connected in series to a 150W load.

for each series. The array PV2 has 18 (i.e. 3×6) SA-5 PV modules connected in 3 series ($s = 3$) and 6 parallel ($p = 6$) for each series. The electrical characteristics for the PV modules SA-5 and SX-10 are give by the Table 2.1. The relationship between the power supplied by the two PV arrays connected in series and the $150W$ load, is given by (6.2).

$$P(V) = 50 \cdot I - 5 \cdot \cdot I \ln(1 - 0.5 \cdot I) + 57 \cdot I - 5.7 \cdot I \ln(1 - 0.556 \cdot I) = 150W \quad (6.2)$$

Using numerical analysis, it can be found that the current supplied by both PV arrays is $I = 1.4874A$, the voltage supplied by the array PV1 is $49.018V$ and for the array PV2 is $51.832V$. Finally, the power produced by the array PV1 is $72.905W$ and by the array PV2 is $77.095W$. It is important to notice that both arrays are operating at the combined power required by the load and not operating at their maximum power levels.

6.4 PVM connected to a RLC Load

Figure 6.4 shows a PVM, Solarex SX-10, under STC connected to a transmission line, L_x, to supply $7.5W$ to a RLC load. The dynamic equations for the PVM connected

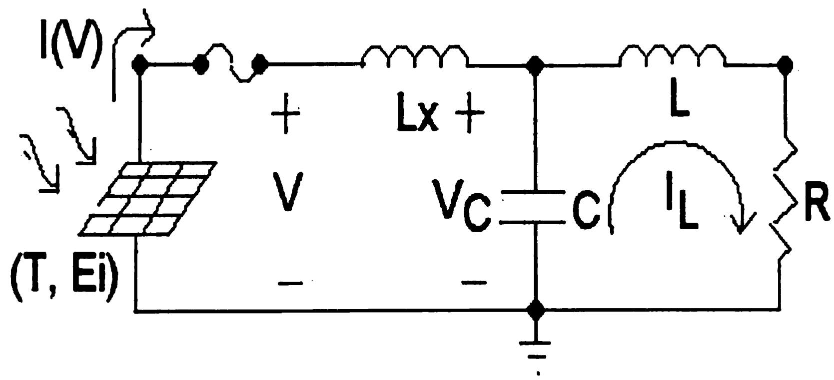

Figure 6.4. PVM connected to a RLC load.

to a RLC load are given by (6.3) - (6.5) with state variables V_C, I_L and I. The voltage produced by the PVM (6.6) is calculated using the inverse of (2.10) with respect to the current, I where the internal resistance, Cx is zero. The supplied apparent power $S(t)$ is calculated by multiplying (6.6) and the solution of (6.5) with respect to the current.

$$\frac{\partial V_C}{\partial t} = \frac{I - I_L}{C} \tag{6.3}$$

$$\frac{\partial I_L}{\partial t} = \frac{V_C - R \cdot I_L}{L} \tag{6.4}$$

$$\frac{\partial I}{\partial t} = \frac{V - V_C}{L_x} \tag{6.5}$$

$$V = Vx + b \cdot Vx \cdot \ln\left[1 - \frac{I}{Ix} + \frac{I}{Ix} \cdot \exp\left(-\frac{1}{b}\right)\right] \tag{6.6}$$

$$S(t) = V \cdot I = P(t) + j \cdot Q(t) \tag{6.7}$$

Simulations were done using Simulink to observe the performance of a PVM connected to an RLC load. The parameters for the SX-10 are $Ix = 0.65A$, $Vx = 21.0V$, $b = 0.8394$, the transmission line L_x is $160\mu H$, and the load parameters are L is $160\mu H$, C is $1000\mu F$ and R is 50Ω.

Figures 6.5 - 6.10 show the simulation waveforms of how the power, voltage, and

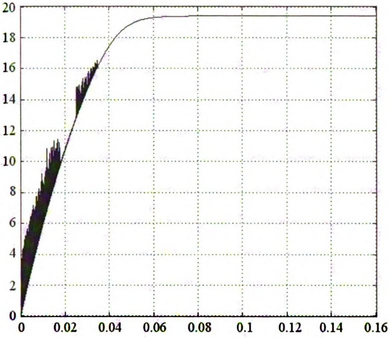

Figure 6.5. PVM SX-10 supplied voltage, V vs. t.

current are changing over time for the PVM connected to an RLC load. Figures 6.5 and 6.8 show the supplied voltage by the PVM and the voltage for the RL load. It is clear that the supplied voltage waveforms have harmonics injected to the PVM by the load. Also, the voltage in the RL load is a smooth waveform without ripple. Figures 6.6 and 6.9 show the supplied current and the load current where a small ripple produced by the change of the voltage in the load current.

The supplied and output power are shown in figures 6.7 and 6.10. Figure 6.10 shows the supplied power reaching the maximum power and then stabilizing to the requiered power for the load. The power in the load is increased and stabilized up to the required level with a small ripple. Finally, these simulations are consistent with the theoretical analysis and, at the same time, prove the effect of nonlinear loads in a photovoltaic module.

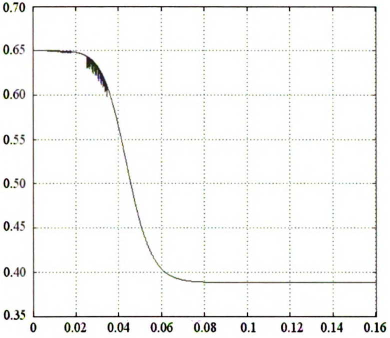

Figure 6.6. PVM SX-10 supplied current, I vs. t.

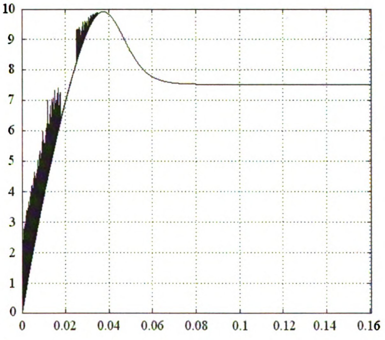

Figure 6.7. PVM SX-10 supplied power, $I \cdot V$ vs. t.

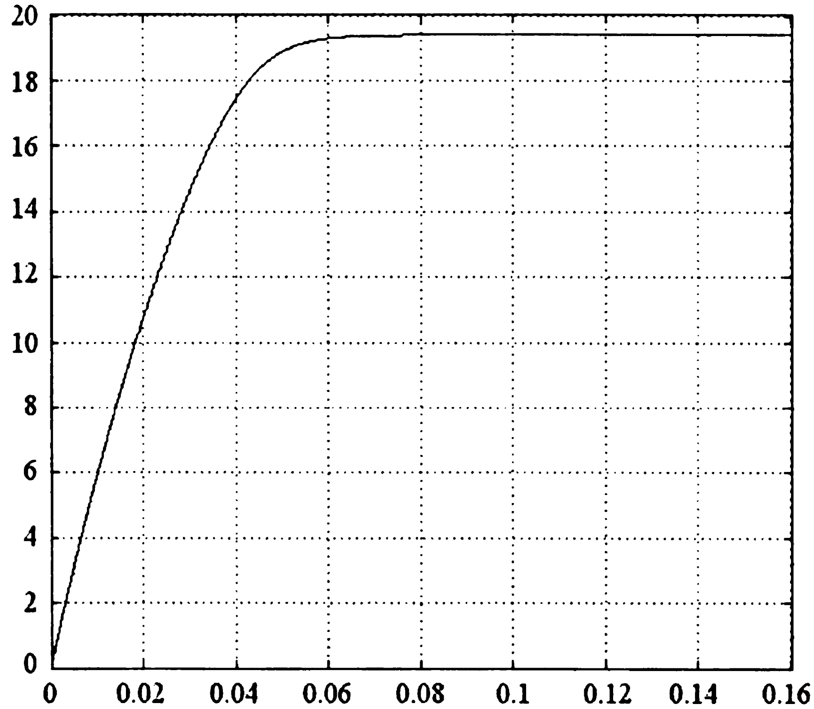

Figure 6.8. V_C Load Voltage, V_C vs. t.

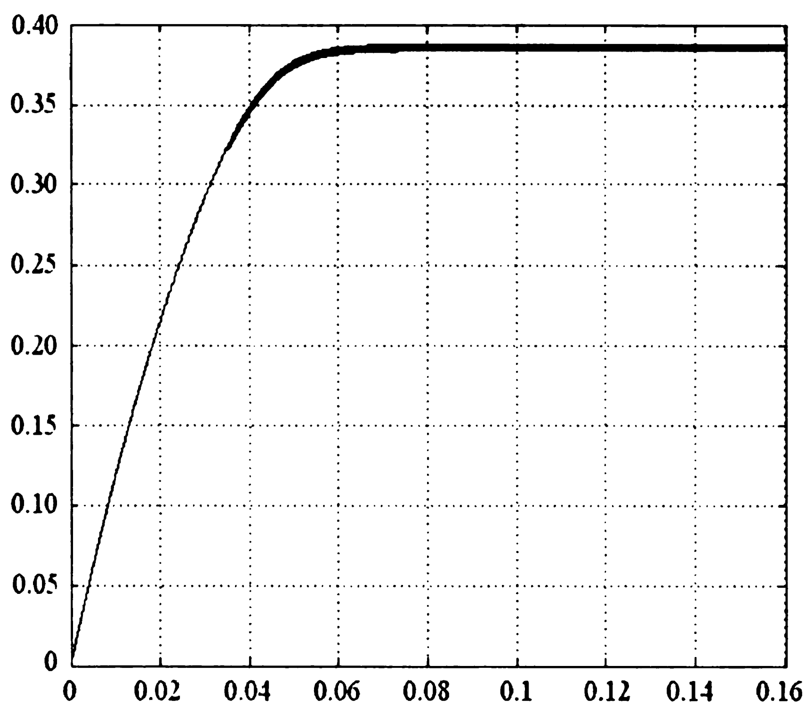

Figure 6.9. I_L Load Current, I_L vs. t.

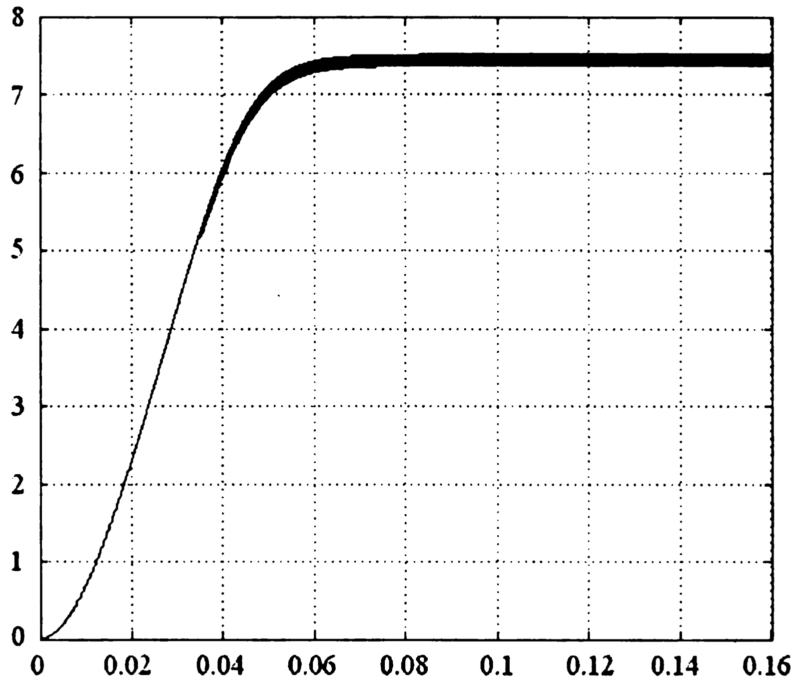

Figure 6.10. $I_L \cdot V_C$ Load Power, $I_L \cdot V_C$ vs. t.

6.5 Optimal Duty Ratio for a dc-dc Converter for PV Applications

Consider a PVM connected to a buck-boost converter to supply power to a resistive load. The objective is to calculate the optimal duty ratio, D, so the PVM will supply P_{max}. The analysis will be done using the steady-state conditions for a buck-boost converter, where all the components are ideal, the inductor current is continuous, the capacitor is large enough to assume a constant output voltage and the switch is closed for time D/f and open for $(1 - D)/f$, where f is the frequency. An advantage of the buck-boost converter is that the magnitude of the output voltage can be either greater than or less than the source voltage, depending on the duty ratio of the switch [116], making it excellent for photovoltaic applications where the weather conditions are changing very fast. The only minor disadvantage for the buck boost converter is the polarity reversal on the output.

The first step for load matching will be done using the relationship between the voltage input and output for a buck-boost converter relationship. The load resistance R_o can be seen as voltage output, V_o, divided by current output, I_o. Using this information, the relationship between the input resistance, R_i, and the output resistance, R_o, is given by (6.8). If V is V_{op}, hence R_i is R_{op}, the optimal duty cycle, D, can be solved. The optimal duty ratio, D, is obtained and only depends on R_o and R_{op}. Switching at the optimal duty ratio guarantees that the power supplied to load is P_{max}.

$$R_o = \frac{V_o}{I_o} = \frac{-D \cdot V_i}{(1-D) \cdot I_o} = \frac{D^2 \cdot V_i}{(1-D)^2 \cdot I_i} = \frac{D^2 \cdot R_i}{(1-D)^2} \tag{6.8}$$

Using (6.8), the optimal duty ratio, D, as a relationship of the optimal resistance, R_{op}, and output resistance, R_o, can be solved and is given in (6.9). Additionally, if the power input and the power output are both P_{max} i.e. $Pi = Po = Pmax$, D can be expressed as a relationship between the optimal voltage, V_{op}, and the output voltage, V_o as given in (6.10).

$$D = \frac{\sqrt{R_o}}{\sqrt{R_o} + \sqrt{R_{op}}} \tag{6.9}$$

$$D = \frac{V_o}{V_o + V_{op}} \tag{6.10}$$

For design purposes, the minimum inductance L_{min} for the buck-boost converter to preserve the continuous current mode using the optimal duty cycle is given in (6.11). The voltage output ripple using the optimal duty cycle is given in (6.12).

$$L_{min} = \frac{R \cdot (1-D)^2}{2 \cdot f} = \frac{R_o \cdot R_{op}}{2 \cdot f \cdot \left(\sqrt{R_o} + \sqrt{R_{op}}\right)^2} < \frac{R_o}{2 \cdot f} \tag{6.11}$$

$$V_{oripple} = \frac{D}{f \cdot C \cdot R_o} = \frac{1}{C \cdot f \cdot \left(R_o + \sqrt{R_o \cdot R_{op}}\right)} \tag{6.12}$$

The same type of procedure is done to calculate the duty cycle for the buck converter or boost converter. Table 6.4 shows the conditions and optimal duty ratio for a buck converter, boost converter and buck-boost converter. The only disadvantage of using a buck or boost converter is the restriction in the values of R_{op} and R_o for both cases.

Table 6.4. Optimal Duty Ratio for Different dc-dc Converters for Load Matching

Converter	for $P_o \leq P_{max}$	for $P_i = P_o = P_{max}$	Conditions
Buck-Boost	$D = \frac{\sqrt{R_o}}{\sqrt{R_o}+\sqrt{R_{op}}}$	$D = \frac{V_o}{V_o+V_{op}}$	none
Boost	$D = 1 - \sqrt{\frac{R_{op}}{R_o}}$	$D = 1 - \frac{V_{op}}{V_o}$	$R_o > R_{op}$
Buck	$D = \sqrt{\frac{R_{op}}{R_o}}$	$D = \frac{V_{op}}{V_o}$	$R_{op} > R_o$

Finally, this method for load matching can be integrated to other algorithms such that the linear reoriented coordinates method, LRCM, which was described in details in Chapter 3. Using the LRCM, the optimal resistance, R_{op}, is calculated under any changes in T or E_i. Also, R_{op} can be calculated using Ix and Vx as given in Chapter 4 using fractional polynomials, then the optimal duty ratio is calculated using the Table 6.4 to control the dc-dc converter and transfer the desired P from the PVM to the load.

6.6 Algorithm and Simulations for a dc-dc Converter using Load Matching

Figure 6.11 shows a proposed algorithm measuring E_i and T to obtain the optimal duty cycle for load matching. Figure 6.12 shows a photovoltaic system with a dc-dc

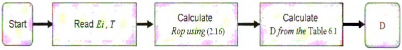

Figure 6.11. Algorithm to calculate the optimal duty ratio given E_i and T.

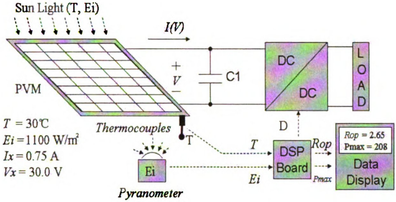

Figure 6.12. Integrated PV power system using load matching and the optimal duty ration given E_i and T.

converter to supply power to a load, using a pyranometer to measure the irradiance level and thermocouples to measure the temperature over the PVM surface. The photovoltaic system has a Sharp ND-208U1 PVM with P_{max} is $208W$, R_{op} is 2.65Ω, V_{op} is $23.48V$, Ix is $0.75A$, Vx is $30V$ and b is 0.1, connected to a dc bus with capacitance $400\mu F$. The dc-dc converter is a $50kHz$ buck-boost converter with inductance $100\mu H$ and capacitance $400\mu F$, and the resistive load is 0.75Ω. Figures 6.13 and 6.14 show the transient results simulations for the photovoltaic system and the dc-dc converter connected to a load. The simulations were done using Simulink. These results show how effective the proposed method can be to calculate the optimal duty ratio to deliver the required power (e.g. P_{max}) using load matching.

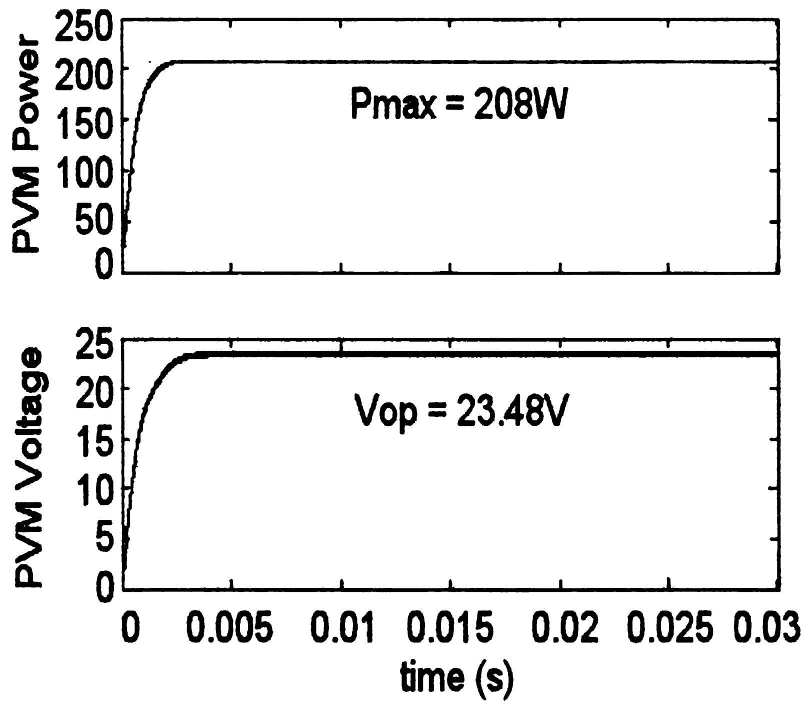

Figure 6.13. PVM power and voltage with respect to the time.

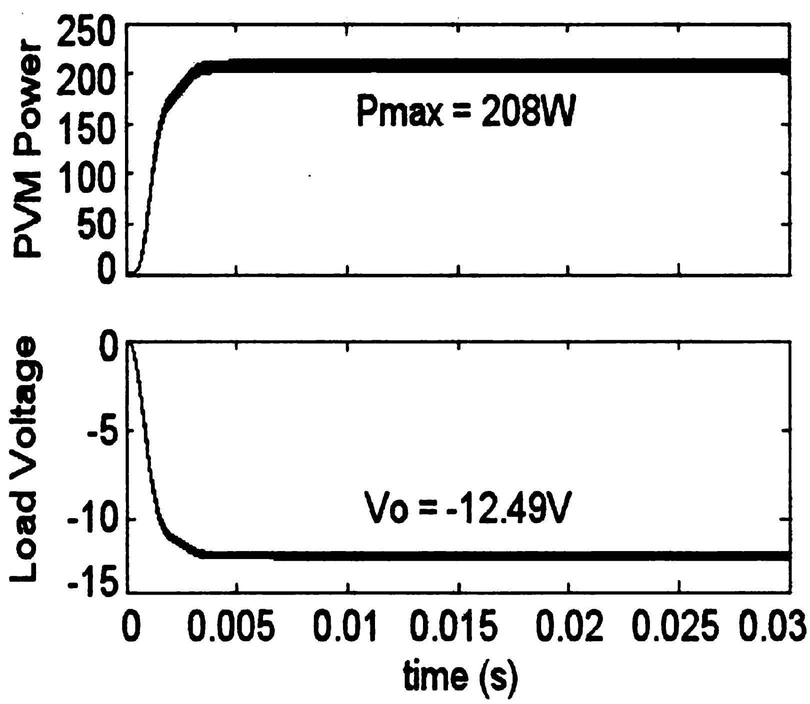

Figure 6.14. Load power and voltage with respect to the time.

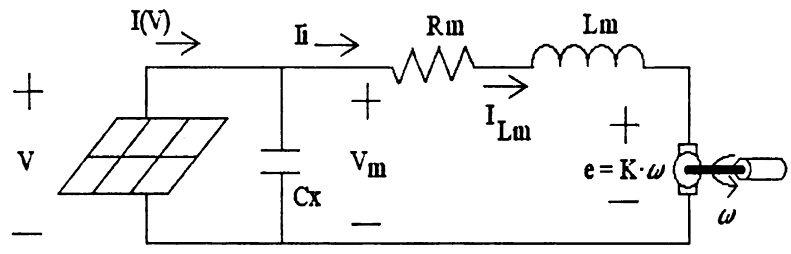

Figure 6.15. PVM connected directly to a dc motor.

6.7 PVM connected to a dc motor

Figure 6.15 shows a PVM connected to a dc motor. Using figure 6.15, the dynamic equations for the system are given by (6.13), (6.15), and (6.14) where Ii is equal to IL and Vm is equal to V. The variable Lm is the armature inductance (H), Rm is armature resistance (Ω), w is the rotor speed (rad/s), Vm is the dc motor terminal voltage (V), I_{Lm} is the dc motor armature current (A), T_L is the load torque ($N \cdot m$), J is the rotor inertia (N/m^2), K is the torque and back emf constant (NmA^{-1}), d is the damping constant (Nms). Now, consider a dc motor with the following parameters Lm is $55mH$, Rm is 7.56Ω, J is $0.068N/m^2$, d is $0.03475Nms$, T_L is zero, and K is $3.475NmA^{-1}$ connected to a PV array of 16 SX-20 PVM's under STC with parameters Ix is $1.29A$, Vx is $21V$, b is 0.0782,p is 4 and s is 4. Simulink was used to simulate the dynamic equations (6.13), (6.15), and (6.14). The results are shown in the figure 6.16. At steady state, the dc motor will be running at $62rad/s$ with a supplied PV power of $285W$ and voltage operation of $89V$. Unfortunately, a PV array connected directly to a dc motor cannot be set to a desired speed electronically. The only way to control the speed is by increasing or decreasing the temperature or effective irradiance level making this type of PV system very impractical.

$$\frac{\partial V}{\partial t} = \frac{Ix}{Cx - Cx \cdot exp\left(\frac{-1}{b}\right)} \cdot \left[1 - exp\left(\frac{V}{b \cdot Vx} - \frac{1}{b}\right)\right] - \frac{I_i}{Cx} \tag{6.13}$$

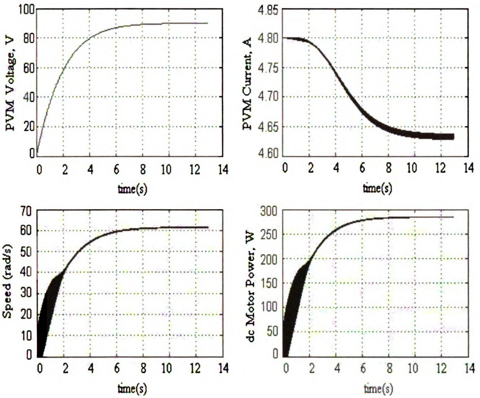

Figure 6.16. Results of SX-20 PV array connected to a dc motor.

$$\frac{\partial w}{\partial t} = \frac{K \cdot I_{Lm}}{J} - \frac{d \cdot w}{J} - \frac{T_L}{J} \tag{6.14}$$

$$\frac{\partial I_{Lm}}{\partial t} = \frac{Vm}{Lm} - \frac{Rm \cdot I_{Lm}}{Lm} - \frac{K \cdot w}{Lm} \tag{6.15}$$

Figure 6.17 shows a PVM connected to a buck-boost converter and a dc motor. Using a buck-boost converter, a dc motor can be controlled to achieve a desired speed. It should be noted that, the maximum speed for a dc motor will depend in the maximum power provided by the PV array. The dynamic equations that describe the figure 6.17 are given by (6.13), (6.15), (6.14), (6.16), (6.17) and (6.18).

$$I_i = S \cdot I_L \tag{6.16}$$

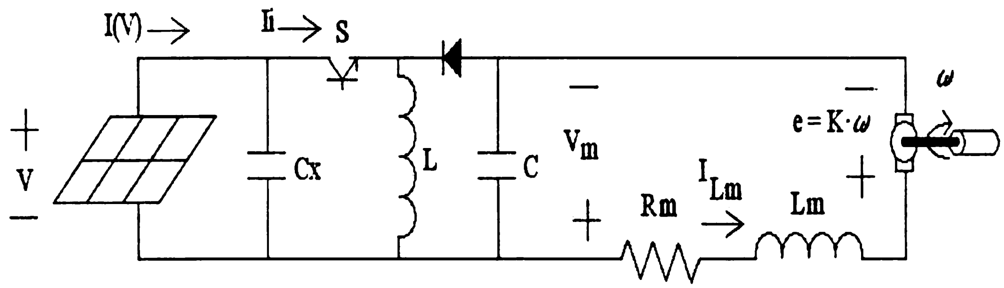

Figure 6.17. PVM connected to a buck-boost converter and a dc motor.

$$\frac{\partial I_L}{\partial t} = \frac{S-1}{L} \cdot Vm + \frac{S}{L} \cdot V \tag{6.17}$$

$$\frac{\partial Vm}{\partial t} = \frac{1-S}{C} \cdot I_L + \frac{I_{Lm}}{C} \tag{6.18}$$

The speed tracking control design is based on the fixed duty ratio, D, to control the buck-boost converter. The fixed duty ratio, D, is calculated using Table 6.4 and the steady state performance of the dc motor as given by (6.19), (6.20) and (6.21). The variable I_{Lm*} is the steady state armature current, wr is the steady state speed, $Vm*$ is the steady state terminal voltage for the dc motor, $P*$ is the power that should be supplied from the PVM to the dc motor for speed wr. Also, the the internal steady state resistance for the dc motor, $R*$, is given by (6.22).

$$I_{Lm*} = \frac{d \cdot wr}{K} + \frac{T_L}{K} \tag{6.19}$$

$$Vm* = Rm \cdot I_{Lm*} + K \cdot wr = \left(\frac{Rm \cdot d}{K} + K\right) \cdot wr + \frac{Rm}{K} \cdot T_L \tag{6.20}$$

$$\begin{aligned} P* &= I_{Lm*} \cdot Vm* = Rm \cdot I_{Lm*}^2 + K \cdot I_{Lm*} \cdot wr \\ &= \left(\frac{d^2}{K^2} \cdot Rm + d\right) \cdot wr^2 + \left(\frac{2 \cdot Rm \cdot d}{K^2} + 1\right) \cdot wr \cdot T_L + \frac{Rm}{K^2} \cdot T_L^2 \end{aligned} \tag{6.21}$$

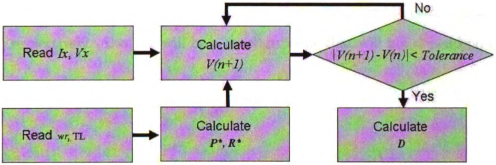

Figure 6.18. Algorithm to calculate the fixed duty ratio, D, using the FPT.

$$R* = \frac{Vm*^2}{P*} = \frac{\left((Rm \cdot d + K^2) \cdot wr + Rm \cdot T_L\right)^2}{(Rm \cdot d^2 + d \cdot K^2) \cdot wr^2 + (2 \cdot Rm \cdot d + K^2) \cdot wr \cdot T_L + Rm \cdot T_L^2} \tag{6.22}$$

It is assumed that the buck-boost converter does not lose power, hence the PVM power is transferred directly to the dc motor. Using the Fixed Point Theorem, it is possible to calculate the voltage of operation, V, to produce the required power for the dc motor, $P*$. The algorithm to calculate V is given by (6.23). The variable ε is the maximum allowed error to stop the iteration. Table 6.4 provides the equation to calculate the duty ratio to transfer desired power using a buck-boost converter. Finally, the fixed duty ratio, D, is calculated by (6.24). As a summary, figure 6.18 show the algorithm to calculate the fixed duty ratio, D, using the Fixed Point Theorem, FPT.

$$\begin{gathered} while|V(n+1) - V(n)| \leq \varepsilon \\ V(n+1) = \frac{P * - P * \cdot exp\left(-\frac{1}{b}\right)}{Ix - Ix \cdot exp\left(\frac{V(n)}{b \cdot Vx} - \frac{1}{b}\right)} \end{gathered} \tag{6.23}$$

$$D = \frac{\sqrt{R_o}}{\sqrt{R_o} + \sqrt{R_{op}}} = \frac{1}{1 + \sqrt{\frac{R_{op}}{R_o}}} = \frac{1}{1 + \sqrt{\frac{V(n+1)^2}{R* \cdot P*}}} \tag{6.24}$$

As a note, if T_L is zero then $P*$, $Vm*$, and $R*$ are simplified to (6.25), (6.26), and (6.27) respectively. Also, $R*$ will be a constant value that will not depend on wr.

$$P* = \left(\frac{d^2}{K^2} \cdot Rm + d\right) \cdot wr^2 \tag{6.25}$$

$$Vm* = Rm \cdot I_{Lm*} + K \cdot wr = \left(\frac{Rm \cdot d}{K} + K\right) \cdot wr \tag{6.26}$$

$$R* = \frac{Vm*^2}{P*} = \frac{(Rm \cdot d + K^2)^2}{(Rm \cdot d^2 + d \cdot K^2)} \tag{6.27}$$

The following example will simulate a PVM connected to buck-boost converter and a dc motor given a variable speed, wr, and T_L which is equal to zero. The parameters for the PVM are the following Ix is $0.3A$, Vx is $21V$, b is 0.08; for the buck-boost converter C is $400\mu F$, L is $100\mu H$, the frequency is $20kHz$; the parameters for the dc motor are Rm is 1Ω, Lm is $0.5HJ$ is $0.01N/m^2$, d is $0.01Nms$, K is $0.1NmA^{-1}$.

$$wr = \begin{cases} 0.1 & \text{if } 0 \le t < 5; \\ 0.21 & \text{if } 5 \le t < 10; \\ 0.15 & \text{if } 10 \le t < 15; \\ 0.20 & \text{if } 15 \le t < 20; \\ 0 & \text{if } 20 \le t \le 25. \end{cases}$$

Figure 6.19 shows the expected transition given the voltage and current for the PVM to produce the required power for the dc motor to run at the reference speed, wr. Figure 6.20 shows the tracking performance given the reference speed, wr. Also, it is shown the changes in the necessary power to produce the required speed. Finally, the same figure shows the transient for the voltage and current supplied by the PVM. These simulations were done using Simulink.

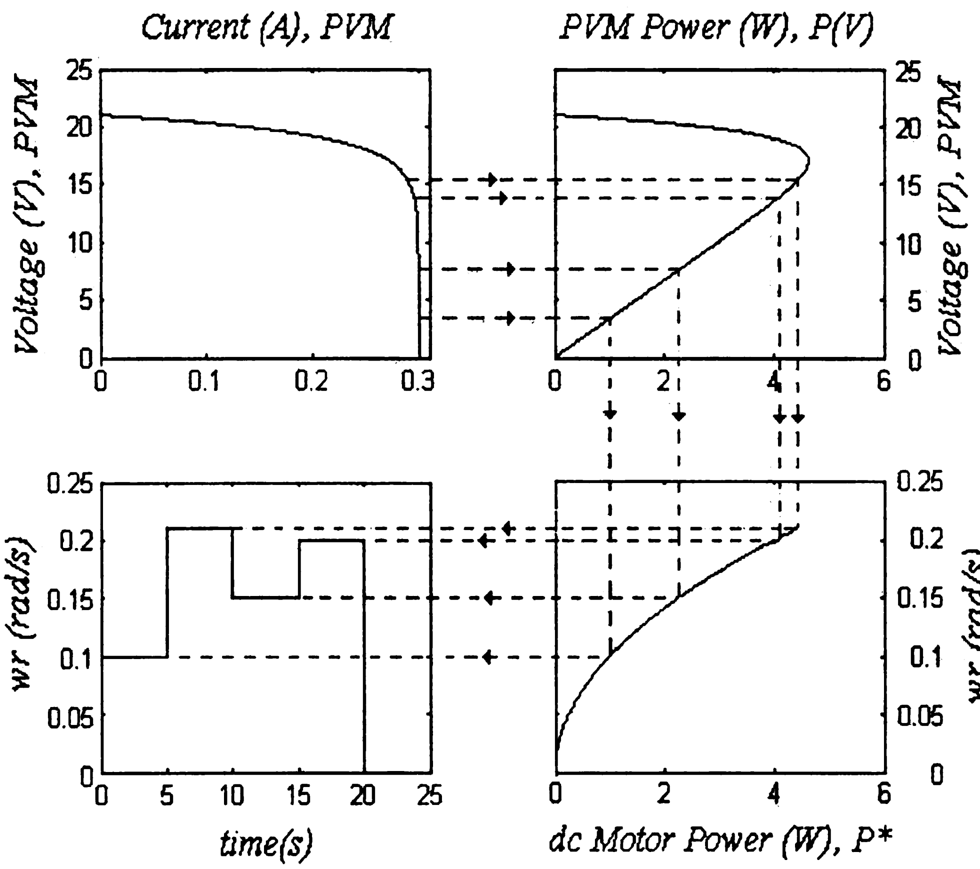

Figure 6.19. Expected transition between the PVM and the dc motor to produce wr.

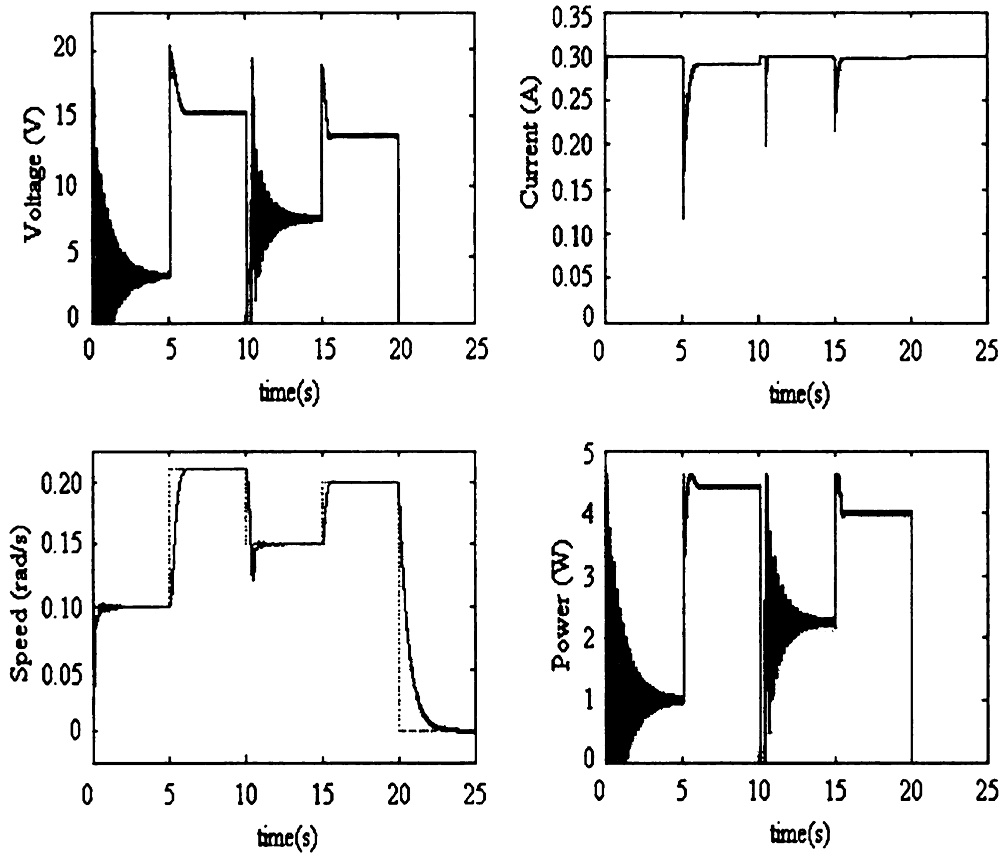

Figure 6.20. Results of a PVM connected to buck-boost converter and a dc motor.

6.8 Z-Source Converter

In the next sections, a photovoltaic system integrated with the Z-source converter for ac power applications is presented. The Z-source converter is an impedance-source power converter [117]. The Z-source concept can be applied to all dc-ac, dc-dc, ac-ac, and ac-dc power conversion [27, 79, 118, 119]. The Z-source is a two-port network that consists of a splits-inductor L_1 and L_2 and capacitors C_1 and C_2 connected in an X shape. L_1 and L_2 can be provided through a split inductor or two separate inductors. The Z-source converter employs a unique impedance network to couple the converter main circuit to the power source, thus providing unique features that cannot be obtained in the traditional voltage-source and current-source converters where a capacitor and inductor are used, respectively [117].

The unique feature of the Z-source connected to an inverter is that the output voltage can be any value between zero and infinity. The Z-source converter is a buck-boost converter that has a wide range of obtainable voltage. Figure 6.21 shows the Z-source and the Z-source dynamic model is described from (6.28) to (6.31). The voltage and current inputs of the Z-source are given by V_d and I_d, and voltage and current outputs are given by V_s and I_s.

$$\frac{\partial V_{C1}}{\partial t} = \frac{1}{C1} \cdot (I_{L2} - I_s) \tag{6.28}$$

$$\frac{\partial V_{C2}}{\partial t} = \frac{1}{C2} \cdot (I_{L1} - I_s) \tag{6.29}$$

$$\frac{\partial I_{L1}}{\partial t} = \frac{1}{L1} \cdot (V_d - V_{C2}) \tag{6.30}$$

$$\frac{\partial I_{L2}}{\partial t} = \frac{1}{L2} \cdot (V_d - V_{C1}) \tag{6.31}$$

$$V_s = V_{C1} + V_{C2} - V_d \tag{6.32}$$

$$I_d = I_{L1} + I_{L2} - I_s \tag{6.33}$$

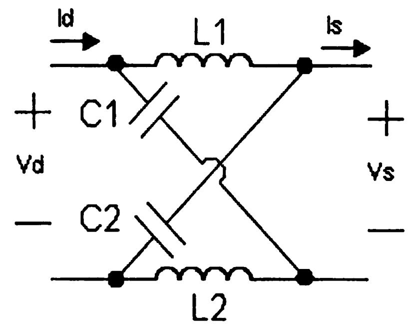

Figure 6.21. Z-Source configuration.

6.9 Proposed PVIS using the Z-Source Converter and Load Matching Control

Figure 6.22 shows the proposed PV inverter system. The PVM is connected to a buck-boost converter, to control the voltage, V_i, of the PVM to it's optimal value, V_{op}. The maximum power for the PVM will result from the optimal voltage, V_{op}. The dc output voltage of the buck-boost converter will charge the battery, Vb, and it is connected to an inverter and the Z-source working under resonance where the dc voltage of the battery will be boosted to the desired ac voltage output. The dynamic equations (6.34) and (6.35) describe a buck-boost converter. The dynamic model for the battery connected to an inductance is given by (6.37) and (6.36). The inverter model is described by (6.38) and (6.39). The load is an induction motor described by (6.40). The proposed PVIS dynamic model is described using (6.28) to (6.41).

$$\frac{\partial V_C}{\partial t} = \frac{S \cdot I_L - I_L - I_z}{C} \tag{6.34}$$

$$\frac{\partial I_L}{\partial t} = \frac{S \cdot V_i + V_C - S \cdot V_C}{L} \tag{6.35}$$

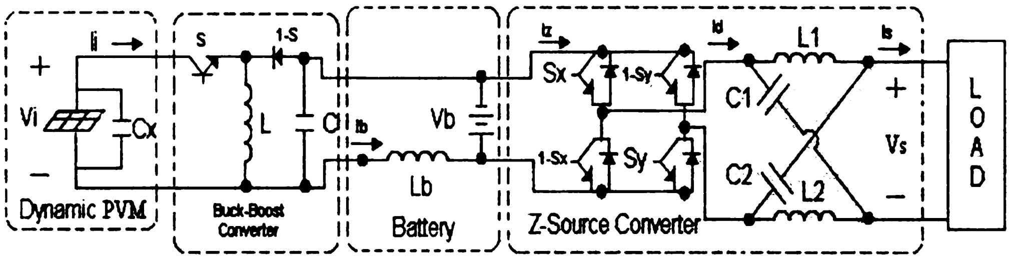

Figure 6.22. Proposed single phase PVIS using the Z-Source converter.

$$\frac{\partial I_{Lb}}{\partial t} = \frac{1}{Lb} \cdot (V_C - V_b) \tag{6.36}$$

$$I_b = I_{Lb} + I_z \tag{6.37}$$

$$V_d = (S_x + S_y - 1) \cdot V_C \tag{6.38}$$

$$I_z = (S_x + S_y - 1) \cdot I_d \tag{6.39}$$

$$\frac{\partial I_s}{\partial t} = \frac{1}{Lm} \cdot (V_s - R_m \cdot I_s) \tag{6.40}$$

$$D = \frac{V_b}{V_b + V_{op}} \tag{6.41}$$

The buck-boost converter is controlled to transfer P_{max} to the battery using the optimal duty ratio, D, given by (6.41). This switching, based on the optimal duty ratio will result in the maximum power and the optimal voltage from the PVM as given in Table 6.4. The components for the proposed PVIS are 13 PVM's SQ80 connected in parallel with an internal capacitance Cx of $39nF$. The electrical characteristics for a PVM SQ80 are given in Table 2.1. Using these values, the maximum power provided by the PV array is around $1040W$ and the optimal voltage is $18.1V$ under STC. The buck-boost converter has an inductance, L, of $0.1mH$ and capacitance, C, of $0.4mF$. The battery should be charged and kept to the rated voltage of $36V$. Also, the bank of batteries is connected to an inductance, Lb, of $0.1mH$. The Z-source was designed to work in resonance to eliminate the use of transformers and filters. The

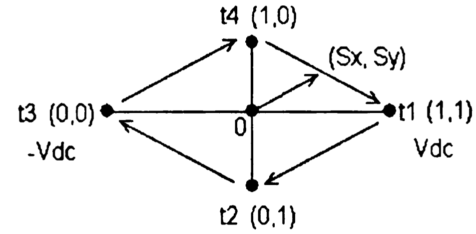

	Sx	Sy	Duration	Vd
t1	1	1	8.1057 ms	-Vb
t2	0	1	1.8943 ms	0
t3	0	0	8.1057 ms	Vb
t4	1	0	1.8943 ms	0

Figure 6.23. Diagram for the phase shifting control with a frequency of $50Hz$.

parameters for the Z-source are: $L1$ is $2mH$, $L2$ is $5mH$, $C1$ is $1mF$ and $C2$ is $6mF$. The load is a single phase induction motor described by a resistance, R_m, of 15Ω and an inductance, L_m, of $0.039H$. The power required for the load is $960W$ with a rated voltage of $120V(rms)$ and a frequency of $50Hz$.

The single phase inverter is controlled using the basic technique of phase shifting control. Figure 6.23 shows the diagram for the phase shifting control with a frequency of $50Hz$ and the duration of time for each state. The inverter voltage output enters the resonant Z-source converter and is amplified 4.7 times. Also, most of the harmonics are eliminated with a THD of less than 3%. Figure 6.24 shows the output voltage, Vd, and output current, Id for the inverter using phase shifting control. Figure 6.25 shows the performance of the resonant Z-source output voltage for the proposed PVIS; hence, the induction motor is receiving a quasi-sinusoidal voltage waveform and sinusoidal current. Finally, advantages of the proposed PVIS are that the use of a transformer is eliminated, harmonics are reduced, and the maximum power and rated output voltage are supplied to the load which in this case is the induction motor.

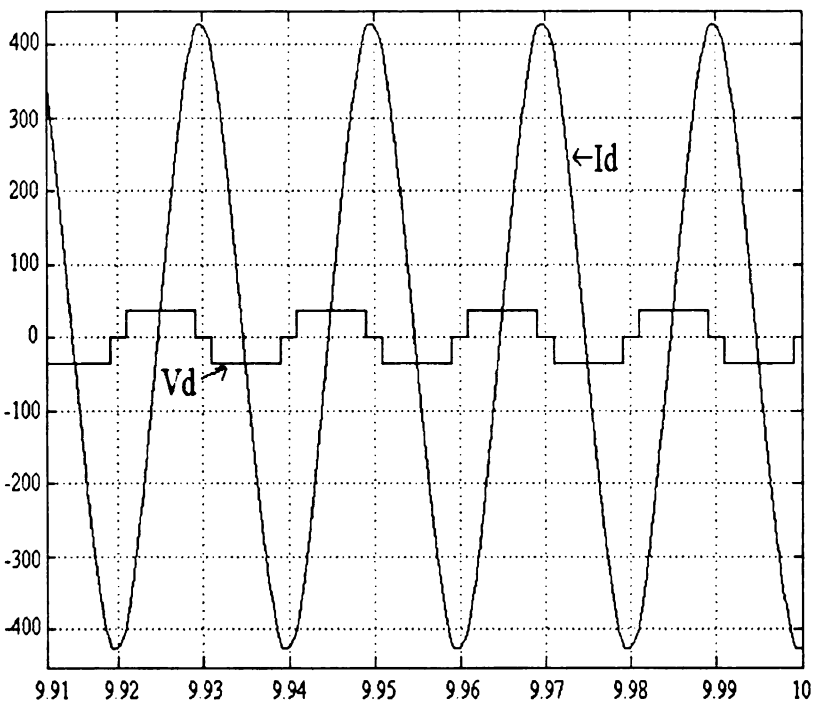

Figure 6.24. Inverter voltage output, Vd and current output Id.

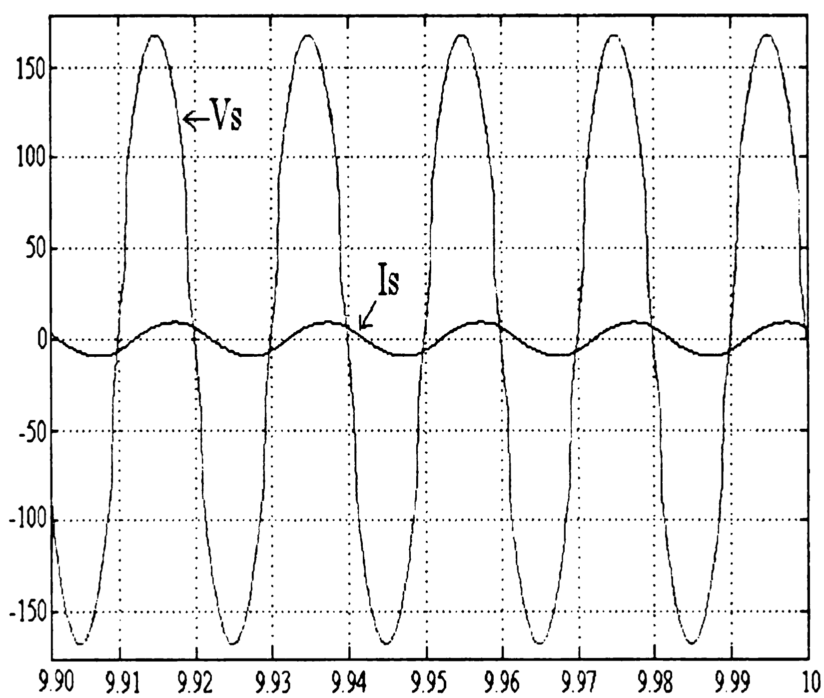

Figure 6.25. Induction motor input voltage, Vs, with a frequency of $50Hz$.

CHAPTER 7

Conclusions

7.1 Summary

This work presented the modeling and analysis of solar distributed generation. All the areas that constitute solar distributed generation were covered in this work, including the modeling and mathematical approximation for a photovoltaic module, algorithms for maximum power point tracking, dc-dc converter control, PV circuit analysis, estimation of the climate conditions, inverter design for residential applications. Each chapter is summarized in the next paragraphs.

Chapter 2 showed an analytical model for a photovoltaic module. The PVM model takes into consideration the manufacturer data sheet, the temperature, and the irradiation level. This model has been verified using different types of PVM's giving excellent results to simulate the I-V and P-V curves. Also, this model can be used to calculate the internal resistance of operation for a PVM. The proposed model has the advantage of producing, not only the I-V curves provided by the manufacturer, but also the P-V curves, R-V curves, P-I curves under changes in the temperature and effective irradiance level. Unfortunately, the proposed PVM cannot provide direct analytical solutions do not exist to calculate the optimal voltage, current and the maximum power using differential calculus. This PVM model was used in other chapters to develop MPPT algorithms, irradiance level and temperature estimation algorithms, PV applications in the area of power systems, etc.

Chapter 3 presented a method called Linear Reoriented Coordinates Method (LRCM). The LRCM is a nontraditional method to be applied for functions without the diffeomorphism property. With the use of the LRCM, solutions to obtain the approximate maximum value f_{max} for a function, $f(x) = x \cdot g(x)$, will be obtained using $g(x)$ and the linear equation, $g_l(x)$. Another application for the LRCM is the approximation for the symbolic solutions of P_{max}, V_{op} and I_{op} for a PVM hence the LRCM can be considered as a MPPT algorithm. Also for PVM applications, the LRCM is more practical for simulations due to the symbolic solutions. Additionally, the LRCM can be integrated into other optimization methods. The LRCM may be applied to other fields like math, geology, civil engineering, economy and mechanical engineering.

Chapter 4 described the Fractional Polynomial Method (FPM) to approximate the exponential functions that describe the performance for a PVM. Also, this chapter described a second method to approximate a fractional polynomial by a sufficiently close integer polynomial. This method is called the Integer Polynomial Approximation Method (IPAM). Several examples were shown and verified using the data of different PVM's. These results proved that the proposed methods FPM and IPAM were excellent to approximate the PVM exponential model and could be applied to other systems. The proposed methods are very useful as tools to solve and approximate certain types of exponential functions keeping the boundary conditions, shape and performance of the original exponential model. The following paragraphs summarize the FPM and the IPAM with the advantages and disadvantages of each approximation or model.

The FPM assumes the same boundary conditions, shape and similar performance as the original PVM model. The FPM is excellent to estimate the analytical solutions for the optimal voltage, current and the maximum power. The parameters n and q are unique values with a direct relationship to the characteristic constant, optimal voltage and open circuit voltage. Also, this method can be considered as an additional alternative Maximum Power Point Tracker, (MPPT) due to the fact that n and q are non-variant. An approximate solution of V_{op} can be obtained measuring the online signals Ix and Vx and used as a reference for maximum power tracking purposes.

The IPAM is an approximation of the FPM. The performance for the integer polynomial is very close to the fractional approximation and uses the parameters n and q previously calculated. The integer polynomial method is useful for Lyapunov analysis, custom polynomial PV source simulation and for ALU programming.

Chapter 5 described four algorithms, which are capable of calculating the effective irradiance level and temperature over a PVM. The proposed algorithms eliminate the use of thermocouples and pyranometers, reducing the cost and complexity of a PV power system. These algorithms have several advantages such as being easy to execute and very efficient at using the data provided by the PVM and having very fast convergence. Three of the algorithms use only the data provided by the voltage sensor and current sensor, and are excellent at tracking changes in the temperature and irradiance level in a geographic region over long periods of time. These algorithms can be integrated into MPPT and other monitoring algorithms, and can be implemented in RT Linux or a fast controller like a DSP. The algorithms have high accuracy (3%), working as effectively a high cost pyranometer without the high price. They also work like an integrated thermocouple without affecting PV power system performance. Finally, these algorithms are excellent for monitoring in remote areas

Chapter 6 presented new contributions to the field of solar energy conversion. One of the contributions was circuit analysis for a PVM connected to different loads. Another of the contributions is the determination of the optimal duty ratio for load matching to transfer the maximum power from a PVM to a load. Also, the optimal duty ratios for different types of dc-dc converters for PV applications were derived. The equations for the optimal duty ratios can be integrated with other algorithms such as LRCM to calculate the PVM internal resistance.

Also, in this chapter was presented a novel single phase photovoltaic inverter system for power applications. The proposed PVIS has the advantages that it takes into consideration the dynamic model for a PVM, it has an optimal duty cycle for the buck-boost converter to transfer the maximum power to the load, and it uses the Z-source converter in resonance to eliminate the use of transformers and filters to the load. The dynamic PVM model is excellent for power applications due to the fact that the model considers the temperature and effective irradiance level and it is useful for calculating the optimal duty ratio for a buck-boost converter. Finally, with the use of a resonant Z-source converter, the desired voltage output can be achieved with minimal harmonics.

Finally, there are some issues that could be explored in the future related to this work. One possibility for future work could be the physical residential implementation of the proposed photovoltaic inverter system using the Z-source converter which can be compared with the traditional photovoltaic inverter system. Research in the area of bifurcations and chaotic behavior in photovoltaic systems could be explored in the future as well. It is possible that the typical problems found in power systems like voltage collapse or instability can be predicted in photovoltaic systems using the proposed PVM model. Future work could be done in applying the techniques developed in this work to a problem where several alternative systems are interconnected and supplying power to different loads. In this type of problem, issues as choosing the correct model to describe sources like wind turbines, fuel cells, geothermic systems could be explore as well as consequences arising from having these alternative power systems connected to the utility grid could be explored. Also, how economically viable they are to produce power and invest in them.

BIBLIOGRAPHY

BIBLIOGRAPHY

[1] University of Texas. Today's Solar Radiation for Austin, Texas. http://ccwf.cc.utexas.edu/ solar/today.html, 2006. cited March 16, 2006.

[2] University of Georgia. Georgia Solar Radiation Database. http://www.griffin.uga.edu/aemn/cgi-bin/AEMN.pl?site=AAAA&report=XO, 2006. cited April 16, 2006.

[3] F. Z. Peng. Editorial Special Issue on Distributed Power Generation. *IEEE Trans. Power Electronics*, 19:1157–1158, September 2004.

[4] G. Batsukh, D. Ochirbaani, C. Lkhagvajav, N. Enebish, B. Ganbat, T. Baatarchuluun, K. Otani, and K. Sakuta. Evaluation of solar energy potentials in Gobi desert area of Mongolia. In *Proc. World Conference on Photovoltaic Energy Conversion*, pages 2262–2264, 2003.

[5] R. Hoffmann and P. Mutschler. The influence of control strategies on the energy capture of wind turbines. In *Proc. IEEE Industry Applications Conference*, volume 2, pages 886–893, Oct. 2000.

[6] P. Mutschler and R. Hoffmann. Comparison of wind turbines regarding their energy generation. In *Proc. IEEE Power Electronics Specialists Conference*, volume 1, pages 6–11, June 2002.

[7] D. Pruitt. The simulation of building integrated photovoltaics in commercial office buildings. In *Proc. International Building Performance Simulation Assoc. Conf.*, pages 685–688, 2001.

[8] J. Wang, F.Z. Peng, J. Anderson, A. Joseph, and R. Buffenbarger. Low cost fuel cell converter system for residential power generation. *IEEE Trans. Power Electronics*, 19(5):1315–1322, Sept. 2004.

[9] J. Wang, F.Z. Peng, J. Anderson, A. Joseph, and R. Buffenbarger. Low cost fuel cell inverter system for residential power generation. In *Proc. IEEE Applied Power Electronics Conference and Exposition*, volume 1, pages 367–373, 2004.

[10] K. Chomsuwan, P. Prisuwanna, and V. Monyakul. Photovoltaic grid-connected inverter using two-switch buck-boost converter. In *Proc. IEEE Photovoltaic Specialists Conference*, pages 1527–1530, May 2002.

[11] T.L Dinwoodie and D.S. Shugar. Optimizing roof-integrated photovoltaics: a case study of the PowerGuard roofing tile. In *Proc. IEEE Photovoltaic Specialists Conference*, volume 1, pages 1004–1007, Dec. 1994.

[12] D. Cruz-Martins, R. Demonti, and R. Ruther. Analysis of utility interactive photovoltaic generation system using a single power static inverter. In *Proc. IEEE Photovoltaic Specialists Conference*, pages 1719–1722, Sept. 2000.

[13] J.M.A. Myrzik and M. Calais. String and module integrated inverters for single-phase grid connected photovoltaic systems - a review. In *Proc. IEEE Power Tech Conf.*, volume 2, pages 23–26, 2003.

[14] S. Saha and V.P. Sundarsingh. Novel grid-connected photovoltaic inverter. *IEE Proceedings Generation, Transmission and Distribution*, 143(2):219–224, March 1996.

[15] State Energy Conservation Office. www.InfinitePower.org. cited on March 17, 2006.

[16] T. Shimizu, O. Hashimoto, and G. Kimura. A novel high-performance utility-interactive photovoltaic inverter system. *IEEE Trans. Power Electronics*, 18(2):704–711, March 2003.

[17] C.R. Sullivan and M.J. Powers. A high-efficiency maximum power point tracker for photovoltaic arrays in solar-powered race vehicle. In *Proc. IEEE Power Electronics Specialists Conference*, pages 574–580, June 1993.

[18] F.Y. Wang, O. Kwan, and T.Y. Yi. Dynamic modeling of rotating flexible platforms. In *Proc. IEEE Conf. on Decision and Control*, pages 1315–1316, Dec. 1992.

[19] J.M.A. Myrzik M. Calais. String and Module Integrated Inverters for Single-Phase Grid Connected Photovoltaic Systems A Review. In *Proc. IEEE Power Tech Conf.*, 2003.

[20] J. Schmid. PV in commercial buildings. In *Proc. IEE Colloquium on Electricity Generation by Commercial Customers Using Photovoltaics*, pages 6/1–6/5, Oct. 1994.

[21] S. Xiaofeng, W. Weiyang, W. Baocheng, and W. Xiaogui. A research on photovoltaic energy controlling system. In *Proc. IEEE International Conference on Electrical Machines and Systems*, volume 1, pages 542–545, Aug. 2001.

[22] B.G. Streetman and S. Baerjee. *Solid State Electronic Devices.* Prentice Hall, 5th edition, 1999.

[23] B. Marion and J. Adelstein. Long-term Performance of the SERF PV Systems. In *Proc. NCPV and Solar Program Review Meeting*, pages 199–201. National Renewable Energy Laboratory, 2003.

[24] C. Prapanavarat, M. Barnes, and N. Jenkins. Investigation of the performance of a photovoltaic AC module. *IEE Proceedings Generation, Transmission and Distribution*, 149(4):472–478, July 2002.

[25] A. Hussein, K. Hirasawa, H. Jinglu, and J. Murata. The dynamic performance of photovoltaic supplied dc motor fed from DC-DC converter and controlled by neural networks. In *Proc. IEEE International Joint Conference on Neural Networks*, volume 1, pages 607–612, May 2002.

[26] K. Khouzam and K. Hoffman. Technical guidelines for the interconnection of PV generation systems in Queensland. In *Proc. IEEE Photovoltaic Specialists Conference*, pages 1349–1352, Oct. 1997.

[27] Y. Huang, M. Shen, and F. Z. Peng. A Z-Source Inverter for Residential Photovoltaic Systems. In *Proc. International Power Electronics Conference*, April 2005.

[28] Resource Assessment Program. Average daily solar radiation per month in usa. http://www.nrel.gov/solar. cited April 21, 2006.

[29] T. Markvart and R.J. Arnold. Integration of photovoltaic converters into the public electricity supply network. In *Proc. IEE Colloquium on Power Electronics for Renewable Energy*, pages 4/1–4/4, June 1997.

[30] V. Quaschning and R. Hanitsch. Influence of shading on electrical parameters of solar cells. In *Proc. IEEE Photovoltaic Specialists Conference*, pages 1287–1290, May 1996.

[31] W. Xiao, W.G. Dunford, and A. Capel. A novel modeling method for photovoltaic cells. In *Proc. IEEE Power Electronics Specialists Conference*, volume 3, pages 1950–1956, June 2004.

[32] L. Shengyi and R. A. Dougal. Dynamic multiphysics model for solar array. *IEEE Trans. Energy Conversion*, 17(2):285–294, June 2002.

[33] T. Markvart. Principles of the radiation damage in solar cells. In *Proc. IEE Colloquium on Solar Cells for Space Applications*, pages 3/1–3/1, Nov. 1988.

[34] A. J. Anderson. Final Report for Task 2.0. subcontract TAD-4-14166-01, NREL, Oak Leaf Place, 1995.

[35] G. Blaesser. PV Array Data Translation Procedure. In *Proc. European Photovoltaic Solar Energy Conference*, 1995.

[36] C.-T Chiang, T.-S. Chiang, and H.-S. Huang. Modeling a photovoltaic power system by CMAC-GBF Photovoltaic Energy Conversion. In *Proc. World Conference on Photovoltaic Energy Conversion*, volume 3 of *3rd*, pages 2431–2434, May 2003.

[37] S. Coors and M. Bohm. Application of the Two-Exponential Model to Correction Procedures for Silicon Solar Cells. In *Proc. EuroSun*, pages 614–619, 1996.

[38] S. Coors and M. Bohm. Validation and comparison of curve correction procedures for silicon solar cells. In *Proc. European Photovoltaic Solar Energy Conference*, pages 220–223, 1997.

[39] Th. F. Elshandatter, M. T. Elhagry, E. M. Abou-Elzahab, and A. A. T. Elkousy. Fuzzy modeling of photovoltaic panel equivalent circuit. In *Proc. IEEE Photovoltaic Specialists Conference*, pages 1656–1659, Sept. 2000.

[40] E.M. Gaddy, R. Cikoski, and D. Mekadenaumporn. Curve fitting solar cell degradation due to hard particle radiation. In *Proc. World Conference on Photovoltaic Energy Conversion*, volume 1, pages 723–725, May 2003.

[41] IEC 891 International Electrotechnical Commission. *Procedures for temperature and irradiance corrections to measured I-V characteristics of crystalline silicon photovoltaic devices*, 1987.

[42] IEC 904 International Electrotechnical Commission. *Photovoltaic devices. Part 1: Measurement of photovoltaic current-voltage characteristics*, 1987.

[43] D.L. King, J.K. Dudley, and W.E. Boyson. PVSIM: a simulation program for photovoltaic cells, modules, and arrays. In *Proc. IEEE Photovoltaic Specialists Conference*, pages 1295–1297, 1996.

[44] C. M. Whitaker, T. U. Townsend, H. J. Wenger, A. Iliceto, G. Chimento, and F. Paletta. Effects of irradiance and other factors on PV temperature coefficients. In *Proc. IEEE Photovoltaic Specialists Conference*, volume 1, pages 608–613, Oct. 1991.

[45] E. I. Ortiz-Rivera and F.Z. Peng. Analytical Model for a Photovoltaic Module using the Electrical Characteristics provided by the Manufacturer Data Sheet. In *Proc. IEEE Power Electronics Specialists Conference*, pages 2087–2091. IEEE, June 2005.

[46] S. Jain and V. Agarwal. A new algorithm for rapid tracking of approximate maximum power point in photovoltaic systems. *IEEE Power Electronics Letters*, 2(1):16–19, March 2004.

[47] Y.-Ch. Kuo, T.-J. Liang, and J.-F. Chen. Novel maximum power-point-tracking controller for photovoltaic energy conversion system. *IEEE Trans. Industrial Electronics*, 48(3):594–601, June 2001.

[48] Y. H. Lim and D. C. Hamill. Simple maximum power point tracker for photovoltaic arrays. *IEEE Power Electronics Letters*, 36(11):997–999, May 2000.

[49] W. Swiegers and J.H.R. Enslin. An integrated maximum power point tracker for photovoltaic panels. In *Proc. IEEE International Symposium on Industrial Electronics*, volume 1, pages 40–44, July 1998.

[50] J.A. Jiang, T.L. Huang, Y.T. Hsiao, and C.H. Chen. Maximum Power Tracking for Photovoltaic Power System. *Tamkang Journal of Science and Engineering*, 8(2):147–153, 2005.

[51] Ch. Hua and Ch. Shen. Study of maximum power tracking techniques and control of DC/DC converters for photovoltaic power system. In *Proc. IEEE Power Electronics Specialists Conference*, volume 1, pages 86–93, 1998.

[52] Ch. Hua, J. Lin, and Ch. Shen. Implementation of a DSP-controlled photovoltaic system with peak power tracking. *IEEE Trans. Industrial Electronics*, 45(1):99–107, Feb. 1998.

[53] T. Hiyama and K. Kitabayashi. Neural network based estimation of maximum power generation from PV module using environmental information. *IEEE Trans. Energy Conversion*, 12(3):241–247, Sept. 1997.

[54] A. Moreno, J. Julve, S. Silvestre, and L. Castaner. A fuzzy logic controller for stand alone PV systems. In *Proc. IEEE Photovoltaic Specialists Conference*, pages 1618–1621, 2000.

[55] T.J. Liang, J.F. Chen, T.C. M, Y.C. Kuo, and C.A. Cheng. Study and Implementation of DSP-based Photovoltaic Energy Conversion System. In *Proc. IEEE Power Electronics and Drive Systems Conference*, volume 1, pages 807–810, 2001.

[56] M.A.S. Masoum, H. Dehbonei, and E.F. Fuchs. Theoretical and experimental analyses of photovoltaic systems with voltage and current-based maximum power-point tracking. *IEEE Trans. Energy Conversion*, 17(4):514–522, Dec. 2002.

[57] Y.H. Lim and D.C. Hamill. Nonlinear phenomena in a model spacecraft power system. In *Proc. Workshop on Computers in Power Electronics*, pages 169–175, July 1998.

[58] J.H.R. Enslin, M.S. Wolf, D.B. Snyman, and W. Swiegers. Integrated photovoltaic maximum power point tracking converter. *IEEE Trans. Industrial Electronics*, 44:769–773, Dec. 1997.

[59] O. Dranga, C.K. Tse, and H.H.C. Iu. Bifurcation behavior of a power-factor-correction boost converter. *International Journal of Bifurcation and Chaos*, 13(10):3107–3114, 2003.

[60] Y.H. Lim and D.C. Hamill. Chaos in spacecraft power systems. *IEEE Power Electronics Letters*, 35(6):510–511, March 1999.

[61] E.I. Ortiz-Rivera and F.Z. Peng. Linear Reoriented Coordinates Method. In *Proc. IEEE Electro/Information Technology Conference*. IEEE, May 2006.

[62] E.I. Ortiz-Rivera and F.Z. Peng. A novel method to estimate the maximum power for a photovoltaic inverter system. In *Proc. IEEE Power Electronics Specialists Conference*, volume 3, pages 2065–2069. IEEE, 2004.

[63] E.I. Ortiz-Rivera. A Novel Method of Area Optimization for a System Modeled with Transcendental Functions. In *Proc. AIAA International Energy Conversion Engineering Conference*. American Institute of Aeronautics and Astronautics, Aug. 2005.

[64] P. Royston and W. Sauerbrei. Stability of multivariable fractional polynomial models with selection of variables and transformations: a bootstrap investigation. *Journal Statistics in Medicine*, 22(4):639–659, Jan. 2003.

[65] G. Ambler and P. Royston. Fractional polynomial model selection procedures: investigation of Type I error rate. *Journal of Statistical Simulation and Computation*, 69:89–108, 2001.

[66] P. Royston, G. Ambler, and W. Sauerbrei. The use of fractional polynomials to model continuous risk variables in epidemiology. *International Journal of Epidemiology*, 28:964–974, 1999.

[67] K. Galkowski and A. Kummert. Fractional polynomials and nD systems. In *Proc. International Symposium on Circuit and Systems*, volume 3, pages 2040–2043, May 2005.

[68] G. Maione. Laguerre approximation of fractional systems. *IEEE Power Electronics Letters*, 38(20):1234–1236, Sept. 2002.

[69] S. Samadi, M. Omair-Ahmad, and M.N.S. Swamy. Exact Fractional-Order Differentiators for Polynomial Signals. *IEEE Power Electronics Letters*, 11(6):529–532, June 2004.

[70] Ch. Liu. Gabor based kernel PCA with fractional power polynomial models for face recognition. *IEEE Trans. Pattern Analysis and Machine Intelligence*, 25(5):572–591, May 2004.

[71] D. Matignon and B. d'Andrea Novel. Observer-based controllers for fractional differential systems. In *Proc. IEEE Conf. on Decision and Control*, pages 4967–4972, Dec. 1997.

[72] S.P. Ellner and J. Guckenheimer. *Dynamic Models in Biology.* Princeton University Press, 1st 2006.

[73] S.G. Gilmour and L.A. Trinca. Fractional Polynomial Response Surface Models. *Journal of Agricultural, Biological, and Eviromental Statistics*, 10(1):50–60, 2005.

[74] Hans Lauwerier. *Fractals Endlessly Repeated Geometrical Figures.* Princeton University Press, 1991.

[75] B.B. Mandelbrot. *The Fractal Geometry of Nature.* W. H. Freeman, 1982.

[76] E.I. Ortiz-Rivera, U.C. Wejinya, and F.Z. Peng. PVM model approximation using fractional polynomials. In *Proc. IEEE Electro/Information Technology Conference*, Aug. 2006.

[77] D. R. Smart. *Fixed Point Theorems.* Cambridge University Press, 1974.

[78] E.I. Ortiz-Rivera and F.Z. Peng. Algorithms to estimate the temperature and effective irradiance over a photovoltaic module using the Fixed Point Theorem. In *Proc. IEEE Power Electronics Specialists Conference*, 2006.

[79] E.I. Ortiz-Rivera and F.Z. Peng. A Dynamic Photovolotaic System Using the Z-Source Converter. In *Proc. AIAA International Energy Conversion Engineering Conference.* American Institute of Aeronautics and Astronautics, Aug. 2005.

[80] Underwriters Laboratories (UL). PVM Specifications. www.ul.com/dge/photovoltaics.

[81] D. Li and P.H. Chou. Maximizing Efficiency of Solar-Powered Systems by Load Matching. In *Proc. IEEE International Symposium on Low Power Electronics and Design*, pages 162–167, Aug. 2004.

[82] SOLAREX. Sa-05 solar panel datasheet. http://www.southwestpv.com/Catalog/PDF/BPcited January 16, 2005.

[83] R. Larson. *Calculus With Analytic Geometry.* D C Heath & Co, 1994.

[84] M.C. Potter. *Principles & Practice of Electrical Engineering: The Most Efficient and Authoritative Review Book for the PE License Exam.* Great Lakes Press, 1st edition, 1998.

[85] K. Holland and F.Z. Peng. Control Strategy for Fuel Cell Vehicle Traction Drive Systems Using the Z-Source Inverter. In *Proc. IEEE Vehicle Power and Propulsion Conference.* IEEE, Sept. 2005.

[86] S. P. Fekete and W. R. Pulleyblank. Area Optimization of Simple Polygons. In *Proc. Annual Computational Geometry*, pages 173–182. Association for Computing Machinery, 1993.

[87] K. Wang and W. K. Chen. Floorplan area optimization using network analogous approach. In *Proc. International Symposium on Circuit and Systems*, volume 1, pages 167–170. IEEE, April 28 May 3 1995.

[88] C.-H. Chen and I.G. Tollis. Efficient area optimization for multi-level spiral floorplans. In *Proc. International Symposium on Circuit and Systems*, volume 1, pages 25–28. IEEE, May 1992.

[89] T. Kim and T. Adali. Complex backpropagation neural network using elementary transcendental activation functions. In *Proc. IEEE International Conference on Acoustics, Speech, and Signal*, volume 2, pages 1281–1284. IEEE, May 2001.

[90] R. Balaniuk, E. Mazer, and P. Bessiere. Fast direct and inverse model acquisition by function decomposition. In *Proc. IEEE International Conference on Robotics and Automation*, volume 2, pages 1535–1540. IEEE, May 1995.

[91] R. Sang-Moon, P. Dong-Jo, and O. Seok-Yong. Inverse mapping using FLS and its application to control. In *Proc. IEEE International Conf. on Systems, Man and Cybernetics*, volume 2, pages 1245–1249. IEEE, October 1995.

[92] M. D. Ercegovac, T. Lang, J.-M. Muller, and A. Tisserand. Reciprocation, square root, inverse square root, and some elementary functions using small multipliers. *IEEE Trans. on Computers*, 49(7):628–637, July 2000.

[93] A. M. Eydgahi and S. Ganesan. Genetic-based fuzzy model for inverse kinematics solution of robotic manipulators. In *Proc. IEEE International Conf. on Systems, Man and Cybernetics*, volume 3, pages 2196–2202. IEEE, October 1998.

[94] H. K. Khalil. *Nonlinear Systems.* Prentice Hall, 3rd edition, 2001.

[95] F. L. Lewis and V. L. Syrmos. *Optimal Control.* Wiley-Interscience, 2nd edition, 1995.

[96] Vesna M. Sekulic Miroljub D. Milojevic. Some comparative considerations of revenue,economy, profit, and profitability functions. *Journal Facta Universitatis Series: Economics and Organization*, 2:81–91, 2004.

[97] H. Petroski. *Design Paradigms: Case Histories of Error and Judgment in Engineering.* Cambridge University Press, 1st edition edition, 1994.

[98] T. J. Rivlin. *An Introduction to the approximation of Functions.* Dover Publications, 1981.

[99] M. Gianquinta and G. Modica. *Mathematical Analysis Aproximation and Discrete Processes.* Birkhauser, 2004.

[100] V. L. Zaguskin. *Handbook of numerical methods for the solution of algebraic and transcendental equations.* Pergamon Press, 1961.

[101] T.F. El Shatter and M.T. Elhagry. Sensitivity analysis of the photovoltaic model parameters. In *Proc. IEEE Midwest Symposium on Circuits and Systems*, pages 914–917, 1999.

[102] R. Gottschalg, M. Rommel, D.G. Infield, and M. J. Kearney. The influence of the measurement environment on the accuracy of the extraction of the physical parameters of solar cells. *Journal Measurement Science and Technology*, 1:797–804, 1999.

[103] D.L. King, W.E. Boyson, and P. Kratochvil. Analysis of factors influencing the annual energy production of photovoltaic systems. In *Proc. IEEE Photovoltaic Specialists Conference*, pages 1356–1361, 2002.

[104] M.W. Davis, A.H. Fanney, and B.P. Dougherty. Evaluating building integrated photovoltaic performance models. In *Proc. IEEE Photovoltaic Specialists Conference*, pages 1642–1645, 2002.

[105] M.A. Abella, E. Lorenzo, and F. Chenlo. Effective irradiance estimation for PV applications. In *Proc. World Conference on Photovoltaic Energy Conversion*, pages 2085–2089, 2003.

[106] Bureau of Meteorology Australian Government. Solar Radiation Definitions. http://www.bom.gov.au/sat/glossary, 2006.

[107] F. Chenlo, N. Vela, and J. Olivares. Comparison between pyranometers and encapsulated solar cells as reference PV sensors-outdoor measurements in real conditions. In *Proc. IEEE Photovoltaic Specialists Conference*, pages 1099–1104, 1990.

[108] D.L. King, W.E. Boyson, B.R. Hansen, and W.I. Bower. Improved accuracy for low-cost solar irradiance sensors. In *Proc. IEEE Photovoltaic Solar Energy Conversion*, pages 1947–1952, 1998.

[109] A. Hunter Fanney, B.P. Dougherty, and M.W. Davis. Performance and characterization of building integrated photovoltaic panels. In *Proc. IEEE Photovoltaic Specialists Conference*, pages 1493–1496, 2002.

[110] C.J. Van Dan Bos and A. Van Dan Bos. Solar radiation sensors: applications, new detector development, characterization and classification according to ISO

9060. In *Proc. IEEE Instrumentation and Measurement Technology Conference*, pages 175–178, 1995.

[111] D.L. King, J.A. Kratochvil, and W.E. Boyson. Temperature coefficients for PV modules and arrays: measurement methods, difficulties, and results. In *Proc. IEEE Photovoltaic Specialists Conference*, pages 1183–1186, April 1999.

[112] Pico Technology Limited. Thermocouple Application Note. http://www.picotech.com/applications/thermocouple.html. cited February 10, 2006.

[113] W. Rakowski. The fixed point theorem in computing magnetostatic fields in a nonlinear medium. *IEEE Trans. Magnetics*, 18:391–392, March 1982.

[114] V. Mainkar and K.S. Trivedi. Sufficient conditions for existence of a fixed point in stochasticreward net-based iterative models. *IEEE Trans. Software Engineering*, 22(9):640–653, September 1996.

[115] S.J. Chiang and C.M. Liaw. Single-Phase Three-Wire Transformerless Inverter. In *IEE Proc. on Electric Power Applications*, volume 141, pages 197–205. IEE, July 1994.

[116] D.W. Hart. *Introduction to Power Electronics*. Prentice Hall, 1st edition, 1996.

[117] F.Z. Peng. Z-source inverter. *IEEE Trans. Industry Applications*, 39(2):504–510, Apr. 2003.

[118] F.Z. Peng, Y. Xiaoming, F. Xupeng, and Q. Zhaoming. Z-source inverter for adjustable speed drives. *IEEE Power Electronics Letters*, 1(2):33–35, June 2003.

[119] F.Z. Peng, A. Joseph, J. Wang, M. Shen, L. Chen, Z. Pan, E.I. Ortiz-Rivera, and Y. Huang. Z-source inverter for motor drives. *IEEE Trans. Power Electronics*, 20(4):857–863, July 2005.